Alma Mater Studiorum · Università di Bologna

Scuola di Scienze
Dipartimento di Fisica e Astronomia
Corso di Laurea Magistrale in Fisica

Primordial tensor modes from inflation and their detectability with GW experiments

Relatore:
Prof. Michele Cicoli

Correlatore:
Prof. Gianmassimo Tasinato

Presentata da:
Alessandro Conigli

Anno Accademico 2017/2018

Sommario

L'obbiettivo di questa tesi è lo studio delle fluttuazioni quantistiche dei modi tensoriali primordiali prodotti durante l'inflazione, con particolare attenzione alla possibilità di rilevare tali modi come onde gravitazionali di background. Una eventuale rilevazione confermerebbe ulteriormente la validità dei modelli inflazionari. Tuttavia, la densità di energia predetta per le onde gravitazionali di background è di gran lunga inferiore alla sensibilità degli attuali rivelatori.
In questo lavoro noi andiamo oltre l'inflazione slow-roll standard e analizziamo nuovi modelli che ci permettono di amplificare le perturbazioni tensoriali su scale al di fuori dell'orizzonte.

Introduciamo un meccanismo che sfrutta una fase transitoria di evoluzione non-attractor per amplificare i modi tensoriali. Procediamo poi con lo studio della fenomenologia del modello, dimostrando la possibilità di amplificare la densità di energia delle onde gravitazionali fino alle scale accessibili dai rivelatori LISA, aLIGO e PTA. Calcoliamo poi il numero di e-folds di fase non-attractor necessari per assicurare la rivelazione di tali onde.

Successivamente, presentiamo un nuovo modello di bigravità, caratterizzato da un termine di accoppiamento tra un tensore privo di massa ed uno massivo. Presentiamo un'analisi dettagliata della dinamica dei due campi tensoriali, derivando vincoli che la massa del campo deve soddisfare per poter amplificare le fluttuazioni prive di massa. Infine, assumiamo che l'accoppiamento sia dominante per un certo numero di e-folds durante l'inflazione e diamo una stima di tale valore per i tre rivelatori sopracitati.

Abstract

The purpose of this thesis is to study quantum fluctuations of primordial tensor modes from inflationary models and to investigate their relation with late-time observables. Their detection would definitely constitute an important hint in favour of inflation models. However their amplitude is predicted to be smaller than the sensitivity of present detectors. In this thesis we instead go beyond the usual slow-roll inflation and discuss two new methods to enhance primordial tensor modes on superhorizon scales.

We first present a mechanism which relies on a transitory non-attractor phase that amplifies the would-be decaying tensor modes. We examine the predictions of the model and we show that gravity waves might be amplified up to the sensitivities of LISA, aLIGO and PTA detectors. We also compute how many e-folds of non-attractor phase are necessary to ensure that the energy density crosses the sensitivity curves of the detectors.

Next, we discuss a new model of bigravity where we assume the existence of massive spin-2 field coupled with a massless tensor mode. We present a detailed analysis of the 2-field dynamics and we derive the constraints on the mass of the field in order to amplify the massless fluctuations om superhorizon scales. We also estimate for the above mentioned detectors the number of e-folds where the coupling term has to be relevant.

Contents

Introduction

The theory of cosmology deals with the origin and the evolution of the universe. The current understanding relies on the application of the general relativity framework to the universe itself. Cosmology provides an explanation to many observational facts with great success, such as the universe expansion, Cosmic Microwave Background (CMB) spectrum and Large Scale Structure (LSS) formation.

Besides its great predictions, standard cosmology is not able to explain questions such as the flatness and horizon problem. These shortcomings are strictly related to the profound question of the initial conditions of the universe, and a possible solution is provided by inflation. The theory of inflation assumes a phase of accelerated expansion of the universe that took place in early times at ultra-high energy. Besides solving some of the hot big bang drawbacks, it was then realized that inflation provides a powerful connection between the universe LSS and its quantum nature. Inflation, together with quantum mechanics, yields a dynamical mechanism for the production of cosmological perturbations on large scales. This is actually one of the rare cases in physics where a prediction based on quantum mechanics and general relativity can be tested experimentally with the present day technology. Indeed, the today's observed cosmic structure evolved from isotropy and homogeneity deviations generated on early times. These deviations may be traced back to quantum fluctuations of the metric and matter fields at the epoch of inflation. Superluminal expansion then stretched fluctuations to a-causal distances, and when inflation ended they eventually re-entered the horizon as classical perturbation. Therefore quantum fluctuations behave as primordial seeds for inhomogeneities, and then they collapse due to gravitational instability.

With the development of precise CMB measurements, inflation became an empirical science, and not only a theoretical speculation. There is great accordance between inflation predictions and the measurements of a nearly scale invariant primordial spectrum of density perturbation. Among these predictions, inflation generally admits the existence of a stochastic background of gravitational waves over a huge range of frequencies, from

those detectable with CMB experiments to those directly accessible with gravitational wave detectors, such as LISA, aLIGO and PTA.
In this dissertation we try to investigate the detectability of the gravitational wave background predicted by inflation at the frequencies probed by the above mentioned detectors. The experimental detection of such background would open up new observational windows for the evolution of the universe at very early times, besides CMB experiments. Indeed a potential observation could give us relevant data about the high energy physics, that will never be accessible by today's particle accelerators.
However the stochastic gravitational wave amplitude is expected to be very week, hence their detection without CMB polarization experiments is so far unlikely.
The purpose of this thesis is to discuss new models which slightly modify the standard slow-roll inflation paradigm in order to enhance the primordial power spectrum of the tensor sector. This would give us a chance to amplify the gravitational wave energy density up to the scales probed by the detectors.
The other main purpose of this thesis is to study the phenomenology predicted by these models, and we try to understand whether or not the primordial spectrum might be enhanced. Then we give an estimate of the required amplification in order to intersects the sensitivity curves of LISA, aLIGO and PTA detectors.

More precisely, this dissertation is organised as follow. In chapter 1 we give a brief introduction of the Friedmann-Robertson-Walker (FRW) space-time and we review the cornerstones of modern cosmology. Working in the general relativity framework we describe the dynamic of homogeneous and isotropic universes, showing the relativistic nature of the expansion and we discuss whether or not it might be accelerated. We then explain how standard Big Bang theory leads to the finely-tuned initial conditions question, namely the flatness and horizon problems. We give a detailed explanation for each of this problems and we show how they can be solved assuming an early period of accelerated expansion called inflation. Finally we discuss the key features of cosmological inflation and we describe how it modifies the causal structure of the space-time. In particular we focus on the physics behind inflation, introducing the notion of the scalar inflaton field as the best candidate which might support the accelerated expansion phase. Eventually we explain the slow-roll approximation which allows us to solve the inflaton dynamics with a perturbative approach and we characterise the number of e-folds required to solve the hot big bang problems.

In chapter 2 we give a brief review of cosmological perturbation theory, trying to explain the mechanism which converts quantum fluctuations during inflation into macroscopic seeds that led to the LSS formation. As pedagogical tool we review the harmonic os-

cillator theory, computing its fluctuations around the ground state. We highlight the choice of the vacuum state, uniquely fixed by the requirement that it is the minimum energy state. Finally, we describe the perturbations production during inflation. In particular we compute the primordial spectrum generated by quantum fluctuations both for the scalar and tensor sector and we discuss its nearly scale invariant behaviour on superhorizon scales.

In chapter 3 we show how to connect the inflation predictions for the tensor sector, *i.e.* the primordial power spectrum, with late-time observables. We solve the equation of motion for the tensor fluctuations derived in chapter 2 at the super and subhorizon scales respectively. Then we match the two solution at horizon crossing in order to fix the integration constant. In particular we focus on the modes that re-entered the horizon during radiation domination, the latter being the cosmologically relevant one for the frequencies probed by detectors. We define the gravitational wave energy density and we show its connection with the primordial power spectrum. According to standard inflation the predicted energy density is well below the sensitivities of actual detectors, therefore relic gravity waves are hard to detect.
We then turn to the discussion of a new model developed by [16] capable to enhance the primordial tensor spectrum in single field inflation. This new mechanism allows us to amplify the would-be decaying tensor mode on superhorizon scales, requiring a transitory non-attractor phase which breaks down standard slow-roll inflation. This phase might be achieved introducing non-canonical kinetic term for the inflaton field, and it can be analytically controlled with tensor duality.
Then we discuss the consequences of a brief non-attractor phase and we investigate how the amplified primordial spectrum could in principle amplify the late-time gravitational wave energy density. In particular we compute how many e-folds of non-attractor inflation are necessary to ensure that the energy density crosses the sensitivity curves of the detectors and we give an estimate of the number of e-folds at which the non-attractor regime should have begun in order to have amplification at the correct frequencies.
After that we review the main noise sources of LISA, aLIGO and PTA experiments and characterise their performance in terms of sensitivity curves. In particular we review the construction of the LISA and aLIGO curves and we propose a new analytical fit for the PTA detector. We conclude the chapter by plotting both the detectors sensitivity and the energy density curves predicted by non-attractor evolution in the same graph, using a consistent protocol. This eventually shows that the stochastic gravitational wave background might be measured by today's detectors if we assume a transient non-attractor phase in between standard slow-roll inflation.

In chapter 4 we discuss a new model which relies on the effective field theory approach: we suppose the existence of a massive spin-2 field coupled with the massless tensor fluctuations and we show that the primordial power spectrum might be enhanced if we set specific constraints on the massive field.
Firstly we discuss a hybrid model of inflation which for the first time introduced a tachyon-like scalar field in order to amplify the production of primordial black holes. Then we develop a similar approach for the tensor sector: starting from effective field theory considerations, we justify the consistency of a lagrangian functional with an interaction term between the massless and the massive tensor field. In particular we assume the coupling term to be relevant for a brief time interval during inflation. Then, solving the equation of motion we investigate the possible enhancement of the massless tensor fluctuations. This might be achieved exclusively for specific values of the mass parameter. We highlight the fact that if we turn off the coupling between the two field, the standard primordial spectrum predicted by slow-roll inflation might be recovered. Finally, in complete analogy with chapter 3, we compute how many e-folds of coupled-fields inflation we need to amplify the energy density up to the desired level accessible by the above mentioned detectors. Eventually, we plot the energy density profile predicted by this model together with the sensitivity curves of the three experiments. Again, this shows us that even in this scenario the detectability of stochastic gravitational wave background might be achieved.

Finally, in the last chapter we sum up the results obtained so far, highlighting the differences between the models discussed in chapter 3 and 4. Then we give possible outcomes for future works.

Chapter 1

Inflationary Universe

1.1 The FRW Universe

The aim of Cosmology is a quantitative description of the evolution and the structure formation of the universe on its largest scales. The current understanding of the universe is based upon the FRW cosmological model which relies on two important observational facts: the expansion of the universe and the so-called Cosmological Principle. The latter tells us that the universe, at least on large scale, is homogeneous and isotropic. The uniformity of the temperature of the CMB constitutes the best observational evidence for the Cosmological Principle: indeed the temperature anisotropies of the CMB spectrum are smaller than one part in 10^5 and this tells us that at the epoch of last scattering (around 300'000 years after the Big Bang) the universe was isotropic and homogeneous with a high degree of precision [1].
From now on we work assuming that the universe is homogeneous and isotropic on large scales and such spaces are characterized by translational and rotational invariance. The only time-dependent four-dimensional spacetime in which the symmetries are clearly manifest and the Cosmological Principle is preserved takes the form

$$\mathrm{d}s^2 = \mathrm{d}t^2 - a^2(t)\left(\frac{\mathrm{d}r^2}{1-kr^2} + r^2\mathrm{d}\Omega^2\right) = g_{\mu\nu}\mathrm{d}x^\mu\mathrm{d}x^\nu \tag{1.1}$$

where $g_{\mu\nu}$ is the FRW metric and $x^\mu \equiv (t, r, \theta, \phi)$ are the comoving coordinates of events on the four-dimensional spacetime. Here $a(t)$ is the cosmic scale factor and it characterizes the relative size of spacelike hypersurfaces Σ at different times [6] together with the time evolution of the universe[1]. The curvature parameter k defines the topology of the

[1]Notice how $a(t)$ is the only time-dependent quantity.

spacelike hypersurface. Indeed, it may have three different values:

$$k = \begin{cases} +1 & \text{for positively curved } \Sigma \\ 0 & \text{for flat } \Sigma \\ -1 & \text{for negatively curved } \Sigma \end{cases} \tag{1.2}$$

As we said previously eq. 1.1 uses a very convenient coordinate system *i.e* the co-moving coordinates: this means that the universe increases in size as $a(t)$ grows, but observers keep fixed coordinates r, θ, ϕ in the absence of peculiar motion, in other words if there are not any forces acting on them. Hence the physical distance can be easily obtained by multiplying the coordinate r with the scale factor, and it is time-dependent even for objects with null peculiar velocities due to the expansion of the universe.
The evolution of the universe, assuming a homogeneous and isotropic FRW metric, is completely determined by the time-evolution of the scale factor $a(t)$. The latter is characterized by the Einstein field equations, once you chose the matter content of the universe. A useful quantity that helps us characterizing the FRW spacetime is the expansion rate, also called Hubble parameter

$$H \equiv \frac{\dot{a}}{a} \tag{1.3}$$

It has units of t^{-1} and is negative for a collapsing universe, positive for an expanding one. In particular, the Hubble parameter sets the time scale of the homogeneous universe[2]: the Hubble time $t \sim H^{-1}$ sets the scale for the age of the universe, while the Hubble length $d \sim H^{-1}$ sets the size of the observable universe [2].

1.2 Einstein equations and stress-energy tensor

The time dependence of the scale factor, which defines the dynamics of the expanding universe, is determined by solving the Einstein field equations

$$R_{\mu\nu} - \frac{1}{2} g_{\mu\nu} R = 8\pi G T_{\mu\nu} \tag{1.4}$$

Here $T_{\mu\nu}$ is the stress-energy momentum tensor and it takes into account the matter content of the universe. This tensor is symmetric

$$T^{\mu\nu} = T^{\nu\mu} \equiv g^{\mu\lambda} T^{\nu}_{\ \lambda} \tag{1.5}$$

[2]We are working with natural units.

and it satisfies the continuity equation

$$\nabla_\mu T^{\mu\nu} = 0 \tag{1.6}$$

where the covariant derivative reduces to the standard one in flats space-time [4].
For consistency with the underlying symmetries of the metric the stress-energy tensor have to be diagonal, while for isotropy the spatial components must be the same. Working on large scales, the simplest realization of such a tensor is that of a perfect fluid

$$T^\mu_{\ \nu} = (\rho + p)u^\mu u_\nu + p\delta^\mu_\nu \tag{1.7}$$

where we denotes with ρ and p the energy density and the pressure respectively, while u^μ is the four-velocity. The latter is known as the fluid velocity field and it reduces to $u^\mu = (1, 0, 0, 0)$ if we use comoving coordinates, *i.e* if we work in reference frame with respect to which the fluid is at rest. In such a frame the stress-energy tensor is simply given by

$$T^\mu_{\ \nu} = \begin{bmatrix} \rho & 0 & 0 & 0 \\ 0 & -p & 0 & 0 \\ 0 & 0 & -p & 0 \\ 0 & 0 & 0 & -p \end{bmatrix} \tag{1.8}$$

Typically, together with the matter content we need to specify an equation of state $p = p(\rho)$ that depends on the properties of the matter itself. Many cosmologically interesting scenarios arise from a linear relationship of the type

$$p = w\rho \tag{1.9}$$

where we introduced the equation of state parameter w.
After these assumptions, we can finally deal with the Einstein field equations: it can be shown that there are only two independent equations, namely the 00-component and one of the ij-components [1]. In particular, the field equations take the form of non linear ordinary differential equations, better known as the Friedmann Equations:

$$H^2 = \frac{8\pi G}{3}\rho - \frac{k}{a^2} \tag{1.10a}$$

$$\dot{H} + H^2 = \frac{\ddot{a}}{a} = -\frac{4\pi G}{3}(\rho + 3p) \tag{1.10b}$$

We denote with dots the derivative with respect to the physical time t.
It is interesting to notice that if the universe is filled with matter which satisfies the strong energy condition $\rho + 3p > 0$ then equation 1.10 implies $\ddot{a} < 0$. Moreover, if we

assume an expanding universe, *i.e.* $\dot{a} > 0$, then we can claim the existence of a singularity in the past $a(t = 0) = 0$. This conclusion depends on the assumption that Friendmann Equation and general relativity are valid up to arbitrary high energies [2] but it is more likely that the singularity determines the breakdown of general relativity itself.

In order to compute the time evolution of the scale factor we combine together the two equation from 1.10 into the continuity equation, which takes the form

$$\frac{\mathrm{d}\rho}{\mathrm{d}t} + 3H(\rho + p) = 0 \tag{1.11}$$

Using the equation of state 1.9 we can rearrange this expression as

$$\frac{\mathrm{d}\ln\rho}{\mathrm{d}\ln a} = -3(1 + w) \tag{1.12}$$

The latter, if integrated, gives the result

$$\rho \propto a^{-3(1+w)} \tag{1.13}$$

We notice that the energy density scales like the inverse of the volume of size $\sim a^3$ if we consider a universe filled with non-relativistic matter ($w = 0$). On the other hand, for a radiation dominated universe ($w = 1/3$) the energy density scales like a^{-4} where the extra factor $1/a$ takes into account the red-shift: the energy of a photon scales like the inverse of its wavelength which in turn scales like $1/a$ [1]. Eventually, if $w = -1$, the energy density ρ is constant in time and this scenario corresponds to a cosmological constant vacuum energy.
Finally we can use the result 1.13 together with the first of the Friedmann eqs. 1.10 to obtain the evolution of the scale factor for a flat universe ($k = 0$)

$$a(t) \propto \begin{cases} t^{2/3(1+w)} & w \neq -1 \\ e^{Ht} & w = -1 \end{cases} \tag{1.14}$$

In principle the early universe was dominated by radiation or relativistic matter, then it was matter dominated and finally the adult universe is dominated by a cosmological constant Λ. As we shall see next, if we assume that inflation happened, there was again a period when the stress-energy tensor was dominated by vacuum energy during the very early phase of the universe.
We report in table 1.1 the solutions for these three different scenarios.

	w	$\rho(a)$	$a(t)$
MD	0	a^{-3}	$t^{2/3}$
RD	$\frac{1}{3}$	a^{-4}	$t^{1/2}$
Λ	-1	a^0	e^{Ht}

Table 1.1: This table shows the possible FRW solutions for a flat universe dominated by matter, radiation or a cosmological constant.

We conclude this section with a brief description of a universe with more than one matter species: if this is the case each species contributes to the energy density and pressure. Hence,

$$\rho = \sum_i \rho_i \qquad\qquad p = \sum_i p_i \tag{1.15}$$

where we denotes with the subscript i each species. In particular if we introduce the critical energy density[3]

$$\rho_c = \frac{3H_0^2}{8\pi G} \tag{1.16}$$

we can define the dimensionless energy density as

$$\Omega_i \equiv \frac{\rho_{i,0}}{\rho_c} \tag{1.17}$$

Finally if we normalize the scale factor evaluated today as $a(t_0) = a_0 = 1$ we may rewrite the first of the Friedmann equations 1.10 as

$$\left(\frac{H}{H_0}\right)^2 = \sum_i \Omega_i a^{-3(1+w_i)} + \Omega_k a^{-2} \tag{1.18}$$

where we parametrize whit $\Omega_k \equiv -k/a_0^2 H_0^2$ the curvature content. If we evaluate this expression today, we end up with the consistency relation

$$\sum_i \Omega_i + \Omega_k = 1 \tag{1.19}$$

On the other hand the second of the Friedmann equations 1.10 evaluated today gives us the condition for accelerated expansion today

$$\frac{1}{a_0^2 H_0^2}\frac{\mathrm{d}^2 a_0}{\mathrm{d}t^2} = -\frac{1}{2}\sum_i \Omega_i(1+3w_i) \tag{1.20}$$

[3]We denote with the subscript 0 a quantity evaluated at the present time t_0.

Indeed we see that accelerated expansion is possible if the condition

$$w_i < -\frac{1}{3} \tag{1.21}$$

is satisfied. This can be achieved if we consider a cosmological constant vacuum-energy domination.

1.3 Causal structure of the spacetime

An outstanding comprehension of the behaviour of light in an expanding universe is a key point to the interpretation of observations: indeed over the last tons the improvements of x-ray, radio and infrared detectors opened a new window to explore the universe.

It is known by physicists that since no massive particle can travel faster than light and the light itself travels at a finite speed there is a fundamental constraint to how far we can see: this is where the concept of horizon comes from.
In this section we focus on the study of the causal structure of the spacetime, which can be understood in terms of conformal diagrams and we develop useful tools that will lead us to the heart of the Big Bang problems and their possible solution with an inflationary epoch at the early stage of the universe.

Once we define the metric for the spacetime of the universe we can study its causal structure, which is determined by the propagation of light in a FRW background.
We know from special relativity that the spacetime interval along the trajectory of a massless photon is determined by

$$\mathrm{d}s^2 = 0 \tag{1.22}$$

According to the equivalence principle, the same holds true in general relativity as we work in a locally inertial reference frame: being the interval invariant, this equation should be valid for light geodesic in any curved spacetime [4].

Given an isotropic universe the radial propagation of light can be easily studied if we work with conformal time η instead of the physical time t. It can be thought as a clock which slows down with the expansion of the universe, and it is defined as

$$\eta \equiv \int \frac{\mathrm{d}t}{a(t)} \tag{1.23}$$

Using conformal time, the metric 1.1 takes the form

$$\mathrm{d}s^2 = a^2(\eta)\big(-\mathrm{d}\eta^2 + \mathrm{d}\chi^2 + \phi_k(\chi^2)(\mathrm{d}\theta^2 + \sin^2(\theta)\mathrm{d}\phi^2)\big) \tag{1.24}$$

where we introduced the coordinate

$$\mathrm{d}\chi^2 = \frac{\mathrm{d}r^2}{1-kr^2} \tag{1.25}$$

and the function $\phi_k(\chi)$ is defined as

$$\phi_k(\chi^2) \equiv \begin{cases} \sinh^2(\chi) & k=-1 \\ \chi^2 & k=0 \\ \sin^2(\chi) & k=+1 \end{cases} \tag{1.26}$$

Thanks to the coordinates η and χ the symmetry of the spacetime are more explicit. In particular by isotropy it is clear the the radial trajectory such that θ, ϕ =const is a geodesic and the propagation of light is determined by the two dimensional line element

$$\mathrm{d}s^2 = a^2(\eta)\big(-\mathrm{d}\eta^2 + \mathrm{d}\chi^2\big) \tag{1.27}$$

This can be recognised as a static Minkowski metric multiplied by the time dependent factor $a^2(\eta)$.

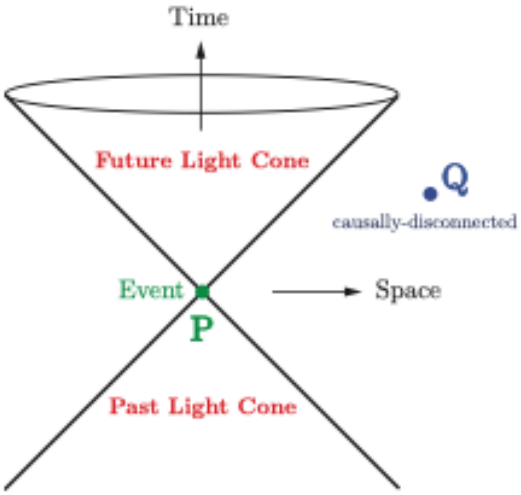

Figure 1.1: The light cone defines the causality of the spacetime: its interior, in which $\mathrm{d}s^2 > 0$, together with the null geodesics $\mathrm{d}s^2 = 0$, defines the region of spacetime causally connected with the event P. On the other hand, causally disconnected region are separated by spacelike interval $\mathrm{d}s^2 < 0$, [2].

Therefore we conclude that radial null geodesics in a FRW background may be described by

$$\chi(\eta) = \pm\eta + \text{const} \tag{1.28}$$

and they correspond to straight lines in the η-χ plane at angles $\pm 45°$. In fig. 1.1 we describe the causal structure in terms of these coordinates. Besides, if we had used physical time t to study light propagation, then the light cones for such a spacetime would be curved [2].

1.3.1 Horizons

In this section we try to answer a crucial question in cosmology: if light travelled only a finite distance since the universe was born, what is the size of the region of the universe in causal contact? This can be easily computed using the results of the previous section: indeed the maximum comoving distance light can propagate from an initial time t_i and a time t is

$$\chi_p(\eta) = \eta - \eta_i = \int_{t_i}^{t} \frac{\mathrm{d}t'}{a(t)} = \int_{a_i}^{a} \mathrm{d}\ln a' \big(aH\big)^{-1} \tag{1.29}$$

where η_i corresponds to the birth of the universe. The quantity $\chi_p(\eta)$ is called the comoving particle horizon and in the last equality we expressed it as a logarithmic integral of the comoving Hubble radius $\big(aH\big)^{-1}$. The maximum physical distance is simply given by multiplying the comoving particle horizon with the scale factor

$$d_p(t) = a(t)\chi_p \tag{1.30}$$

There is an important difference between Hubble radius and particle horizon and it is crucial to keep in mind this distinction: while the scale characterised by the particle horizon relies on kinematical consideration, the Hubble radius is a dynamical scale that determines the rate of expansion [4]. In particular the Hubble horizon represents the distance travelled by particles in the time which takes the scale factor to double [5], [1]. In essence the Hubble radius gives us a different way to understand whether particles are causally connected: if particles are separated by a distance greater than the particle horizon $\chi_p(\eta)$ they could have never communicate between each other, while if they are separated by a distance greater than the comoving Hubble radius $\big(aH\big)^{-1}$ they cannot talk to each other at a given time η. This open the possibility that particle horizon is much bigger than the Hubble radius at the present time, so that they cannot communicate today but they were in causal contact at earlier epochs.
We underline that in the standard Hot Big Bang model the particle horizon is finite and it is equal to the Hubble radius[4] and this is the reason why they are interchangeable in the context of standard cosmology. On the other hand, as we shall see later on, if we consider inflationary models where the strong energy condition is violated and the

[4]Up to a numerical factor.

universe undergoes an accelerated expansion the two quantity are drastically different: indeed the particle horizon grows exponentially with respect to the Hubble radius and by the end of the inflation they differ by a factor e^N where N is the number of e-folds. Finally we note that the Hubble radius determines whether or not a physical length scale $\lambda = 2\pi a/k$ is within the Hubble radius itself: if $k/(aH) \ll 1$ then the physical scale is outside the horizon, while for $k/(aH) \gg 1$ the length lies inside the Hubble radius.

1.4 The drawbacks of the Big Bang theory

Observations over decades of the CMB, which gives us a snap-shot of the early universe, showed us that at the epoch of recombination the universe was surprisingly isotropic and homogeneous on all scales, with anisotropies of the order of 10^{-5}.
In this section, given the laws that govern the evolution of the universe, we try to understand which initial conditions led to such isotropy and homogeneity, and we show that the standard Big Bang model requires a fine-tuned set of initial conditions to explain the current state of the universe. It would be disappointing if only a specific set of initial conditions allows the universe to evolve as we see it, making what we observe an improbable accident [2]. In the next section we will show how this problem can be solved if we assume a stage of accelerated expansion of the universe: indeed one of the major achievements of inflation is its ability to let the universe evolve out of generic initial conditions.

In order to specify the initial conditions, we consider [6] a spatial slice of constant time Σ. On this surface there are two independent sets of initial conditions that characterize matter: the particles positions and their velocities.
In particular, the spatial distribution is described by the energy density $\rho(x)$ as a function of the coordinates. Experimental evidences show that inhomogeneities at the last scattering epoch were much smaller then today, and we know that such inhomogeneities grow with time due to gravitational instability. Thus we expect that these fluctuations were even smaller during the early phase of the universe and in the standard Big Bang model there are no dynamical reason to explain the smoothness of the early universe. Besides, this is even more annoying since, as we show in a while, at the CMB epoch there were a large number of causally disconnected regions, and in the conventional model there is no reason why these regions show similar physical behaviour[5]. This is often referred to as the horizon problem.

On the other hand, besides the initial spatial distributions, we have to specify the

[5]Remember that the CMB spectrum shows us that the universe is almost homogeneous on all scales.

initial field of velocities for a complete characterization of the Cauchy problem of the universe [4]. It turns out that the initial velocities must obey the Hubble law to ensure that the universe is kept homogeneous at late time. Together with the horizon problem, this fine-tuning of the initial velocities is even more dramatic because they have to be matched between causally disconnected regions. This second problem regarding the initial velocities is often called the flatness problem.
In the next paragraphs we analyse in detail these two shortcomings of the standard cosmology model.

1.4.1 Horizon problem

The standard cosmological model shows that at a red shift of about$z = 1100$, photons decoupled from baryonic matter and started a free-stream path, until they reach us basically untouched [1]. In particular this event is know as recombination and it defines the so called last-scattering surface. Let us consider the length corresponding to the present Hubble radius, *i.e.* the scales entering the horizon today, at the time of last-scattering. This is simply

$$\lambda_H(t_{ls}) = d_p(t_0)\frac{a_{ls}}{a_0} = d_p(t_0)\frac{T_0}{T_{ls}} \tag{1.31}$$

where T stands for the temperature. If we consider a universe filled by a fluid with equation of state w, we have

$$H^2 \propto \rho \propto a^{-3(1+w)} \propto T^{3(1+w)} \tag{1.32}$$

The behaviour depends on whether or not $1 + w$ is positive or negative. Taking into account standard cosmology *i.e.* $w \geq 0$ we conclude that the Hubble radius $(H)^{-1}$ always decreases monotonically as you go back in time, but with a different law than the physical length. In particular, at last-scattering epoch and assuming matter domination, *i.e.* $w = 0$, the Hubble radius takes the value

$$H_{ls}^{-1} = d_p(t_0)\left(\frac{T_0}{T_{ls}}\right)^{3/2} \ll \lambda_H(t_{ls}) \tag{1.33}$$

In other words, the physical lengths corresponding to the present day Hubble radius were larger than the Hubble horizon itself at the time of recombination. In particular, the ratio between the volumes associated with these two scales is given by

$$\frac{\lambda_H^3(T_{ls})}{H_{ls}^{-3}} = \left(\frac{T_0}{T_{ls}}\right)^{-3/2} \simeq 10^6 \tag{1.34}$$

Therefore we showed that there were almost 10^6 different casually disconnected regions: this means that the physical scales that enters the horizon today were far outside the horizon at the epoch of last-scattering. However, CMB observations tells us that the universe was extremely homogeneous at that time. How is it possible the so many causally-disconnected regions show the same physical behaviour?

For a better comprehension of the horizon problem it is convenient to think in terms of the conformal time. We recall that in conformal time the light cones look the same as in Minkowski spacetime, and since the light determines the causality, a conformal spacetime diagram provides a good tool to visualize horizons. During radiation or matter domination, the scale factor as a function of the conformal time behaves as

$$a(\eta) \propto \begin{cases} \eta & \text{RD} \\ \eta^2 & \text{MD} \end{cases} \tag{1.35}$$

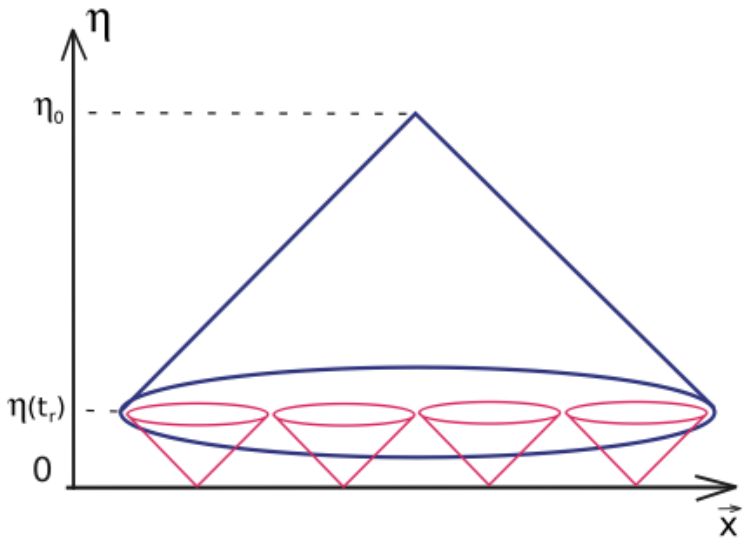

Figure 1.2: Conformal diagram corresponding to standard cosmology. Two points on a surface η = const are in causal contact if their past light cone intersect at least at the big bang singularity $\eta_i = 0$, [3].

Therefore if we assume that the universe has always been dominated by radiation or matter we end up with the existence of the Big Bang singularity at $\eta = 0$:

$$a(\eta_i = 0) = 0 \tag{1.36}$$

From the diagram in figure 1.2 it is evident how the last scattering surface consists of numerous causally disconnected regions, not in thermal equilibrium. Therefore the homogeneity of the CMB becomes a serious puzzle, and we see later on how the inflation paradigm allows us to solve this problem.

1.4.2 The flatness problem

General relativity teaches us that the spacetime is a dynamical entity that evolves in response to the matter content. On the other hand cosmological observations suggest that the universe is perfectly approximated by a flat Euclidean space. How is that possible? To address this problem we start from the Friedman equation

$$H^2 = \frac{8\pi G}{3}\rho(a) - \frac{k}{a^2} \tag{1.37}$$

which can be written, introducing the critical density, as

$$\Omega(a) - 1 = \frac{k}{H^2 a^2} \tag{1.38}$$

From this equation we deduce that if the universe were perfectly flat, then $\Omega = 1$ would holds true at all the times. Besides, if even a small curvature is present, then we have to take into account the time dependence of $\Omega(a)$ and things can be tricky: the critical value $\Omega = 1$ is an unstable fixed point [2].
Given a radiation domination, the Hubble parameter evolves as $H^2 \propto a^{-4}$ and we get

$$\Omega - 1 \propto a^2 \tag{1.39}$$

while in matter domination, $H^2 \propto a^{-3}$ implies

$$\Omega - 1 \propto a \tag{1.40}$$

In both scenarios the time dependent quantity $\Omega - 1$ decreases as we go backwards in time. Experimental evidences suggest us $\Omega_0 = 1$ at the present day. Therefore we can deduce the value of $\Omega(a)$ at the Plank era, at which the temperature of the universe was $T_{Pl} \sim 10^{19}$ Gev. Indeed given the present day CMB temperature $T_0 = 10^{-13}$ Gev, we have:

$$\frac{|\Omega - 1|_{T=T_{Pl}}}{|\Omega - 1|_{T=T_0}} \approx \frac{a_{Pl}^2}{a_0^2} \approx \frac{T_0^2}{T_{Pl}^2} \approx \mathcal{O}(10^{-64}) \tag{1.41}$$

Therefore we can conclude that without inflation the almost flatness observed today requires at early times an extreme fine-tuning of the value $\Omega - 1$, which needs to be very close to zero without being exactly zero.

In the last two paragraphs we described the horizon and flatness problem of the Big Bang model. It is important to highlight that these problem are not inconsistencies of the model: if we assume that the universe was isotropic and homogeneous over superhorizon scales and that the initial value of the dimensionless energy density was extremely close to unity, then the universe evolves according to the experimental results. These are just drawbacks in the predictive power of the standard cosmological model.
The power of the inflationary theory relies on its ability to describe dynamically these initial conditions, without assuming a priori fine-tuning.

1.5 Inflationary universe

In the previous section we stressed out that at the heart of the horizon and flatness problem there is the fact that the comoving Hubble radius $\big(aH\big)^{-1}$ is an increasing function of time in the hot Big Bang model. In particular, recalling the definition of the particle horizon

$$\chi_p(\eta) = \int_0^t \frac{\mathrm{d}t'}{a(t')} = \int_{-\infty}^{\ln a(t)} \mathrm{d}\ln a' \big(aH\big)^{-1} \tag{1.42}$$

we see that due to its behaviour the Hubble radius gives most of the contribute to the integral 1.42 at late time. In essence this means that the amount of conformal time elapsed between the singularity and the CMB production is much smaller than the time between recombination and the present day [7], as figure 1.2 shows.
Therefore we are led to the following simple idea that could help us solving the Big Bang puzzle: what if we invert the behaviour of the Hubble radius in the very early universe, assuming it decreased in time for a sufficiently long period?
Let us explain why a shrinking comoving Hubble sphere really solves the drawbacks of the standard cosmology. In section 1.3 we said that if particles are separated by a distance greater than the Hubble radius $\big(aH\big)^{-1}$ they cannot communicate with each other now, while if they are separated by distances greater than the particle horizon $\chi_p(\eta)$ they could have never talked to each other. In particular, there is a chance that the comoving particle horizon is much bigger than the Hubble radius today: if this is the case, particles that cannot talk to each other now were in causal contact in the past. Eventually this might happen if we assume a decreasing phase of the Hubble radius during the early times, and that is the idea behind inflation. In this new scenario we see that the integral

in eq 1.42 takes most of the contribution from the lower limit and the nowadays particle horizon is greater than the Hubble radius.
Once we understand the mechanism that underlies the evolution of these two cosmological horizons we can explain how inflation manages to solve the Big Bang drawbacks.

According to our definition of inflation in terms of the Hubble radius, we discuss what a shrinking Hubble sphere implies. Indeed the condition

$$\frac{\mathrm{d}}{\mathrm{d}t}\big(aH\big)^{-1} = \frac{-\ddot{a}}{\big(aH\big)^2} = -\frac{1}{a}\left(\frac{\dot{H}}{H^2}+1\right) < 0 \qquad \Longrightarrow \qquad \epsilon \equiv -\frac{\dot{H}}{H^2} < 1 \tag{1.43}$$

tells us that inflation is a phase of accelerated expansion $\ddot{a} > 0$ of the universe: the Hubble parameter remains approximately constant, while the scale factor grows very fast. Taking into account the Friedmann equation

$$\frac{\ddot{a}}{a} = -\frac{4\pi G}{3}(\rho + 3p) \tag{1.44}$$

together with the accelerated expansion, why find a third condition for inflation expressed as the violation of the strong energy condition

$$\rho + 3p < 0 \tag{1.45}$$

A specific example of matter which satisfies this inequality is given by the cosmological constant [4], for which $p = -\rho$. In this scenario the solution to the Einstein field equation is a de Sitter universe. In particular we have the exact de Sitter solution in the limit $\epsilon \to 0$ for which the space expands exponentially

$$a(t) \propto e^{Ht} \tag{1.46}$$

while the Hubble parameter remains constant. Again, since $H \simeq$ const and the scale factor grows exponentially we see that the comoving Huble radius $\big(aH\big)^{-1}$ decreases during the inflationary process, just as we said before. However, inflation should ends with a graceful exit towards hot big bang evolution. Therefore the exact de Sitter solution fails to attempt all the necessary conditions for a successful inflation: it can be used just as a zero order approximation when you deal with realistic models.

Finally we show how inflation addresses the Big Bang problems: during inflation the Hubble parameter is almost constant and the scale factor as a function of the conformal time evolves like

$$a(\eta) = -\frac{1}{H\eta} \tag{1.47}$$

This means that the initial singularity $a = 0$ is pushed to the infinite past $\eta \to -\infty$ and if we assume an exact de Sitter solution we see that the scale factor diverges at $\eta = 0$,

which corresponds to the infinite future $t \to \infty$. Therefore we see that the inflation phase introduces additional conformal time between recombination and the singularity [7]. A graphical representation is given in fig. 1.3: as you can see the conformal time is extended to negative values and the horizon problem is solved.

Inflation manages to solves elegantly the flatness problem as well. We saw in the previous section that the Friedmann equation can be rewritten as

$$\Omega - 1 = \frac{k}{a^2 H^2} \tag{1.48}$$

Since the scale factor grows exponentially during inflation we conclude that the value $\Omega = 1$ is an attractor in this phase and this solves the flatness problem.
In order for this problem to be solved such that the present day value $\Omega_0 - 1$ approaches unity, we define the so called e-folds number as

$$\mathrm{d}N = \mathrm{d}\ln a = H\mathrm{d}t \qquad \Longrightarrow \qquad N = \ln\left(\frac{a_f}{a_i}\right) \tag{1.49}$$

where a_f, a_i denote the value of the scale factor at the end and the beginning of inflation.

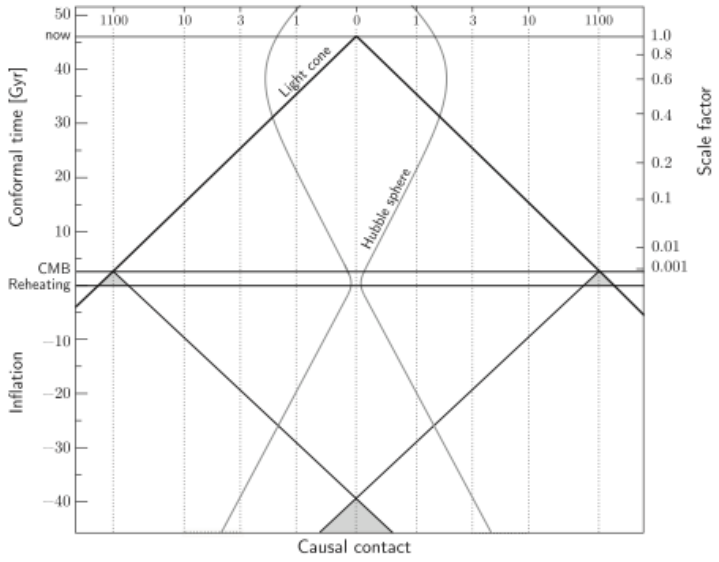

Figure 1.3: Conformal diagram for inflationary model. During the accelerated expansion the Hubble sphere decreases and then grows again during standard hot big bang [7].

In particular the necessary condition to solve flatness and horizon problem is that the largest scale observed today was smaller than the Hubble radius during inflation epoch. This condition gives us a value of about $N = 60$ e-fold for the duration of inflation.

In the picture 1.3 the value $\eta = 0$, instead of marking the singularity, represents the smooth transition from inflation to the standard cosmology. The horizon problem is evidently solved: all the points of the CMB are causally connected in the past.
Besides solving the drawbacks of standard cosmology thanks to the decreasing Hubble radius, inflation also explains the quantum-mechanical origin of cosmological perturbation, as we discuss in chapter 2.

1.6 The physics of inflation

So far we introduced the main idea behind inflation and we learned that in general relativity it is required a negative pressure in order to let the universe expand exponentially within a fraction of second. Here we present a theoretical model and the physical condition under which we can realize the required equation of state. According to [4], the natural candidate to realize inflation is a scalar field ϕ, called inflaton. Without specifying its nature, we use the scalar field as a clock to parametrize the evolution of the energy density during inflation. In figure 1.4 we give an example of inflaton potential.

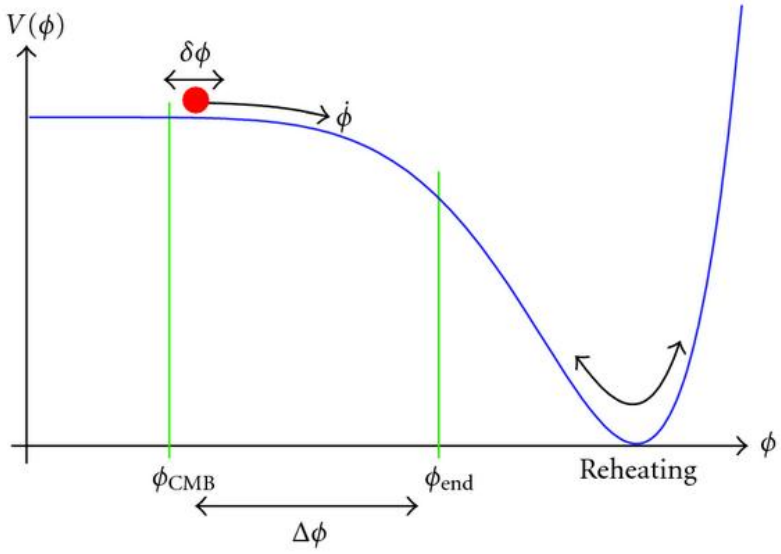

Figure 1.4: Example of potential for a single field inflation model. Courtesy of [3].

We have accelerated expansion when the potential energy $V(\phi)$ dominates over the kinetic term $\frac{1}{2}\dot{\phi}^2$. Indeed, inflation ends when the kinetic term becomes relevant if compared to the potential energy. Besides, CMB primordial perturbations are produced by

the quantum fluctuations of the inflaton at the beginning of inflation, and the energy density of the latter is transferred to radiation during the reheating process.

The inflaton field minimally coupled to gravity evolves according to the action

$$S = \int \mathrm{d}^4x\sqrt{-g}\mathcal{L} = \int \mathrm{d}^4x\sqrt{-g}\left[\frac{1}{2}R + \frac{1}{2}g^{\mu\nu}\partial_\mu\phi\partial_\nu\phi - V(\phi)\right] = S_{EH} + S_\phi \tag{1.50}$$

hence, its dynamics is governed by the sum of the Einstein-Hilbert action S_{EH} and the action of a scalar field S_ϕ with canonical kinetic term [2].
According to the Euler-Lagrange equations of motion

$$\partial^\mu \frac{\delta\left(\sqrt{-g}\mathcal{L}\right)}{\delta\partial^\mu\phi} - \frac{\delta\left(\sqrt{-g}\mathcal{L}\right)}{\delta\phi} = 0 \tag{1.51}$$

we get for the scalar field ϕ

$$\ddot{\phi} + 3H\dot{\phi} - \frac{\nabla^2\phi}{a^2} + V_{,\phi} = 0 \tag{1.52}$$

We denote with $V_{,\phi}$ the derivative of the potential with respect to the field. It is evident the presence of the friction term $3H\dot{\phi}$, which can significantly restraint the field ϕ for large values of the potential.
Starting from the action 1.50 we might compute the stress-energy tensors as

$$T_{\mu\nu} = -\frac{2}{\sqrt{-g}}\frac{\delta S}{\delta g^{\mu\nu}} = \partial_\mu\phi\partial_\nu\phi - g_{\mu\nu}\left(\frac{1}{2}\partial^\lambda\phi\partial_\lambda\phi + V(\phi)\right) \tag{1.53}$$

Assuming a FRW metric 1.1, the corresponding energy density ρ and pressure p for the inflaton perfect fluid are

$$\rho = T_{00} = \frac{\dot{\phi}^2}{2} + V(\phi) + \frac{\left(\nabla\phi\right)^2}{2a^2} \tag{1.54a}$$

$$p = \frac{T_i^i}{3} = \frac{\dot{\phi}^2}{2} - V(\phi) - \frac{\left(\nabla\phi\right)^2}{6a^2} \tag{1.54b}$$

From these two equation we see that if the gradient term were dominant, according to the equation of state $p = w\rho$ we would get

$$p = -\frac{\rho}{3} \tag{1.55}$$

which is not enough to support inflation, as we claimed in 1.45.
Therefore we restrict ourselves to the case of a homogeneous inflaton field $\phi(t, \boldsymbol{x}) \equiv \phi(t)$. In this way, the resulting equation of state is

$$w = \frac{p}{\rho} = \frac{\frac{1}{2}\dot{\phi}^2 - V}{\frac{1}{2}\dot{\phi}^2 + V} \tag{1.56}$$

Hence we showed that a scalar inflaton field can actually lead to a negative-pressure stress-energy tensor, with the consequential accelerated expansion, if the potential V dominates on the kinetic term.

1.6.1 Slow-roll regime

If we work with a homogeneous inflaton field, then eq. 1.52 becomes

$$\ddot{\phi} + 3H\dot{\phi} + V_{,\phi} = 0 \tag{1.57}$$

This equation can be recognised as the harmonic oscillator equation with a friction term $3H\dot{\phi}$. It is a known fact that a large friction term reduces the initial velocities and establishes a slow-roll regime in which the acceleration $\ddot{\phi}$ can be neglected with respect to the friction term. From the Friedman equation we know that $H^2 \propto \rho \sim V$, thus we expect the friction term to be relevant for large values of the potential V. Indeed, neglecting $\ddot{\phi}$ and assuming the approximation $\dot{\phi}^2 \ll V$, equation 1.57 simplifies to

$$3H\dot{\phi} + V_{,\phi} \approx 0 \tag{1.58}$$

while the Hubble parameter can be expressed as

$$H \equiv \frac{\mathrm{d}\ln a}{\mathrm{d}t} \approx \sqrt{\frac{8\pi G}{3}V(\phi)} \tag{1.59}$$

Taking into account 1.58 we can rewrite the Hubble parameter as

$$\frac{\mathrm{d}\ln a}{\mathrm{d}t} = \dot{\phi}\frac{\mathrm{d}\ln a}{\mathrm{d}\phi} \approx -\frac{V_{,\phi}}{3H}\frac{\mathrm{d}\ln a}{\mathrm{d}\phi} \tag{1.60}$$

Using 1.59 we get

$$-V_{,\phi}\frac{\mathrm{d}\ln a}{\mathrm{d}\phi} \approx 8\pi G V \tag{1.61}$$

Integrating this last expression, we obtain the evolution of the scale factor as a function of the inflaton

$$a(\phi) \approx a_i \exp\left(8\pi G \int_{\phi}^{\phi_i} \mathrm{d}\phi \frac{V}{V_{,\phi}}\right) \tag{1.62}$$

Finally, if we assume a power law potential $V(\phi) = \lambda\phi^n$ we get

$$a(\phi(t)) \approx a_i \exp\big(4\pi G(\phi_i^2 - \phi^2(t))\big) \tag{1.63}$$

It is evident that the accelerated expansion takes place if the inflaton decreases in time from its initial value.

Eventually, we stress out that these solution are valid only in the slow-roll approximation regime

$$\dot{\phi}^2 \ll V \qquad \ddot{\phi} \ll 3H\dot{\phi} \sim -V_{,\phi} \tag{1.64}$$

In particular, with the help of 1.58 and 1.59 they can be expressed in terms of condition on the shape potential

$$\epsilon_v(\phi) \equiv \left(\frac{V_{,\phi}}{V}\right)^2 \ll 1 \qquad \eta_v(\phi) \equiv \left|\frac{V_{,\phi\phi}}{V}\right| \ll 1 \tag{1.65}$$

The background evolution is determined by eq. 1.59, indeed

$$H^2 \approx \frac{8\pi G}{3} V \approx \text{const} \tag{1.66}$$

hence the spacetime is approximately de Sitter

$$a(t) \sim e^{Ht} \tag{1.67}$$

Inflation takes over when the slow-roll condition 1.65 are broken, *i.e* when $\epsilon_v(\phi) \approx 1$. Using these approximations we can compute the number of e-folds for inflation: denoting with ϕ_i and ϕ_f the values of the inflaton field at the beginning and at the end of inflation respectively, we have

$$N \equiv \ln \frac{a_f}{a_i} = \int_{t_i}^{t_f} H \mathrm{d}t \approx \int_{\phi_i}^{\phi_f} \frac{H}{\dot{\phi}} \mathrm{d}\phi \approx 8\pi G \int_{\phi_f}^{\phi_i} \frac{V}{V_{,\phi}} \mathrm{d}\phi \tag{1.68}$$

where we used the results 1.58 and 1.59 in the last step.
In order to solve completely the flatness and the horizon problem we require a duration of inflation of at least

$$N \equiv \ln \frac{a_f}{a_i} \geq 60 \tag{1.69}$$

The precise value for the total number of e-folds depends on the energy scale at which inflation take course and on the details of reheating after inflation [2].

We conclude this chapter spending few words on different models of inflation: even if we restrict ourselves to the single-field inflation case, there are plenty of available models and they are divided into three main categories: large-field, small-field and hybrid. It is a challenging question whether or not a model explain rigorously the physics of inflation: indeed inflation happened at extreme high energy scales and any description of this epoch requires an extrapolation of the known laws of physics. Luckily, experimental data from the CMB measurements can discriminate between inflation models [5].

Chapter 2

Quantum origin of primordial fluctuations

It is a known fact in cosmology that the LSS of the universe can be explained assuming primordial inhomogeneities, seen as seeds of the structure formation. Indeed, the temperature anisotropies observed in the CMB spectrum prove that the universe was not perfectly homogeneous at the time of recombination. Moreover, the same observations suggest us that the inhomogeneities were very small ($\sim 10^{-5}$), therefore we are allowed to treat them as linear perturbation around a homogeneous background.
In principle, before the development of the inflationary paradigm, these perturbations were postulated *ad hoc* and their power spectrum was specifically built to be in accordance with observations [4]. The drawback of this method is evident: any experimental data could be described by imposing proper initial conditions.
Besides solving the horizon and flatness problem, cosmic inflation explains in a dynamical way the origin of primordial perturbations and predicts their statistics. As we shall see later on, primordial perturbations are generated by quantum fluctuations of the inflaton scalar field[1]. These fluctuations are produced on subhorizon scales, and due to the accelerated expansion they exit the horizon once their comoving wavelength becomes greater than the Hubble radius $\left(aH\right)^{-1}$. In terms of physical coordinates, fluctuations undergo a superluminal expansion, and they are stretched to non-causal distances. When inflations ends, leaving space to the standard Hot Big Bang evolution, they eventually re-enter the horizon as classical density perturbation and then collapse to form the LSS under the effect of gravity.

[1]We are working in the context of a simple inflationary model: single-field inflation in slow-roll approximation.

2.1 Cosmological perturbations: generalities

In order to fully comprehend the important mechanism behind the generation of perturbation from quantum fluctuations, we need a background of perturbation theory and this is going to be the topic of this section.

The smallness of inhomogeneities at the time of decoupling allows us to treat perturbation linearly: indeed, the Einstein equations at first order in perturbations approximate with very high accuracy the non linear solution.
The winning strategy to treat perturbation is to divide all quantities $X(t,x)$ into the sum of to terms: a homogeneous background $\bar{X}(t)$ that depend on cosmic time only, and a perturbation $\delta X(t,x)$ term that is spatially dependent

$$X(x,t) = \bar{X}(t) + \delta X(t,x) \tag{2.1}$$

We are dealing with very small perturbations, therefore the linearised Einstein equation

$$\delta G_{\mu\nu} = 8\pi G \delta T_{\mu\nu} \tag{2.2}$$

approximates the general solution with great precision.

One of the crucial facts during the study of cosmological perturbation is that the split of equations 2.1 into background and perturbation terms is not unique because it depends on the gauge choice, *i.e* the choice of the coordinate. Let us try to explain why this is true: according to 2.1, the perturbation can be defined as the difference between the value X in the real perturbed spacetime, and the value $\bar{X}$ of the very same variable in the unperturbed spacetime. On the other hand, it is a known fact from differential geometry that if we want to properly compare tensors quantities, we need a map which allows us to identify points of the background spacetime with points of the perturbed one. This is in essence a gauge choice, and the freedom we have in changing this map is a gauge transformation. Therefore we conclude that the split of 2.1 is not unique. If we do not make attention during the gauge choice we can either remove a real perturbation or introduce a fake one. In order to resolve this ambiguity we have to take into account the complete set of perturbation [2]: we need both the metric and the matter perturbations and we can change from one to the other with a gauge transformation. Eventually, in order to avoid confusion, we will study fluctuations of gauge invariant quantities: indeed they cannot be removed, by definition, with a gauge transformation.

One of the advantages of the homogeneous and isotropic background is that it constitutes a maximally symmetric space and these symmetries allow us to decompose the matter and metric perturbations into three independent components: scalar, vector and tensor. This is called in the literature scalar-vector-tensor (SVT) decomposition, and

it turns out to be a powerfull techniques, as we shall see in a moment. We claim that a generic perturbation has helicity m if under the rotation of the coordinate system by an angle θ it is multiplied by $e^{im\theta}$. In particular, scalar vector and tensor have helicity $0, \pm 1, \pm 2$ respectively [2]. Eventually, the SVT decomposition allows us to treat each perturbation[2] independently, because each type evolves individually.
As a final general remark we claim that perturbations are more easily treated in Fourier space, and it can be shown that traslation invariance means that the different Fourier modes do not interact. These features of maximally symmetric spaces allow us to considerably simplify the study of cosmological perturbations.
After this general introduction we can explicitly define the perturbations for both metric and matter around the homogeneous FRW background.

Metric perturbations

Here we define the inflaton and metric perturbation around the FRW universe and according to 2.1 we have

$$\phi(t, \boldsymbol{x}) = \phi(t) + \delta\phi(t, \boldsymbol{x}) \qquad g_{\mu\nu}(t, \boldsymbol{x}) = \bar{g}_{\mu\nu}(t) + \delta g_{\mu\nu}(t, \boldsymbol{x}) \tag{2.3}$$

where the metric perturbations may be parametrized in terms of the line element as

$$\begin{aligned} \mathrm{d}s^2 &= g_{\mu\nu}\mathrm{d}x^\mu \mathrm{d}x^\nu \\ &= -(1+2\Phi)\mathrm{d}t^2 + 2aB_i\mathrm{d}x^i\mathrm{d}t + a^2\big[(1-2\Psi)\delta_{ij} + E_{ij}\big]\mathrm{d}x^i\mathrm{d}x^j \end{aligned} \tag{2.4}$$

Using the SVT decomposition we can rewrite the metric perturbation as follow

$$B_i \equiv \partial_i B - S_i \qquad \partial^i S_i = 0 \tag{2.5}$$

and

$$E_{ij} \equiv 2\partial_i\partial_j E + 2(\partial_i F_j + \partial_j F_i) + h_{ij} \qquad \partial^i F_i = 0, \quad h^i_i = \partial^i h_{ij} = 0 \tag{2.6}$$

We note the presence of two vector perturbation S_i and F_i. It can be shown [3] that vector perturbations of the metric always decay in time, hence they do not play a fundamental role in standard cosmology and from now on we neglect them. We will focus mainly on scalar and tensor perturbations, which can be related to experimental observable quantity in the late universe: density fluctuations and gravitational waves respectively.
The main difference between scalar and tensor perturbations is that the latter are gauge-invariant, while the former change under a change of the coordinate system, hence they

[2] At the linear level

are not gauge invariant.
Indeed, if we take into account the gauge transformation

$$t \to t + \alpha \tag{2.7a}$$

$$x^i \to x^i + \delta^{ij}\beta_j \tag{2.7b}$$

using the invariance of the spacetime interval, we see that the scalar metric perturbations change as

$$\Phi \to \Phi - \dot{\alpha} \tag{2.8a}$$

$$B \to B + a^{-1}\alpha - a\dot{\beta} \tag{2.8b}$$

$$E \to E - \beta \tag{2.8c}$$

$$\Psi \to \psi + H\alpha \tag{2.8d}$$

Matter perturbations

In this paragraph we define the stress-energy perturbation $\delta T_{\mu\nu}$.
The latter is related with the metric perturbations by the Einstein equations and after inflation, the perturbed terms of the stress-energy tensor are [3]

$$\delta T^0_0 = \delta\rho \tag{2.9a}$$

$$\delta T^0_i = -(\rho + p)v_i \tag{2.9b}$$

$$\delta T^i_j = -\delta^i_j \delta p \tag{2.9c}$$

where v_i represents the perturbation of the velocity field. Being scalar quantity, under a gauge transformation they change as

$$\delta\rho \to \delta\rho - \dot{\bar{\rho}}\alpha \tag{2.10a}$$

$$\delta p \to \delta p - \dot{\bar{p}}\alpha \tag{2.10b}$$

We stress out that we are dealing with a perfect fluid, and in most cases this approximation is enough for our purpose. If the matter cannot be represented by a perfect fluid, then the perturbation δT^i_j contains an extra term Σ^i_j, called the anisotropic stress.

2.1.1 Gauge invariant quantities

As we mentioned above, the split of equation 2.1 is not unique, but depends on the gauge choice. If we do not proceed carefully, the gauge choice can either introduce fake perturbations or remove real ones. In particular, we said that tensor perturbations are gauge invariant, but this is not true for scalar perturbations. To avoid confusion, it is convenient to introduce gauge invariant variables for the scalar sector.
An important scalar quantity which is invariant under the gauge transformation is the curvature perturbation ζ, defined as [9]

$$-\zeta \equiv \Psi + \frac{H}{\dot{\bar{\rho}}}\delta\rho \tag{2.11}$$

This quantity gives us a measure of the spatial curvature of constant density hypersurfaces [2] and besides being a gauge invariant variable it has the important property of being constant outside the horizon[3].

There is another relevant gauge invariant quantity, which geometrically measures the spatial curvature of comoving hypersurfaces. It is called comoving curvature perturbation and it is defined by

$$\mathcal{R} \equiv \Psi - \frac{H}{\dot{\bar{\phi}}}\delta\phi \tag{2.12}$$

These two quantities can be related via the Einstein equations and it turns out that they satisfy

$$-\zeta = \mathcal{R} + \frac{k^2}{(aH)^2}\frac{2\bar{\rho}}{3(\bar{\rho}+\bar{p})}\Psi_B \tag{2.13}$$

with

$$\Psi_B \equiv \psi + a^2 H(\dot{E} - B/a) \tag{2.14}$$

is the Bardeen potential [9]. From this relation we conclude that on superhorizon scale, *i.e.* for $k \ll aH$, ζ and $\mathcal{R}$ are equal. Therefore their correlation function is the same at horizon crossing and they are constant on superhorizon scales. Using the linear gauge perturbations discussed before, it can be shown that both $\mathcal{R}$ and ζ are truly gauge invariant variables.

Statistical approach

So far we described a precise picture of cosmological perturbations and finally we need to compare them with experimental data. This can be achieved using a statistical approach:

[3]This holds true for adiabatic matter perturbation [2].

even if we have just one universe, thanks to the ergodic hypothesis we can substitute the average over different realizations with the average over sufficiently large volumes, which can be considered as statistically independent. Eventually, the connection between theoretical computations and experimental results relies on the so called Power Spectrum $P(k)$. It is a statistical average of a certain signal as analysed in terms of its scale (or frequency) content. From a mathematical point of view it is defined as the Fourier coefficient of the Fourier transform of the two point correlation function. Therefore, taking into account the comoving curvature perturbation $\mathcal{R}$, we write its two point correlation function as

$$\langle \mathcal{R}(x)\mathcal{R}(y)\rangle = \int \frac{\mathrm{d}^3k}{(2\pi)^3}\frac{\mathrm{d}^3k'}{(2\pi)^3}\langle \mathcal{R}_k\mathcal{R}_{k'}\rangle e^{i\boldsymbol{k}\cdot\boldsymbol{x}}e^{i\boldsymbol{k'}\cdot\boldsymbol{y}} \tag{2.15}$$

where we denote with $\langle\ldots\rangle$ the ensemble average of the fluctuations.
Finally, the power spectrum $P_{\mathcal{R}}(k)$ is defined as

$$\langle \mathcal{R}_k\mathcal{R}_{k'}\rangle = (2\pi)^3\delta(\boldsymbol{k}+\boldsymbol{k'})P_{\mathcal{R}}(k) \tag{2.16}$$

We will use the dimensionless power spectrum, defined as

$$\Delta^2_{\mathcal{R}} = \frac{k^3}{2\pi^2}P_{\mathcal{R}}(k) \tag{2.17}$$

If the variable under exam is gaussian then its power spectrum contains all the statistical information. It can be shown that in single field inflation model the primordial non gaussianity in negligible [10]. Therefore all the statistical information are encoded in the power spectrum of $\mathcal{R}$ and we do not need to take into account higher order correlation functions[4].
It is possible to define, in the very same way, the power spectrum for each of the two polarizations of the tensor mode h_{ij}

$$\langle h_k h_{k'}\rangle = (2\pi)^3\delta(\boldsymbol{k}+\boldsymbol{k'})P_h(k), \qquad \Delta^2_h = \frac{k^3}{2\pi^2}P_h(k) \tag{2.18}$$

The total power spectrum of tensor modes is then defined as the sum of the power spectrum of the two polarization

$$\Delta^2_T \equiv 2\Delta^2_h \tag{2.19}$$

In the next sections we will compute both $\Delta^2_{\mathcal{R}}$ and Δ^2_T starting from quantum fluctuations.

[4]Indeed, higher order correlation functions describe the non gaussianity of the field.

2.2 Harmonic oscillator

As a pedagogical tool, we will start with a review of the quantum mechanical treatment of the Harmonic Oscillator (HO). Indeed, it constitutes a simple example, but still contains most of the important physical consideration.
The Fourier analysis tells us that the majority of complex physical systems can be expanded as a collection of HOs with different frequencies and amplitude [2]. Being one of the few physical system which can be solved analytically, the HO turns out to be extremely important. In particular, we will see that a free quantum field in a curved background can be thought of as a set of HOs with time dependent frequencies.

In classical mechanics, a time dependent frequency HO is described by the action

$$S = \frac{1}{2}\int \mathrm{d}t\big(\dot{x}^2 - m^2\omega^2(t)x^2\big) \tag{2.20}$$

where we denote with x the deviation from the equilibrium state of a particle. From now on we will set for simplicity $m = 1$.
The equation of motion can be easily obtained from the variation of the action

$$\frac{\delta S}{\delta x} = 0 \quad \Longrightarrow \quad \ddot{x} + \omega^2(t) = 0 \tag{2.21}$$

Quantization

Adopting the canonical quantization paradigm, we proceed in the standard way defining the conjugate momentum

$$p \equiv \frac{\delta L}{\delta \dot{x}} = \dot{x} \tag{2.22}$$

and then we impose the canonical commutator at equal time

$$[\hat{x}, \hat{p}] = i\hbar \tag{2.23}$$

where the classical variables x, p have been promoted to quantum operators $\hat{x}, \hat{p}$.
We are working in the Heisenberg picture, where states are time independent while operators evolve in time. Hence, the position operator $\hat{x}$ might be expanded as

$$\hat{x} = v(t)\hat{a} + v(t)^*\hat{a}^\dagger \tag{2.24}$$

where we introduced the creation and annihilations operators.
For consistency, the complex mode function $v(t)$ satisfies the equation of motion 2.21

$$\ddot{v} + \omega^2(t)v = 0 \tag{2.25}$$

The canonical commutator of equation 2.23 becomes

$$\langle v, v\rangle \left[\hat{a}, \hat{a}^\dagger\right] = 1 \tag{2.26}$$

where we introduced the scalar product

$$\langle v, w\rangle \equiv \frac{i}{\hbar}\left(v^* \partial_t w - w \partial_t v^*\right) \tag{2.27}$$

If we assume that the solution v is such that the scalar product is positively defined, we can rescale the function itself in order to properly normalize the scalar product

$$\langle v, v\rangle = 1 \quad \Longrightarrow \quad \left[\hat{a}, \hat{a}^\dagger\right] = 1 \tag{2.28}$$

In particular according to 2.27 , the creation and annihilations operator are identified by the relations

$$\hat{a} = \langle v, \hat{x}\rangle \tag{2.29a}$$

$$\hat{a}^\dagger = -\langle v^*, \hat{x}\rangle \tag{2.29b}$$

Finally, we can proceed with the construction of the Fock space: the vacuum state is defined as

$$\hat{a}\,|0\rangle = 0 \tag{2.30}$$

while excited states are defined in terms of the action of $\hat{a}^\dagger$ on the vacuum state, *i.e*

$$|n\rangle \equiv \frac{1}{\sqrt{n}}(\hat{a}^\dagger)^n\,|0\rangle \tag{2.31}$$

It easy to show that a state like that is an eigenstate of the number operator $\hat{N} = \hat{a}^\dagger\hat{a}$, indeed

$$\hat{N}\,|n\rangle = n\,|n\rangle \tag{2.32}$$

The careful reader probably noticed that we have not determined uniquely the mode functions $v(t)$. Since the definition of annihilation operator is based upon the mode functions, we conclude that every change in $v(t)$ that leaves invariant the solution $x(t)$ determine a change in the definition of the vacuum state. In particular, it turns out that for HOs with time dependent frequency $\omega(t)$ there is no unique choice of the vacuum state, because the decomposition of $\hat{x}$ in eq. 2.24 is not unique. As we see later on, this is what happens when we deal with curved spacetime.

On the other hand, if the frequency is time independent there exists a preferred choice of the vacuum state $|0\rangle$ as the ground energy state of the Hamiltonian.

Indeed, if we evaluate the Hamiltonian operator for a generic mode function $v(t)$ taking into account eq. 2.24, we get

$$\begin{aligned}\hat{H} &= \frac{1}{2}\hat{p}^2 + \frac{1}{2}\omega^2\hat{x}^2 \\ &= \frac{1}{2}\left[(\dot{v}^2 + \omega^2 v^2)\hat{a}\hat{a} + (\dot{v}^2 + \omega^2 v^2)\hat{a}^\dagger\hat{a}^\dagger + (\left|\dot{v}^2\right| + \omega^2\left|v^2\right|)(\hat{a}\hat{a}^\dagger + \hat{a}^\dagger\hat{a})\right]\end{aligned} \tag{2.33}$$

It is now easy to compute the action of the Hamiltonian operator on the ground state $|0\rangle$. Indeed, recalling $\left[\hat{a}, \hat{a}^\dagger\right] = 1$ and $\hat{a}\,|0\rangle = 0$ we obtain

$$\hat{H}\,|0\rangle = \frac{1}{2}(\dot{v}^2 + \omega^2 v^2)\hat{a}^\dagger\hat{a}^\dagger\,|0\rangle + (\left|\dot{v}^2\right| + \omega^2\left|v^2\right|)\,|0\rangle \tag{2.34}$$

Therefore, if we require the vacuum to be an eigenstate of $\hat{H}$ the first term must be zero, and this implies

$$\dot{v} = \pm i\omega v \tag{2.35}$$

Recalling the definition of the scalar product 2.27, we see

$$\langle v, v\rangle = \mp\frac{2\omega}{\hbar}|v|^2 \tag{2.36}$$

If we assume the scalar product to be positively defined and properly normalize, we chose the minus sign equation from 2.35

$$\dot{v} = -i\omega v \tag{2.37}$$

and its solution is simply

$$v(t) = \sqrt{\frac{\hbar}{2\omega}}e^{-i\omega t} \tag{2.38}$$

With this choice of the mode function, the vacuum state is uniquely defined as the ground state of the Hamiltonian. The latter can be written as

$$\hat{H} = \hbar\omega\left(\hat{N} + \frac{1}{2}\right) \tag{2.39}$$

for which

$$\hat{H}\,|0\rangle = \frac{\hbar\omega}{2} \tag{2.40}$$

Fluctuations around the ground state

Finally, we consider the expectation value of $|\hat{x}|^2$ around the ground state, which is

$$\begin{aligned}\langle 0|\,|\hat{x}|^2\,|0\rangle = \langle 0|\,\hat{x}^\dagger\hat{x}\,|0\rangle &= \langle 0|\,(v^*\hat{a}^\dagger + v\hat{a})(v\hat{a} + v^*\hat{a}^\dagger)\,|0\rangle \\ &= |v(\omega,t)|^2\,\langle 0|\,\left[\hat{a}, \hat{a}^\dagger\right]\,|0\rangle = |v(\omega,t)|^2\end{aligned} \tag{2.41}$$

Therefore we see that the ground state fluctuations of the position around the vacuum are completely characterized by the square of the mode function

$$\langle 0| \, |\hat{x}|^2 \, |0\rangle = |v(\omega, t)|^2 = \frac{\hbar}{2\omega} \tag{2.42}$$

We reviewed so far all the necessary background to compute the power spectrum of primordial fluctuations, which is going to be the topic of the next section.

2.3 Primordial perturbations from quantum fluctuations

In this section we finally study the quantum fluctuations of the inflaton: we will see that this approach provides a dynamical way to generate primordial perturbations that led to the LSS of the universe.
In particular, cosmologically relevant fluctuations are created quantum mechanically inside the Hubble horizon

$$k \gg aH \tag{2.43}$$

The comoving scales k^{-1} remain constant during inflation, while the Hubble radius $\left(aH\right)^{-1}$ shrinks as we explained in the previous sections. Eventually, fluctuations exit the horizon and undergo to the so called super horizon regime, hence

$$k \ll aH \tag{2.44}$$

This is better explained in figure 2.1: in standard inflation the amplitude of the perturbations is not affected by causal physics on super horizon scales. Therefore, fluctuations freeze out until they re-enter the horizon. When inflation ends and the standard Hot Big Bang begins, the comoving Hubble horizon grows in time and all fluctuations re-enter the horizon. After these general remarks we can proceed with the detail computation of quantum fluctuations and their power spectrum, keeping in mind the HO results.

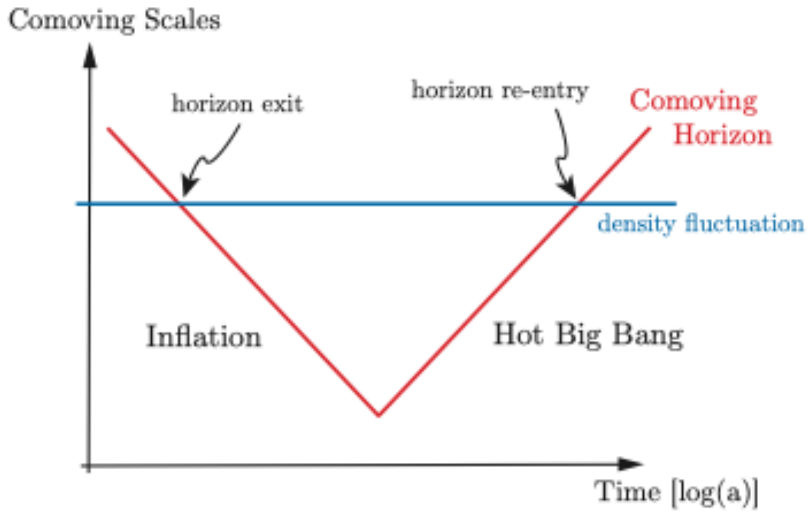

Figure 2.1: Dynamics of perturbations in the inflationary universe [2].

2.3.1 Scalar perturbations

The starting point for the computation of scalar fluctuations is the action describing the dynamics of a single field slow-roll inflation model. We are interested in linear equation of the perturbations, hence the action must be expanded to second order in fluctuations. From the latter we derive the equation of motion for the comoving curvature perturbation $\mathcal{R}$ in the standard HO form. Then we will solve the equation considering different approximation regimes.
The action for the single field, in units where $8\pi G = 1$ is given by

$$S = \frac{1}{2}\int \mathrm{d}^4x\sqrt{-g}\big[R - g^{\mu\nu}\partial_\mu\phi\partial_\nu\phi - 2V(\phi)\big] \tag{2.45}$$

Before expanding the action, we need to fix the gauge in order to avoid time and spatial reparametrisation. In particular, following the approach developed by Maldacena [10], we leave the inflaton field unperturbed while all the scalar degrees of freedom are contained in the metric fluctuation $\mathcal{R}$. Hence, we impose

$$\delta\phi = 0, \qquad g_{ij} = a^2\big[(1-2\mathcal{R})\delta_{ij} + h_{ij}\big], \qquad \partial h_{ij} = h^i_i = 0 \tag{2.46}$$

After the gauge fixing we can finally expand the action 2.45 to the second order in $\mathcal{R}$. What we get is

$$S_{(2)} = \frac{1}{2}\int \mathrm{d}^4x a^3 \frac{\dot\phi^2}{H^2}\big[\dot{\mathcal{R}}^2 - a^2\big(\partial_i\mathcal{R}\big)^2\big] \tag{2.47}$$

The latter can be simplified if we change to conformal time η and we introduce the new quantity

$$v \equiv z\mathcal{R}, \qquad z^2 \equiv a^2 \frac{\dot{\phi}^2}{H^2} \tag{2.48}$$

where v is known as the Mukhanov variable. Then, the action, after integration by parts, takes the form

$$S_{(2)} = \frac{1}{2}\int \mathrm{d}\eta \mathrm{d}^3x \left[(v')^2 - (\partial_i v)^2 + \frac{z''}{z}v^2\right] \tag{2.49}$$

where with $'$ we denote, as usually, the derivative with respect to the conformal time η. It is now convenient to move into Fourier space. Thus we define the expansion for the field v as

$$v(\eta, \boldsymbol{x}) = \int \frac{\mathrm{d}^3k}{(2\pi)^3} v_k(\eta) e^{i\boldsymbol{k}\cdot\boldsymbol{x}} \tag{2.50}$$

Substituting this expansion in equation 2.49 and computing the equation of motion, we end up with the so called Mukhanov equation

$$v_k'' + \left(k^2 - \frac{z''}{z}\right)v_k = 0 \tag{2.51}$$

Since the function z is strictly related to the background dynamics, the Mukhanov equation is very hard to solve. Thus we will consider a series of approximation, like the pure de Sitter limit and the slow-roll regime, in order to solve it analytically.

Quantization

In complete analogy with the harmonic oscillator we proceed with the quantization of the field v. This can be achieved promoting the field itself and its conjugate momentum v' to quantum operator, hence

$$\hat{v} = \int \frac{\mathrm{d}^3k}{(2\pi)^3}\left[v_k(\eta)\hat{a}_k e^{i\boldsymbol{k}\cdot\boldsymbol{x}} + v_k^*(\eta)\hat{a}_k^\dagger e^{-i\boldsymbol{k}\cdot\boldsymbol{x}}\right] \tag{2.52}$$

Equivalently we can promote to quantum operators the Fourier modes, using the decomposition

$$\hat{v}_k = v_k(\eta)\hat{a}_k + v_{-k}^*(\eta)\hat{a}_{-k}^\dagger \tag{2.53}$$

If we normalize the mode function as

$$\langle v_k, v_k\rangle \equiv \frac{i}{\hbar}\left(v_k^* v_k' - v_k^{*'} v_k\right) = 1 \tag{2.54}$$

then the creation and annihilation operators satisfy the canonical commutation relation

$$\left[\hat{a}_k, \hat{a}^\dagger_{k'}\right] = (2\pi)^3 \delta(\boldsymbol{k} - \boldsymbol{k}') \tag{2.55}$$

We stress out that equation 2.54 is one of the boundary condition for the Mukhanov equation 2.51. The second one is determined once we chose a proper vacuum state.

Bunch-Davies vacuum

The standard choice of vacuum state for fluctuations is the Minkowski ground state of a comoving observer in the past, $\eta \to -\infty$ or equivalently $k \gg aH$, [2]. Under this approximation, the Mukhanov equation 2.51 simplifies to

$$v_k'' + k^2 v_k = 0 \tag{2.56}$$

The analogy with the modes equation of a standard harmonic oscillator with time independent frequency is evident. We already showed that there exists a unique solution to this equation if we require the vacuum state to be the minimum energy state of the Hamiltonian. Thus we impose, together with 2.54, the second boundary condition

$$\lim_{\eta \to -\infty} v_k = \frac{e^{-ik\eta}}{\sqrt{2k}} \tag{2.57}$$

where we set $\hbar = 1$. The two boundary conditions completely set the mode functions on all scales [2].

De Sitter limit

In the previous chapter we defined inflation as a period of shrinking Hubble radius:

$$\frac{\mathrm{d}}{\mathrm{d}t}\big(aH\big)^{-1} = -\frac{1}{a}(1-\epsilon), \qquad \epsilon \equiv -\frac{\dot{H}}{H^2} < 1 \tag{2.58}$$

If we assume a pure de Sitter phase, *i.e* $\epsilon \to 0$ then the scale factor is related to the conformal time by the relation

$$a(\eta) = -\frac{1}{H\eta} \tag{2.59}$$

where η takes negative values[5] Thus if we consider the de Sitter limit

$$\frac{z''}{z} = \frac{a''}{a} = \frac{2}{\eta^2} \tag{2.60}$$

[5]Recall that $\eta \in (-\infty, \infty)$.

and the Mukhanov equation 2.51 becomes

$$v_k'' + \left(k^2 - \frac{2}{\eta^2}\right) v_k = 0 \tag{2.61}$$

By direct substitution it is easy to verify that an exact solution of this equation is

$$v_k = \alpha \frac{e^{-ik\eta}}{\sqrt{2k}} \left(1 - \frac{i}{k\eta}\right) + \beta \frac{e^{ik\eta}}{\sqrt{2k}} \left(1 + \frac{i}{k\eta}\right) \tag{2.62}$$

where α and β are two free parameters and they represent the non uniqueness of the mode functions [2]. This solution can be uniquely fixed if we impose the boundary conditions 2.54 and 2.57, together with the subhorizon limit $|k\eta| \gg 1$. Indeed, in this case we fix $\alpha = 1$ and $\beta = 0$ and this lead us to a unique definition of the so called Bunch-Davies mode function

$$v_k = \frac{e^{-ik\eta}}{\sqrt{2k}} \left(1 - \frac{i}{k\eta}\right) \tag{2.63}$$

Zero-point fluctuations and power spectrum

We already computed the expectation value of $|\hat{x}|^2$ for the standard harmonic oscillator and we found

$$\langle 0| \, |\hat{x}|^2 \, |0\rangle = |v(\omega, t)|^2 = \frac{1}{2\omega} \tag{2.64}$$

Here we proceed with the very same computation for the field $\mathcal{R}$. Recalling the definition of the Mukhanov variable

$$v \equiv z\mathcal{R}, \qquad z^2 \equiv a^2 \frac{\dot{\phi}^2}{H^2} \tag{2.65}$$

and the definition of the power spectrum as the Fourier mode of the two point correlation function, we have

$$\begin{aligned} \langle \mathcal{R}_k, \mathcal{R}_{k'} \rangle &= \frac{H^2}{a^2\dot{\phi}^2} \langle v_k, v_{k'} \rangle = (2\pi)^3 \frac{H^2}{a^2\dot{\phi}^2} \delta(\boldsymbol{k} + \boldsymbol{k'}) |v_k(\eta)|^2 \\ &= (2\pi)^3 \frac{H^2}{a^2\dot{\phi}^2} \delta(\boldsymbol{k} + \boldsymbol{k'}) \frac{1}{2k^3\eta^2} (1 + k^2\eta^2) \\ &= (2\pi)^3 \delta(\boldsymbol{k} + \boldsymbol{k'}) \frac{H^2}{\dot{\phi}^2} \frac{H^2}{2k^3} (1 + k^2\eta^2) \end{aligned} \tag{2.66}$$

where we used the result 2.63 and we took in mind that for a de Sitter background

$$a(\eta) = -\frac{1}{H\eta} \tag{2.67}$$

On superhorizon scales $|k\eta| \ll 1$ we see that the power spectrum approaches to a constant

$$\langle \mathcal{R}_k, \mathcal{R}_{k'} \rangle = (2\pi)^3 \delta(\boldsymbol{k} + \boldsymbol{k'}) \frac{H^2}{\dot{\phi}^2} \frac{H^2}{2k^3} \tag{2.68}$$

This property reflects the fact that $\mathcal{R}$ is constant on superhorizon scales, as we explained in 2.1.1. Finally we can compute the power spectrum at horizon crossing, *i.e* at $a(\eta_\times)H(\eta_\times) = k$. This is given by

$$\langle \mathcal{R}_k, \mathcal{R}_{k'} \rangle = (2\pi)^3 \delta(\boldsymbol{k} + \boldsymbol{k'}) \frac{H_\times^2}{\dot{\phi}_\times^2} \frac{H_\times^2}{2k^3} \tag{2.69}$$

The power spectrum at horizon crossing determines the future power spectrum until a given fluctuation re-enters the horizon, since $\mathcal{R}$ is constant on superhorizon scales.
Eventually, the dimensionless power spectrum is defined as

$$\Delta^2_{\mathcal{R}}(k) \equiv \frac{k^3}{2\pi^2} P_{\mathcal{R}}(k) = \frac{H_\times^2}{(2\pi)^2} \frac{H_\times^2}{\dot{\phi}_\times^2} \tag{2.70}$$

This result is explicitly extended to quasi de Sitter background because we computed it at a specific instant: the horizon crossing. Indeed, different scales exit the horizon at slightly different times and $H_\times$ has different values due to its slow time-evolution.

2.3.2 Tensor perturbations

We already discuss the quantization of primordial fluctuations for the scalar sector, and here we move on to the tensor sector, where a similar approach might be applied.
It is clear from equations 2.9 that the stress energy tensor does not have spin two components, therefore tensor modes are purely gravitational and they do not have sources [3]. After this remarks what we need is the action for the gravitational waves and this may be derived if we expand the Einstein action up to the second order in the metric perturbation h_{ij}. Here h_{ij}, already encountered in eq. 2.46, is the spin two transverse traceless perturbation. Its dynamics is governed by the action

$$S = \frac{1}{64\pi G} \int \mathrm{d}\eta \mathrm{d}^3x a^2 \left[(h'_{ij})^2 - (\partial_l h_{ij})^2 \right] \tag{2.71}$$

We recognise the analogy with the action of a massless scalar field, up to the over all factor. We might define the Fourier decomposition of the tensor mode

$$h_{ij} = \sum_{s=+,\times} \int \frac{\mathrm{d}^3k}{(2\pi)^3} \epsilon^s_{ij}(k) h^s_k e^{i\boldsymbol{k}\cdot\boldsymbol{x}} \tag{2.72}$$

where $\epsilon^s_{ij}(k)\epsilon^{s'}_{ij}(k) = 2\delta_{ss'}$ and $\epsilon_{ii} = k^i\epsilon_{ij} = 0$. Substituting the decomposition in the tensor action, we get

$$S = \sum_s \frac{1}{32\pi G}\int \mathrm{d}\eta \mathrm{d}^3k a^2\left[(h^{s\prime}_k)^2 - k^2(h^s_k)^2\right] \tag{2.73}$$

If we introduced the canonical normalised field

$$v^s_k = \frac{a}{\sqrt{32\pi G}}h^s_k \tag{2.74}$$

we get

$$S = \sum_s \frac{1}{2}\int \mathrm{d}\eta \mathrm{d}^3k\left[(v^{s\prime}_k)^2 - \left(k^2 - \frac{a''}{a}\right)(v^s_k)^2\right] \tag{2.75}$$

we recognize it as two copies of the action for scalar perturbation of eq. 2.49.
Indeed each polarization satisfies the equation

$$(v^s_k)'' + \left(k^2 - \frac{a''}{a}\right)v_k = 0 \tag{2.76}$$

The latter might be expressed in terms of the physical fluctuation h^s_k into the form

$$(h^s_k)'' + 2\frac{a'}{a}(h^s_k)' + k^2h^s_k = 0 \tag{2.77}$$

which is going to be useful in chapter 3.

Quantization and power spectrum

We just showed that each polarization of the tensor mode behaves as a massless scalar field in the de Sitter space

$$h^s_k = \frac{\sqrt{32\pi G}}{a}v^s_k \tag{2.78}$$

Since we already computed the power spectrum for the scalar sector, we can simply write down

$$\begin{aligned}\langle \hat{h}^s_k(\eta)\hat{h}^s_{k'}(\eta)\rangle &= (2\pi)^3\delta(\boldsymbol{k}+\boldsymbol{k'})\frac{32\pi G}{a^2}\langle v^s_k(\eta)v^s_{k'}(\eta)\rangle \\ &= (2\pi)^3\delta(\boldsymbol{k}+\boldsymbol{k'})\frac{32\pi G}{a^2}\frac{1}{2\eta^2k^3}(1+\eta^2k^2) \\ &= (2\pi)^3\delta(\boldsymbol{k}+\boldsymbol{k'})32\pi G\frac{H^2}{2k^3}(1+\eta^2k^2)\end{aligned} \tag{2.79}$$

where we used the results from the previous section together with the expression of the scale factor for a de Sitter background,

$$a(\eta) = -\frac{1}{H\eta} \tag{2.80}$$

In the superhorizon limit, $|k\eta| \ll 1$, we end up with

$$\langle \hat{h}^s_k(\eta)\hat{h}^s_{k'}(\eta)\rangle = (2\pi)^3\delta(\boldsymbol{k}+\boldsymbol{k'})32\pi G\frac{H^2}{2k^3} \tag{2.81}$$

Finally, we can write down the dimensionless power spectrum for a single polarization mode, evaluated at horizon exit

$$\Delta^2_h = \frac{H^2_\times}{\pi^2 M^2_{pl}} \tag{2.82}$$

where we introduced the Planck mass $M^2_{pl} = 1/8\pi G$.
Thus the dimensionless power spectrum for tensor fluctuations, taking into account both the polarizations, is simply

$$\Delta^2_T = 2\Delta^2_h = \frac{2H^2_\times}{\pi^2 M^2_{pl}} \tag{2.83}$$

This last expression gives us the result for the power spectrum of the tensor fluctuation produced by inflation, evaluated at horizon crossing.

Chapter 3

From Inflation to late-time observables

The aim of this chapter is to discuss how the predictions of inflation on the primordial tensor perturbations can be transferred at late time as a contribution to the GW energy density. Firstly, we proceed with the study of cosmological perturbation, starting with the equations of the linear theory previously derived to analyse the evolution of tensor perturbations in the framework of the hot big bang theory. In particular, we connect primordial fluctuations with late-time observable, introducing the notion of gravitational wave energy density. The reason why we are so interested in studying tensor perturbations in details relies on the possible detection of the theoretically predicted stochastic gravitational wave background via direct detections with future spaced-based interferometers and Pulsar Timing Array (PTA) experiments.
Then we presents a new mechanism developed by [16] to amplify the primordial spectrum of the tensor sector in single field inflation scenario. Requiring a transitory non-attractor phase, tensor fluctuations might be enhanced by several orders on superhorizon scales.
Moreover, we compute the duration of the non-attractor phase to ensure that the energy density crosses the sensitivity curves of LISA, aLIGO and PTA detectors.
We then review the main noise sources of these interferometers, providing good analytical fits for their sensitivity curves. Finally, we plot in the same graph the amplified energy density together with the detectors sensitivity curves.

3.1 Tensor perturbations as relic gravitational waves

We are assuming homogeneity and isotropy on large scales and this leads us to the FRW metric which reads, using conformal time, as

$$\mathrm{d}s^2 = a^2(\eta)\big(-\mathrm{d}\eta^2 + \mathrm{d}\vec{x}^2\big) \tag{3.1}$$

where we assumed a flat background. Let us recall that tensor perturbations are described by the transverse traceless tensor h_{ij}. The latter can be decomposed in momentum representation in the basis of helicity-2 tensors in the very same way we discussed in chapter 2:

$$h_{ij} = \sum_{s=+,\times} \int \frac{\mathrm{d}^3k}{(2\pi)^3} \epsilon^s_{ij}(k) h^s_k e^{i\boldsymbol{k}\cdot\boldsymbol{x}} \tag{3.2}$$

where we denote with the index s the two possible polarizations. Moreover, we know that each polarization obeys the equation 2.77, *i.e.*

$$(h^s_k)'' + 2\frac{a'}{a}(h^s_k)' + k^2 h^s_k = 0 \tag{3.3}$$

describing the propagation of gravitational waves at the speed of light. For simplicity from now on we neglected the polarization index, taking into account the single polarization mode.

Evolution Regimes

Before exploring deep down the solutions of this equation we first need to step back for a while and analyse the different regimes of evolution. Indeed the solutions strongly depend on the relation between the Hubble parameter H and the physical momentum $q = \frac{k}{a}$. In particular it is possible to distinguish two different regimes, called respectively *Subhorizon* and *Superhorizon* regimes. The former occurs when the physical wavelength is small compared to the comoving Hubble radius $(aH)^{-1}$, hence when it is satisfied the following inequality

$$k \gg a(\eta)H(\eta) \tag{3.4}$$

On the other hand during superhorizon regime the opposite inequality holds and this means that the Hubble size is smaller than the physical wavelength

$$k \ll a(\eta)H(\eta) \tag{3.5}$$

According to inflation the combination $(aH)^{-1}$ decreases in time, hence the physical momentum $q(t) = k/a(t)$ necessarily decreases faster than $H(t)$ as shown in figure 3.1.

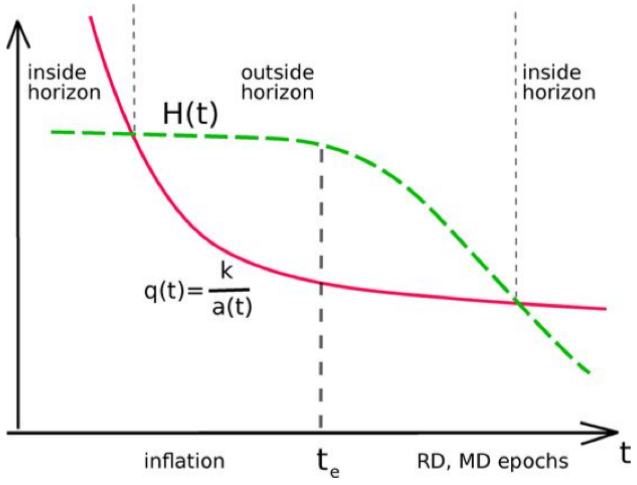

Figure 3.1: Given a conformal momentum k the figure describes the dependence of the physical momentum and Hubble parameter at inflation epoch and later on [3].

This property of inflation is related to the solution of the horizon and flatness problem of the hot big bang theory. Hence we conclude that during inflation a mode is first subhorizon, and then superhorizon, with the situation being inverted at radiation or matter domination: fluctuations are created on all length scale, and the cosmologically relevant ones start their lives inside the horizon. However while the comoving wavenumber k is constant, the Hubble size shrinks during inflation, so eventually all fluctuations exit the horizon. After inflation the Hubble radius grows again and fluctuations re-enter the horizon. The larger the physical wavelength, the later the perturbations re-enters the horizon. In particular, scales of cosmological interest came back within the Hubble size at relatively recent times.
In the next section we solve the eq 3.3 at superhorizon and subhorizon regimes respectively and then we match the solutions at horizon crossing $k = a(\eta)H(\eta)$

3.1.1 Superhorizon regime

We begin considering the superhorizon regime, hence $k \ll \frac{a'}{a}$ (or equivalently $|k\eta| \ll 1$). This allow us to neglect the last term in 3.3 and we are left with

$$h'' + 2\frac{a'}{a} = 0 \tag{3.6}$$

The general solution of this equation is given by the sum of two different terms

$$h(\eta) = h_i + \mathcal{C} \cdot \int \frac{\mathrm{d}\eta}{a^2(\eta)} \tag{3.7}$$

where h_i and $\mathcal{C}$ are two integration constant. We notice that one of the solutions is a constant mode[1] whether the other one is a decaying mode, and we always assume the latter to be negligible at horizon re-entry. This assumption is not hard to understand but deserves a better explanation: if the decaying mode was large enough not to be negligible at horizon re-entry, it was even larger at early times, but this is in contrast with the viewpoint of an homogeneous and isotropic universe at early stages. On the other hand if this mode was not substantially large at early times, it soon became negligibly small. Therefore we are led to the conclusion that decaying modes are always negligible[2]. Of course this reasoning holds true if we assume slow-roll inflation during which the scale factor grows with time, but it breaks down if we consider a non-attractor regime: in this case, the second term of 3.7 becomes a growing mode, and this is going to be the topic of the next section.

To summarize, we focus on the modes that "freeze-out" outside the horizon and their value at horizon exit determines the future power spectrum until the wavelength of a given fluctuation becomes smaller than the Hubble size and the subhorizon regime sets in.

3.1.2 Subhorizon regime

We now move on to subhorizon perturbations and we consider $k \gg a'/a$. To fully solve eq 3.3 we make use of a trick that allow us to get rid of the first derivative. The basic idea is to introduce the unknown function $f(\eta) = a(\eta)h(\eta)$ and rewrite the equation as

$$f'' + \left(k^2 - \frac{a''}{a}\right) f = 0 \tag{3.8}$$

Since $|k\eta| \gg 1$ and in quasi-de Sitter space $a \propto \eta^{-1}$ we can neglect the last term and we are left with the equation of the harmonic oscillator, whose general solution is given by

$$h(\eta) = \frac{A}{a(\eta)} \cos(k\eta + \alpha) \tag{3.9}$$

We notice that after horizon re-entry the amplitude of the gravitational wave decays in inverse proportion to the scale factor. This general result is valid both for MD and

[1] With the subscript (i) we refer to the amplitude initial value.

[2] This assumption concerns scalar perturbation as well.

RD epochs. The two free parameters A and α can be determined by matching 3.9 with the constant mode of the superhorizon regime. The borderline between the two regimes occurs at $k\eta_\times \simeq 1$ and the function 3.9 at that time is found to be $h = Aa^{-1}(\eta_\times)$ and equating it to the constant mode h_i we finally find a first estimate of the amplitude after the horizon re-entry

$$h(\eta) = h_i \frac{a(\eta_\times)}{a(\eta)} \cos(k\eta + \alpha) \tag{3.10}$$

At a given time, the dependence of the amplitude h on momentum is completely determined by the scale factor time evolution $a(\eta_\times) \simeq a(k^{-1})$, if we assume that h_i are the same for all wavelengths. Keeping in mind this statement we now want to determine the amplitude at both RD and MD epochs.

During RD era, in which we have $k \gg k_{eq}$ with the subscript eq standing for matter-radiation equality, the scale factor depends linearly on the conformal time $a(\eta) \propto \eta$, while during MD, $k \ll k_{eq}$, the scale factor grows with the square of the conformal time $a(\eta) \propto \eta^2$. To summarize:

$$h(k) \propto h_i k^{-1} \qquad k \gg k_{eq} \tag{3.11a}$$

$$h(k) \propto h_i k^{-2} \qquad k \ll k_{eq} \tag{3.11b}$$

We are still missing the phase α and to determine it we have to fully solve eq 3.3. In what follow we mainly focus on RD-entering modes because as we will see they match with the range of frequencies analysed by interferometers. For these modes we have $a'/a = \eta^{-1}$ and this means that eq 3.3 is nothing but the Bessel equation, whose solution that tends to a constant as the conformal time tends to zero is given by

$$h(\eta) = h_i \frac{\sin(k\eta)}{k\eta} \tag{3.12}$$

where we focused on the Bessel solution that tends to a constant mode in order to match the solution with the superhorizon constant mode previously discussed. The assumption of the absence of decaying modes uniquely fixes the phase in this solution. We have to keep in mind that this expression is valid only at $\eta \sim \eta_\times$ and to obtain the value of the amplitude $h(\eta)$ at later times we have to make use of the time-independence of the ratio $a(\eta)/\eta$ at the horizon crossing, hence

$$h(\eta) = h_i \frac{a(\eta)}{\eta_\times} \frac{\sin(k\eta)}{ka(\eta)} \tag{3.13}$$

Let us recall now that deep down at radiation domination, making use of the entropy conservation, we can rewrite the Friedman equation as

$$\begin{aligned} H^2 &= \frac{8\pi}{3} G \frac{\pi^2}{30} g_\star T^4 \\ &= \left(\frac{g_{\star,0}}{g_\star}\right)^{1/3} \Omega_{rad} H_0^2 \left(\frac{a_0}{a}\right)^4 \end{aligned} \tag{3.14}$$

Hence we express the conformal time as

$$\eta = \int_0^t \frac{\mathrm{d}\tilde{t}}{a(\tilde{t})} = \int_0^a \frac{\mathrm{d}\tilde{a}}{\tilde{a}^2 H(\tilde{a})} = \left(\frac{g_\star}{g_{\star,0}}\right)^{1/6} \frac{1}{a_0 H_0 \sqrt{\Omega_{rad}}} \frac{a}{a_0} \tag{3.15}$$

and this allow us to rewrite the ratio

$$\frac{a(\eta_\times)}{\eta_\times} = a_0^2 H_0 \sqrt{\Omega_{rad}} \left(\frac{g_{\star,0}}{g_\star(\eta_\times)}\right)^{1/6} \tag{3.16}$$

This gives us the final expression for the time evolution of the amplitude of subhorizon RD-entering mode. At a present time, the formula gives us[3]

$$h(\eta_0) = h_i \frac{H_0 \sqrt{\Omega_{rad}}}{q_0} \left(\frac{g_{\star,0}}{g_\star(\eta_\times)}\right)^{1/6} \sin(k\eta_0) \tag{3.17}$$

where $q_0 = \frac{k}{a_0}$ is the physical momentum today.

3.2 Gravitational wave energy density

The main property of a relic gravitational wave background of cosmological origin is its frequency spectrum: indeed it is expected to be isotropic, stationary and unpolarized. The intensity of such a background can be characterized by the dimensionless energy density, defined as [3]:

$$\Omega_{gw}(k) \equiv \frac{1}{\rho_c} \frac{\mathrm{d}\rho_{gw}}{\mathrm{d}\log(k)} \tag{3.18}$$

where ρ_c is the critical density given by

$$\rho_c = \frac{3H_0^2}{8\pi G}$$

and ρ_{gw} is the energy density of the stochastic background.
The results of the previous section can be used to compute such a density in the present

[3]We will use this result later on.

Universe. Once the wavelength is smaller than the Hubble horizon the modes are not affected anymore by the Universe expansion, and the tensor perturbation quadratic action reduces to the free gravity waves action in Minkowski space-time[4]

$$S = \sum_s \frac{1}{64\pi G} \int \mathrm{d}^4x \left[\left(\partial_t h^s\right)^2 - \partial_k h^s \partial_k h^s \right] \tag{3.19}$$

Hence the hamiltonian functional is given by

$$H = \sum_s \frac{1}{64\pi G} \int \mathrm{d}^3x \left[\left(\partial_t h^s\right)^2 + \partial_k h^s \partial_k h^s \right] \tag{3.20}$$

Next, Fourier expanding the amplitude and computing the T_{00} component of the stress-energy tensor we immediately get the energy density ρ_{gw}

$$\rho_{gw} = \frac{M_{pl}^2}{32\pi} \int \frac{\mathrm{d}q_0}{q_0} \left(q_0 \Delta_{T,0}\right)^2 \tag{3.21}$$

where Δ_T^2 is the dimensionless tensor spectrum defined in chapter 2 as

$$\Delta_T^2 = \frac{k^3}{2\pi^2} P_T(k) \tag{3.22}$$

With $\Delta_{T,0}^2$ we denote the power spectrum evaluated today. Of course this quantity is strictly connected with the primordial spectrum.
It is now easy using the result 3.17 and the definition 3.18 to obtain the gravitational wave energy density in the present Universe

$$\Omega_{gw} = \frac{1}{12} \Omega_{rad} \left(\frac{g_{\star,0}}{g_\star(\eta_\times)} \right)^{1/3} \Delta_T^2 \tag{3.23}$$

The predicted energy density is very small, therefore relic gravity waves are hard to detect. However the required sensitivity might be reached by future space-based interferometers like LISA or with Pulsar Timing Array (PTA) techniques. The figure 3.2 shows for a variety of gravitational wave experiments the sensitivities to a relic gravitational wave background as a function of momentum k and frequency f. The line k_{eq} separates modes that entered the horizon at matter domination (smaller frequencies) and radiation domination, the latter being the ones we are interested in.

[4]We assume a flat background space.

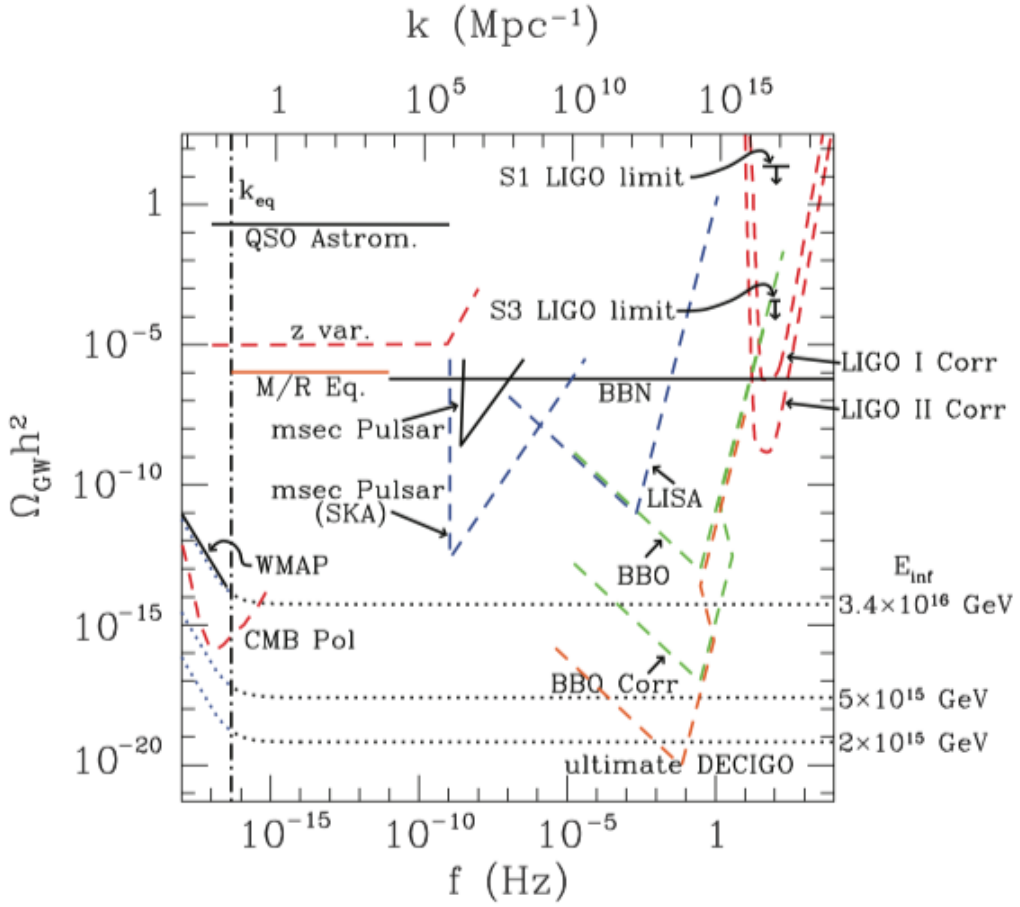

Figure 3.2: The dashed curves stand for the projective sensitivities of the various detectors, while the solid curves denote the current upper limit [13].

3.3 Tensor fluctuations enhancement

In the previous section we obtained the energy density of relic GW in the present universe assuming a flat primordial power spectrum. We can see from fig 3.2 that the predicted energy density for different inflation models is well below the sensitivity curves of the actual detectors, hence we are led to the conclusion that direct detection of stochastic background is so far unlikely.
Here we present a new mechanism developed by [16] that allows us to amplify the primordial fluctuations of the tensor sector. Then in section 3.4 we translate this enhanced power spectrum into late-time energy density, ensuring that it crosses LISA, LIGO and PTA sensitivity curves.

Assuming a single filed inflation background, they showed that tensor fluctuations might be enhanced if we assume a non-attractor phase of inflation: indeed, this transitory regime raises the would-be decaying tensor mode at superhorizon scales. Before exploring this mechanism we briefly discuss similar models applied to the scalar sector, in order to gain familiarity with this scenario.

3.3.1 Analogies with the scalar mode

We already saw in 2.3.1 that in a single field inflationary scenario the dynamics is governed by the action 2.45. Then we expanded the latter to the second order in the scalar curvature perturbation $\mathcal{R}$, obtaining eq. 2.47, which in conformal time takes the form

$$S_{(2)} = \frac{1}{2}\int \mathrm{d}\eta \mathrm{d}x^3 z^2 \left[\mathcal{R}'^2 - \left(\partial_i \mathcal{R}\right)^2\right] \tag{3.24}$$

where the scalar pump field z is

$$z = a\frac{\dot{\phi}}{H} \tag{3.25}$$

and we denote with ϕ the scalar inflaton field. As we studied earlier, in standard single field inflation scenarios $\dot{\phi}$ and H are approximately constant, while the scale factor $a \propto e^{Ht}$ grows exponentially. Hence, the scalar pump field z increases in time and the inflation is said to be in an attractor phase: the scalar curvature perturbation $\mathcal{R}$ remains constant at superhorizon scales and its power spectrum is almost scale invariant.
However there are models in which the rapid change in the potential slope breaks the slow-roll conditions, then the standard inflation is not an attractor anymore and the quantity z might decrease for a brief time interval. If this happens the would-be decaying solution of eq 2.51 in the superhorizon regime becomes relevant, and the modes that exit the horizon during this phase might be amplified by several orders. As a consequence the primordial power spectrum of the curvature perturbation $\mathcal{R}$ is enhanced and these predictions can be tested with CMB experiments.
Before discussing the tensor sector, it is worthwhile to present with some more details the theories behind these results, hence we describe the so called ultra slow-roll system as presented by [11]. According to this model the slow-roll inflation, besides ending when the field potential is steep and curved, breaks down when it becomes too flat and the ultra slow-roll regime sets in.

Ultra slow-roll inflation

In chapter 1 we studied the physics behind inflation and we saw that the dynamic of the inflaton is governed by the Klein Gordon equation 1.57:

$$\ddot{\phi} + 3H\dot{\phi} + V_{,\phi} = 0 \tag{3.26}$$

In particular, we achieved slow-roll inflation requiring the parameter

$$\epsilon \equiv -\frac{\dot{H}}{H^2} \tag{3.27}$$

to be smaller than unity. In this standard scenario the term $\ddot{\phi}$ in equation 3.26 is negligible[5] and it reduces to

$$3H\dot{\phi} \approx -V_{,\phi} \tag{3.28}$$

The latter shows us that the friction term depends on the slope term. Inflation proceeds in the standard regime and it ends when slow-roll conditions are broken.

However, there is a chance for the potential to became extremely flat and if this happens the slope term in equation 3.26 can be neglected. Hence, we are left with

$$\ddot{\phi} + 3H\dot{\phi} \approx 0 \tag{3.29}$$

and this shows us that the friction term now depends on the acceleration $\ddot{\phi}$.
In this scenario, the slow-roll conditions do not hold anymore and a super slow-roll regime sets in.
Thus, if we are in slow-roll regime but the slope $V_{,\phi}$ decreases drastically, then by virtue of equation 3.28 it drags down the friction term as well. Arguably this reduces the kinetic energy density

$$E_{kin} = \frac{1}{2}\dot{\phi}^2$$

However this value cannot decrease arbitrarily quick: indeed the fastest it can shrinks is $E_{kin} \propto a^{-6}$, and this is called free-fall because it corresponds to a scalar field with null potential density $V = 0$, whose dynamics is governed by eq. 3.29. Therefore we conclude that if the decreasing slope $V_{,\phi}$ forces the derivative $\dot{\phi}$, hence the kinetic energy density, to reduce faster than the free-fall case, then slow-roll condition are broken and super slow-roll begins.

[5]Indeed, we saw that accelerated expansion is sustained for a sufficient amount of time only if $\left|\ddot{\phi}\right| \ll \left|3H\dot{\phi}\right|, |V_{,\phi}|$.

We conclude with a brief comment on the power spectrum behaviour during super slow-roll inflation. In section 2.3.1 we analysed the primordial fluctuations for the scalar curvature perturbation, then we computed its power spectrum. This was given by

$$\Delta^2_{\mathcal{R}}(k) \equiv \frac{k^3}{2\pi^2} P_{\mathcal{R}}(k) = \frac{H^2_\times}{(2\pi)^2} \frac{H^2_\times}{\dot{\phi}^2_\times} \tag{3.30}$$

In standard slow-roll inflation the potential energy dominates over the kinetic term and the variation of $\dot{\phi}$ is very small, hence the power spectrum $\Delta^2_{\mathcal{R}}(k)$ remains almost constant and as we said it is roughly scale invariant. On the other hand, things are different during ultra slow-roll inflation: indeed in this regime we have $\dot{\phi}^2 = 2E_{kin} \propto a^{-6} \propto e^{-6\Delta N}$, where with ΔN we denote the elapsing ultra slow-roll e-folds. This means that during ultra slow-roll the power spectrum goes like

$$\Delta^2_{\mathcal{R}}(k) \propto e^{6\Delta N} \tag{3.31}$$

Therefore we conclude that the curvature perturbations grow exponentially during this phase and the primordial power spectrum for the scalar sector might be enhanced by several orders of magnitude.

3.3.2 Tensor sector

The amplification of scalar perturbations recently lived a renovated interest, since these scenarios can lead to the production of primordial black hole [16]. In this section we explain how a similar enhancement might be achieved for primordial tensor modes, if we require a phase of non-attractor inflation.
During the last decades accurate measures of CMB polarization set constraints on the amplitude of the tensor spectrum at very large scales, without giving us further information about much smaller scales.
On the other hand interferometers and other GWs experiments might probe a stochastic background at these smaller scales in the next future. Thus, scenarios of inflation where the primordial power spectrum is amplified at the scales of these detectors give us predictions that are easier to verify, instead of CMB polarization experiments [16]. In essence, this is the reason why the enhancement of the tensor modes of primordial perturbations constitutes a phenomenologically interesting topic.
Hence we describe this new mechanism developed by [16] that allow us to amplify the tensor spectrum in single field inflation at arbitrary scales. It relies on the assumption that the inflaton dynamic goes through a phase of non attractor regime that enhances the tensor perturbations on super-horizon scales.

We already saw in chapter 2 the linearised tensor fluctuations around a FRW background, define by the line element

$$\mathrm{d}s^2 = -\mathrm{d}t^2 + a^2(t)\big((1-2\mathcal{R})\delta_{ij} + h_{ij}\big)\mathrm{d}x^i\mathrm{d}x^j \tag{3.32}$$

where with h_{ij} we denote as usually the transverse spin-2 tensor perturbations which satisfies the traceless condition

$$\partial_i h_{ij} = h^i_i = 0 \tag{3.33}$$

Here we consider a non minimal coupling between the metric and the inflaton field ϕ, so that we end up with a time dependent function in the action for tensor modes that allows us to enhance the spectrum. Indeed, expanding the Einstein action up to the second order in the metric perturbation we get [17]

$$S = \frac{1}{8}\int \mathrm{d}t\mathrm{d}^3x a^3(t)\left[\mathcal{G}_T(t)(\partial_t h_{ij})^2 - \frac{\mathcal{F}_T(t)}{a^2(t)}(\partial_l h_{ij})^2\right] \tag{3.34}$$

where we set $M_{pl}^2 = 1/(8\pi G) = 1$. In contrast with the previously derived equation 2.71 here we have two time dependent functions, *i.e.* $\mathcal{G}_T(t), \mathcal{F}_T(t)$ that characterise the non minimal coupling of the tensor kinetic term with the scalar field. If we introduce, in analogy with the scalar fluctuations, the tensor pump field

$$z_T^2 = \frac{a^2}{4}\sqrt{\mathcal{G}_T\mathcal{F}_T} \tag{3.35}$$

and define a new time variable

$$\mathrm{d}t = a\left(\frac{\mathcal{G}_T}{\mathcal{F}_T}\right)^{1/2}\mathrm{d}\tilde{\eta} \tag{3.36}$$

we might re-write the above action in a more convenient way

$$S = \frac{1}{2}\int \mathrm{d}\tilde{\eta}\mathrm{d}^3x z_T^2(\tilde{\eta})\left[(h'_{ij})^2 - (\partial_l h_{ij})^2\right] \tag{3.37}$$

where we denote with primes the derivative with respect to $\tilde{\eta}$. Here we recognize the action of a free field in a time dependent background. In particular it is interesting to notice that if we impose $\mathcal{G}_T = \mathcal{F}_T = 1$ then the new time variable $\tilde{\eta}$ behaves like the conformal time and we recover the usual scenario discussed in the previous chapters.

Besides the presence of the two time dependent functions, the analogies with standard inflation are evident and we can proceed as discussed in 3.1. Indeed, in Fourier space the equation of motion reads

$$h'' + 2\frac{z'_T}{z_T}h' + k^2 h = 0 \tag{3.38}$$

Actually we just substituted the scale factor a in Mukhanov equation 3.3 with the tensor field pump z_T. However the non minimal kinetic mixing encoded in $\mathcal{G}_T(t), \mathcal{F}_T(t)$ might considerably change the evolution of tensor perturbations with the subsequent primordial spectrum enhancement. If we focus on superhorizon regime, *i.e.* $k^2 \ll |z_T'/z_T|$ we can neglect the last term in eq. 3.38 and the general solution of the motion equation under this approximation is given by

$$h(\tilde{\eta}) = \mathcal{C}_1 + \mathcal{C}_2 \int \frac{\mathrm{d}\tilde{\eta}'}{z_T^2(\tilde{\eta}')} \tag{3.39}$$

where $\mathcal{C}_1$ and $\mathcal{C}_2$ are two integration constant. As we discussed in section 3.1.1, during standard slow-roll inflation the second term on the r.h.s. decreases always in time and its contribution is negligible at horizon re-entry. Hence the tensor perturbations together with the primordial power spectrum remain constant on superhorizon scales.
On the other hand in this case we might have a very different behaviour of the would-be decaying tensor mode which lead us to different predictions: indeed if the function z_T decreases rapidly in time the term proportional to $\mathcal{C}_2$ becomes dominant with respect to the constant mode $\mathcal{C}_1$ and the tensor amplitude is enhanced. If this happens the would-be decaying mode is no longer suppressed by the scale factor and the system undergoes to the so called non attractor regime.
In particular this occurs if the ratio z_T'/z_T changes sign, *i.e.*

$$\frac{z_T'}{z_T} < 0 \qquad \Longrightarrow \qquad \text{non-attractor regime} \tag{3.40}$$

This condition might be achieved, even for a short period of time, if the tensor pump field z_T has a strong time dependence, inducted by the presence of the two functions $\mathcal{G}_T(t), \mathcal{F}_T(t)$. Actually the above condition for the non-attractor regime determines a break down of the standard slow-roll inflation: this implies that the dynamics of the tensor amplitude cannot be described in terms of the usual slow-roll equations and we have to introduce the idea on tensor duality, which allows us to control the system analytically besides being in the non-attractor phase.

Duality and tensor modes

The concept of duality for the scalar sector has already been introduced by Wands [18]: he showed that the power spectrum produced during inflation from quantum primordial fluctuations is invariant under a transformation of the homogeneous background field. In essence this allows us to produce a scale invariant spectrum from inflation regimes far from the usual slow-roll approximation.

This degeneracy of the spectrum is present even in the gravitational wave sector and we might apply the very same argument to the brief transient non-attractor phase in order to control analytically the evolution of tensor perturbations. For a better comprehension of the idea of tensor duality we recall the action 3.37. The latter can be written in the standard form

$$S = \frac{1}{2}\int \mathrm{d}\tilde{\eta}\mathrm{d}^3x z_T^2(\tilde{\eta})\left[(q'_{ij})^2 - (\partial_l q_{ij})^2 + \frac{z''_T}{z_T}q_{ij}^2\right] \tag{3.41}$$

where we introduced the canonical normalized tensor field

$$h_{ij} = \frac{q_{ij}}{z_T} \tag{3.42}$$

The above action corresponds to the usual action for an harmonic oscillator with a mass $\mu^2 = z''_T/z_T$ which evolves in time, and it can be quantized and investigated if it satisfies specific conditions. In particular we realize that the action 3.41 remains invariant under a general transformation of the function $z_T(\tilde{\eta})$ which leaves the ratio z''_T/z_T unchanged. Moreover such a redefinition leaves invariant the equations of motion of the canonically normalized field q_{ij} hence the solution is the same.
According to [18] the most general transformation which leaves the ratio

$$\frac{\bar{z}''_T}{\bar{z}_T} = \frac{z''_T}{z_T} \tag{3.43}$$

invariant might be written as

$$\bar{z}_T(\tilde{\eta}) = z_T(\tilde{\eta})\left(c_1 + c_2\int \frac{\mathrm{d}\tilde{\eta}'}{z_T^2(\tilde{\eta}')}\right) \tag{3.44}$$

where c_1, c_2 are two integration constants. It is worthwhile to highlights that the action 3.41 contains the same canonical variable q_{ij} after the transformation law of the tensor pump field z_T and this constitutes the key feature of tensor duality. Indeed this condition allows us to introduce a new tensor perturbation $\bar{h}_{ij}$ which can be related to the old tensor amplitude h_{ij} thanks to the common canonical variable q_{ij}:

$$\begin{cases} h_{ij} = \frac{q_{ij}}{z_T} \\ \\ \bar{h}_{ij} = \frac{q_{ij}}{\bar{z}_T} \end{cases} \qquad \Longrightarrow \qquad \bar{h}_{ij} = \frac{z_T}{\bar{z}_T}h_{ij} \tag{3.45}$$

The new field $\bar{h}_{ij}$ is called the tensor dual of h_{ij}. The dynamics of the tensor dual is governed by the very same action 3.41 if we substitute z_T with $\bar{z}_T$. Thus we conclude that both the tensor perturbation and its dual follow the same statistics, since they are

associated with the same canonical variable q_{ij}. Eventually this allows us to correlate the dual power spectrum with the original one with the only difference of an overall factor

$$\bar{\Delta}_T^2 = \left(\frac{z_T}{\bar{z}_T}\right)^2 \Delta_T^2 \tag{3.46}$$

In particular if the overall ratio is bigger than unity the dual tensor spectrum is enhanced as we desired. This shows that, thanks to tensor duality, if we control analytically the power spectrum of h_{ij} then we might control the dual spectrum for the amplitude $\bar{h}_{ij}$.

So far we discussed in a general way the non-attractor phase and tensor duality and now we want to correlate them by computing the tensor dual of a slow-roll phase. Hence we consider a quasi de-Sitter background space where the inflaton field is such that the functions $\mathcal{G}_T(t), \mathcal{F}_T(t)$ are almost constant in time and the slow-roll approximation is satisfied. In this regime we know from the previous chapters that the power spectrum is scale invariant and it is constant at superhorizon scales. In particular if we neglect the time dependence of the Hubble parameter it is found to be [16]

$$\Delta_T = 2\frac{\mathcal{G}_T^{1/2}}{\mathcal{F}_T^{3/2}}\frac{H_\times^2}{\pi^2} \tag{3.47}$$

Recalling the definition 3.35, the function z_T during slow-roll inflation is simply

$$z_T^2 = \frac{a^2}{4}\sqrt{\mathcal{G}_T\mathcal{F}_T} \propto a^2 \tag{3.48}$$

On the other hand, keeping in mind the duality condition of eq. 3.44, which can be rewritten as

$$\partial_{\tilde{\eta}}\left(\frac{\bar{z}_T}{z_T}\right) \propto \frac{1}{z_T^2} \tag{3.49}$$

we might determine the properties of the tensor dual of the slow-roll phase. Recalling the relation which connects the two time variable $\tilde{\eta}$ and t the above equation becomes

$$\partial_t\left(\frac{\bar{z}_T}{z_T}\right) \propto \frac{1}{a^3} \tag{3.50}$$

If we consider the background as a pure de Sitter space we obtain

$$\frac{\bar{z}_T}{z_T} \propto \frac{1}{a^3} \qquad \Longrightarrow \qquad \bar{z}_T^2 \propto \frac{1}{a^4} \tag{3.51}$$

Thus we showed that if slow-roll inflation is an attractor phase with the the tensor pump field z_T increasing in time, then the tensor dual of such a phase has a time-decreasing

function $\bar{z}_T$. This tells us that the dual phase is a non-attractor and recalling the solution 3.39 we conclude that in this regime the tensor perturbations grow at superhorizon scales, with the subsequent amplification of the primordial power spectrum. The latter, according to 3.46 has an amplitude given by

$$\bar{\Delta}_T^2 = \left(\frac{z_T}{\bar{z}_T}\right)^2 \Delta_T^2 \propto a^6 \Delta_T^2 \tag{3.52}$$

We know that during inflation the scale factor a grows exponentially, hence we conclude the mechanism we just described allows us to properly amplify the power spectrum in the dual regime where equation 3.51 holds true. In particular, the requirement

$$\bar{z}_T^2 \propto \frac{1}{a^4} \tag{3.53}$$

together with the definition 3.35

$$\bar{z}_T^2 = \frac{a^2}{4}\sqrt{\bar{\mathcal{G}}_T \bar{\mathcal{F}}_T} \tag{3.54}$$

implies that in the dual phase the two functions must satisfy the relation

$$\sqrt{\bar{\mathcal{G}}_T \bar{\mathcal{F}}_T} \propto \frac{1}{a^6} \tag{3.55}$$

which eventually determines the non-attractor regime of the tensor fluctuations.
Using tensor duality it is possible to build specific models of single field inflation which are able to enhance the tensor fluctuations on superhorizon scales. For further details see [16]. In what follow we will mainly use the results 3.52 in order to study the phenomenology predicted by a brief non attractor phase in between standard slow-roll inflation.

3.4 Non-attractor regime

In this section we investigate how a non attractor phase of the tensor sector, with the consequent enhancement of the power spectrum, could in principle amplify the total energy density of the gravitational wave background in the present Universe. The dynamic of a non-attractor phase has already been discussed in the previous section.
We first justify the idea of a non attractor regime during inflation and then we move toward a quantitative study of the power spectrum evolution in the presence of such a regime. Then we estimate the new energy density predicted by the modified power spectrum and we examine how many e-folds of non attractor inflation are necessary to ensure that the energy density crosses LISA, LIGO and PTA sensitivity curves.

The CMB and LSS observations provide an estimate of the spectrum of inhomogeneities in the Universe on very large scale and they both strongly support the paradigm of cosmological inflation.
However, we know from the inflationary theory that large scales modes were the first to exit the horizon and being far outside of it at recombination they have not been affected by subhorizon evolution. Hence, they allow us to directly observe just a small fraction of the inflationary evolution. Indeed, CMB and LSS probe the range of wave numbers $10^{-4}\text{Mpc}^{-1} < k < 0.1\text{Mpc}^{-1}$, corresponding to about 7 out of the 60 e-folds of inflation and this leaves the remaining e-folds largely unknown [31].
It is therefore legit to suppose that at smaller scales there has been a short period ΔN of non-attractor regime during which slow-rolls conditions were broken. We already studied in the previous section how this transitory non-attractor phase let the tensor fluctuations grow at superhorizon scales, amplifying the would-be decaying tensor mode. Our purpose is to compute again the energy density predicted by the modified power spectrum. In particular, we consider a short period of non-attractor phase in between the slow-roll inflation. Let us recall the expression 3.52 for the dimensionless power spectrum during a non-attractor phase

$$\bar{\Delta}_T^2 = \left(\frac{z_T}{\bar{z}_T}\right)^2 \Delta_T^2 \propto a^6 \Delta_T^2 \tag{3.56}$$

This relation shows us that the power spectrum during the dual phase grows like the sixth power of the scale factor.
Indeed, if we assume the presence of a non-attractor phase for a brief time interval between usual slow-roll inflation, the power spectrum profile might be viewed as[6]

$$\Delta_T^2 = \mathcal{P}_T = 2\frac{H_\times^2}{\pi^2} \times \begin{cases} 1 & a < a_i \quad \text{slow-roll} \\ \left(\frac{a}{a_i}\right)^6 & a_i < a < a_f \quad \text{non-attractor} \\ \left(\frac{a_f}{a_i}\right)^6 & a > a_f \quad \text{slow-roll} \end{cases} \tag{3.57}$$

where we note with $a_i \equiv a(N_i)$ the scale factor when the non-attractor phase stars, while $a_f \equiv a(N_f)$ when the latter ends. We want to translate the enhancement of the primordial power spectrum achieved by the non-attractor phase into energy density amplification in the present Universe. Hence we start again from the formulas of the previous section and making use of eq. 3.21 and the definition 3.18 we get the amplified

[6]We are assuming H to be constant during the inflation process.

dimensionless energy density

$$\Omega_{gw} = \frac{1}{6}\Omega_{rad}\left(\frac{g_{\star,0}}{g_\star(\eta_\times)}\right)^{1/3}\frac{H_\times^2}{\pi^2} \times \begin{cases} 1 & a < a_i \\ \left(\frac{a}{a_i}\right)^6 & a_i < a < a_f \\ \left(\frac{a_f}{a_i}\right)^6 & a > a_f \end{cases} \tag{3.58}$$

We note that one of the main advantages of the non-attractor hypothesis is that it really increases the stochastic gravitational wave energy density by a factor of a^6, hence we expect that such a mechanism ensures that the energy density crosses the detectors sensitivity curves with just few e-folds of non-attractor regime.

Before computing the e-folds number of the non attractor regime, we need a relation between the frequencies (scales) and the e-folds number during inflation. To this end, let us recall the definition of the horizon crossing

$$\frac{k}{a(\eta_k)} = H_\times(\eta_k) \tag{3.59}$$

During inflation, the scale factor rapidly evolves in time while the Hubble parameter remains almost constant. Hence, chosen a conformal momentum $k_\star$ at one's convenience we get

$$\frac{k}{k_\star} = \frac{a(\eta_k)}{a(\eta_{k_\star})} = e^{N(\eta_k)-N(\eta_{k_\star})} \tag{3.60}$$

where we chose the sign convention that counts the numbers of e-folds from the start of inflation: with this convention N becomes larger as we go forward in time and increases as the scale factor increases. We are assuming that inflation ended at $N = 60$ e-folds.

To determine how many e-folds of non-attractor inflation are necessary and whether or not background gravitational radiation will be detectable by a specific gravitational wave detector, it is essential to know the sensitivity of the instrument [15].
Typically such sensitivities are represented by plotting the minimum value of the gravitational wave amplitude detectable by the instrument versus the frequency of the wave itself, as we saw in fig 3.2. We will provide in the next section the analytical fit for these curves.
According to the literature [13] we consider as inflation energy scale the value $E_{inf} = 2 \times 10^{15}$GeV, which corresponds to an energy density of $\Omega_{gw}h_0^2 \sim 10^{-19}$, where h is the dimensionless Hubble parameter.
The LISA, aLIGO and PTA sensitivities are provided by [31] and the table 3.1 summarizes the observational windows, together with the number of e-folds from the start of inflation at which the corresponding modes were generated. In particular, the number of e-folds was obtained using eq 3.60 and setting as arbitrary momentum $k_{CMB} \simeq 0.05\text{Mpc}^{-1}$.

GW @	k [Mpc^{-1}]	$N_{estim.}$	$(\Omega_{gw}h_0^2)_{min}$
LISA	$10^{11} - 10^{14}$	$28.3 - 35.2$	4.5×10^{-12}
aLIGO	$10^{16} - 10^{17}$	$39.8 - 42.13$	3.2×10^{-6}
PTA	$10^{6} - 10^{8}$	$16.8 - 21.4$	0.9×10^{-10}

Table 3.1: First column: list of different interferometers under exam. Second columns: observational windows in terms of the order of magnitude of the wave number of the primordial modes. Third column: estimate number of e-folds at which those modes exit the horizon. Fourth column: minimum value of gravitational wave amplitude detectable by each experiment.

Given all these ingredients we can finally determine how many e-folds ΔN of non-attractor are necessary for each of the three detectors. Indeed, recalling the definition of the e-folds number

$$\mathrm{d}N = \mathrm{d}\ln(a) = H\mathrm{d}t \qquad \Rightarrow \qquad N = \log\left(\frac{a_f}{a_i}\right) \tag{3.61}$$

and taking into account the predicted energy density value $\Omega_{gw}h_0^2 \sim 10^{-19}$ before the non-attractor regime sets in, we can estimate the duration of the non attractor regime in order to get the desired amplification. Keeping in mind the expression of the amplified power spectrum during inflation 3.58, the enhancement is given by

$$\left(\frac{a_f}{a_i}\right)^6 = e^{6\Delta N} = \frac{(\Omega_{gw}h^2)_{min}}{\Omega_{gw}h^2} = \frac{(\Omega_{gw}h^2)_{min}}{10^{-19}} \tag{3.62}$$

Hence, the required e-folds number might be expressed as

$$\Delta N = \frac{1}{6}\ln\left(\frac{(\Omega_{gw}h^2)_{min}}{10^{-19}}\right) \tag{3.63}$$

where with $(\Omega_{gw}h^2)_{min}$ we mean the minimum value of gravitational wave energy density detectable by each experiment. Taking into account the fourth column of table 3.1 we are able to obtain the value ΔN for the three different detectors and finally fix the value $N_i = N_{estim.} - \Delta N$ at which the non-attractor regime should have set in to ensure the amplification of the energy density at the correct frequencies. We report the results in table 3.2.

GW @	ΔN	N_i
LISA	2.9	$25.4 - 32.3$
aLIGO	5.2	$34.6 - 36.9$
PTA	3.4	$13.4 - 18$

Table 3.2: First column: estimated duration of the non-attractor phase. Second column: number of e-folds at which the non-attractor regime should have begun.

Finally, with these results we can represent graphically the equation 3.58, taking into account the three different detectors. In order to have a smooth transition regime between the non-attractor and the slow-roll phases we considered the following analytical approximation of eq 3.58

$$\Omega_{gw}(N)h_0^2 = 10^{-19}\frac{1+e^{6(N-N_i)}}{1+e^{6(N-N_i)}e^{-6\Delta N}} \tag{3.64}$$

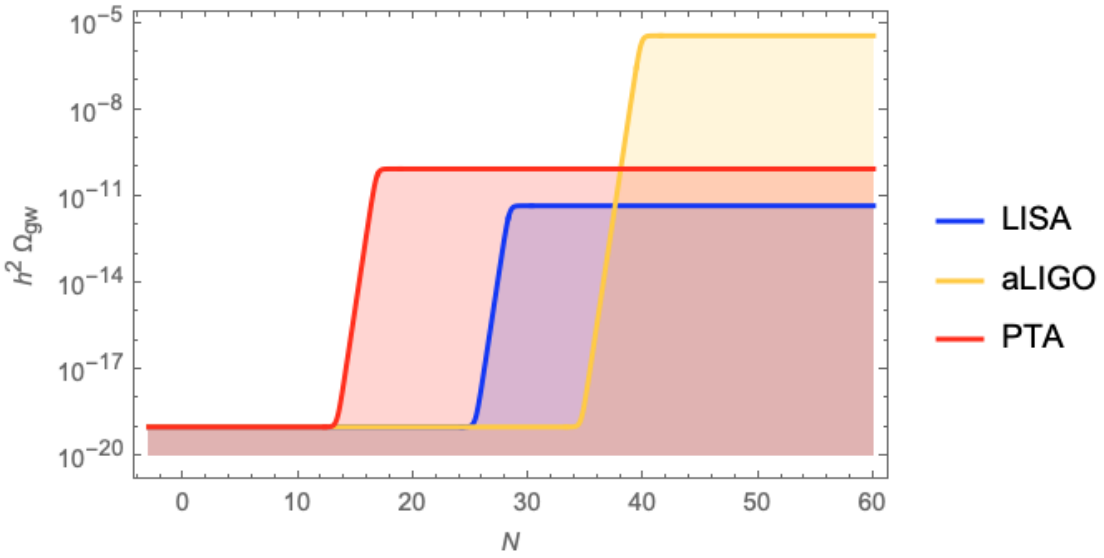

Figure 3.3: We considered the energy density amplification as given by 3.58 for three different detectors. We assumed the inflation to end at $N = 60$ e-folds. Each curve represents the desired amplification for every detector under exam. The presence of a non-attractor phase ensures that the energy density crosses the sensitivity of the above mentioned detectors if the growing phase takes place for a sufficiently large number of e-folds.

The plot 3.3 shows the amplification of primordial energy density due to the intermediate non-attractor phase for all the detectors we analysed in this section. Notice how according to the results of table 3.2 we were able to enhance the power spectrum up to the desired level. Indeed, we show in section 3.6 that the latter really crosses aLIGO, LISA and PTA sensitivities curves at the correct frequency range.According to table 3.2 the aLIGO interferometer requires a longer non-attractor phase if compared with PTA and LISA, since its minimum value of detectable energy density is higher - see 3.1
In this plot we assumed the Hubble parameter H to be constant during both slow-roll and non-attractor inflation epochs and we neglected the inheritance of the subhorizon modes. The latter assumption allowed us to consider a flat power spectrum during the slow-roll phases.

3.5 Energy density and sensitivity curves

In this section we discuss a method to parametrize the sensitivity of a GW detector and, together with the results so far obtained, we try to summarize these information on a sensitivity-curves plot. There are several methods to describe such sensitivities and the gravitational wave energy density, hence we discuss the different conventions - and their relations - commonly used in the literature, in order to adopt a consistent protocol between detectors and sources that allows us to plot both the information on the very same graph.

3.5.1 Power spectral density

We begin making contact with what happens in a GW detection experiment and we focus on the response of a single detector. Its performance is completely characterized by the so called power spectral density (PSD), and the latter can be defined with the following method. Typically the total output of the detector can be expressed as a superposition of a possible signal $h(t)$ and the noise $n(t)$

$$s(t) = n(t) + h(t) \tag{3.65}$$

where we assume, for simplicity, that the noise is stationary and Gaussian [33]. Considering the average over an ensemble of realization[7], the noise auto-correlation function $C(t_1, t_2)$ is defined by

$$C(t_1, t_2) \equiv \langle n(t_1) n(t_2) \rangle \tag{3.66}$$

[7]More precisely, we are working with a single realisation, but with the ergodic hypothesis the ensemble average can be replaced with a time average.

Under the assumption of stationarity, hence assuming the detector performance being time independent, this quantity depends only on $\tau = |t_1 - t_2|$. In this case it is possible to introduce the PSD [34] as the Fourier transform of eq. 3.66

$$S_n(f) \equiv \frac{1}{2}\int_{-\infty}^{\infty} \mathrm{d}\tau C(\tau) e^{-2\pi i f \tau} \qquad\qquad f \geq 0 \tag{3.67}$$

Using the following convention for the Fourier transform

$$\tilde{x}(f) = \mathcal{F}\{x(t)\}(f) = \int_{-\infty}^{\infty} \mathrm{d}t x(t) e^{-2\pi i f t} \tag{3.68a}$$

$$x(t) = \mathcal{F}^{-1}\{\tilde{x}(f)\}(t) = \int_{-\infty}^{\infty} \mathrm{d}f \tilde{x}(f) e^{2\pi i f t} \tag{3.68b}$$

it is easy to show, with the help of 3.67, that for a stationary noise background

$$\langle \tilde{n}(f)\tilde{n}^*(f')\rangle = \frac{1}{2}\delta(f - f')S_n(f) \tag{3.69}$$

Detector output and GW signals are both real quantities: thus we have to impose the reality condition on the Fourier coefficients. This gives us

$$\tilde{n}(-f) = \tilde{n}^*(f) \qquad\qquad \tilde{h}(-f) = \tilde{h}^*(f) \tag{3.70}$$

therefore we conclude that $S_n(f)$ is an even function and this fact allows us to rewrite the Fourier integrals over all frequencies as an integrals over the positive frequencies only; hence the $S_n(f)$ is called *one-side* PSD.
It is easy to show [33] that the PSD, if integrated over all positive frequencies, gives us the mean square noise amplitude

$$\overline{|n(t)|}^2 = \int_0^{\infty} S_n(f) \tag{3.71}$$

Thanks to this interesting property, the square root of the PSD, also called amplitude spectral density, is one of the most commonly used quantity in sensitivity curves plots. Introducing the dimensionless strain amplitudes[8] $h_c(f)$ and $h_n(f)$ for the source amplitude and the noise counterpart respectively, we have

$$\sqrt{S_n(f)} = h_n(f) f^{-1/2} \tag{3.72a}$$

$$\sqrt{S_h(f)} = h_c(f) f^{-1/2} \tag{3.72b}$$

[8]Designed to include the effect of integrating and inspiralling signal [33].

It is evident that the PSDs have the dimensions of time but, being defined in the frequency domain, it is conventional in the literature to use the dimensions of Hz^{-1}, hence both $\sqrt{S_n(f)}$ and $\sqrt{S_h(f)}$ have dimensions of $\mathrm{Hz}^{-1/2}$.

A second way of describing the GW amplitude is the characteristic strain itself: the advantage of this convention is that when plotting on a log-log scale it is possible to relate the signal-to-noise ratio with the area between the source and the detector curves [12].

Energy density

Finally we describe a third way to characterize the spectrum, and it involves the energy density per logarithmic interval of frequency $\Omega_{gw}(f)$. We recall the definition 3.18

$$\Omega_{gw}(f) = \frac{1}{\rho_c}\frac{\mathrm{d}\rho_{gw}}{\mathrm{d}\log f} \tag{3.73}$$

where f is the frequency of the stochastic background GW with energy density ρ_{gw} and ρ_c is the value of the critical energy density given by

$$\rho_c = \frac{3H_0^2}{8\pi G} \tag{3.74}$$

The energy density description is the most commonly used in sensitivity curves for stochastic GW background and it has the advantage of having an explicit physical interpretation.

Relation between the descriptions

In this work we deal with stochastic GW background therefore, for consistency with the existing literature, we wish to plot in the same graph both the signal and the sensitivity curves of the detectors we analysed using the energy density parametrization. Typically the sensitivity curves are given in terms of the PSD, the latter being the quantity that fully characterizes the performance of a GW detector, as mentioned earlier. Hence, we need to relate all possible ways for describing the spectrum and it can be shown that the following relations hold true [12],[33]

$$H_0^2\Omega_{gw}(f) = \frac{2\pi^2}{3}f^3 S_n(f) = \frac{2\pi^2}{3}f^2[h_c(f)]^2 \tag{3.75}$$

Writing the Hubble constant H_0 as

$$H_0 = h_0 \times 100 \text{ km s}^{-1}\text{Mpc}^{-1} \tag{3.76}$$

where h_0 parametrize the today's experimental uncertainty and using 3.75 we easily obtain the desired relation[9]

$$\Omega_{gw}(f)h_0^2 = 6\pi^2 f^3 S_n(f) \times 10^{34} \tag{3.77}$$

As we see later on thanks to this equation we will be able to plot the sensitivity curves in the energy density domain.

3.5.2 Sensitivity curves

So far we discussed the response of a single detector in a very general way and we introduced the necessary quantities to characterize its performance. In this section we focus on the sensitivities of the detectors we took into account in 3.4 In particular, we review how the sensitivity curves for LISA and aLIGO are constructed, and we propose a new analytical fit for IPTA curve.

aLIGO Interferometer

In order to have good chances of detection, gravitational wave interferometers must aim to extremely ambitious sensitivity. In this subsection we analyse the possible noise sources to see what sensitivity can be achieved. We distinguish two main categories of noise, know as optical read-out noise and displacement noise. The former is intrinsic to the technique[10] that an interferometer uses to detect the signal, while the latter denotes all other sources that have nothing to do with gravitational waves detection.
The optical read-out noise can be thought as a combination of two different effects: the shot noise and the radiation pressure

$$S_n(f)|_{opt} = S_n(f)|_{shot} + S_n(f)|_{rad} \tag{3.78}$$

The shot noise is a quantum effect that arises from the photons emitted by the laser: these discrete quanta of light, arriving randomly at the test masses, produce fluctuations in the light intensity that can be misunderstood as gravitational wave signal. Being a random process, the error increases with the square root of the number N_γ of photon used [34]. In order to reduce this noise we should increase the laser power[11], however this improves the radiation pressure generated by the photons on the mirror itself. Since

[9] We made use of the conversion 1 Mpc $= 3 \times 10^{22}$ m.

[10] Typically we detect the displacement induced by the gravitational wave on the test masses, using a laser beam that bounces between them [35].

[11] This result can be achieved either increasing the recycling factor or the input laser power.

the number of photons arriving at the test masses fluctuates, the radiation pressure generates a stochastic force that shakes the mirrors [35] and it cannot being compensated by a mechanism that keep the mirrors in place.
It can be shown [35] that the shot noise is proportional to $P_{bs}^{1/2}$ while the radiation pressure to $P_{bs}^{-1/2}$, where we denote with P_{bs} the laser input power. Here we explicitly see the effects of the Heisenberg uncertainty principle: we increase the laser power to reduce the shot noise, improving the position sensing accuracy[12], but this eventually ends up with a greater disturbance of the conjugate variable. Indeed, the momentum transferred to the mirror impinges a recoil on the mirror itself, and this leads to a measure disturbance able to mask a gravitational wave signal. The interesting fact is that we are working with a quantum system to measure a purely classical quantity, such as the gravitational wave amplitude. Luckily the uncertainty principle does not impose constraint on the level of accuracy of position measurements, but only on the simultaneous measurements of conjugated variables. Therefore it is possible to overcome this difficulty adopting specific interferometer configurations that reduce the uncertainty effect on the variable being measured, decreasing the accuracy of the unmeasured conjugated variable. One of the best results so far obtained was achieved during the upgrade of the German interferometer GEO600 and it is described in [39].

Next we move on the discussion of displacement noise: the complete computation of these noises is a very technical subject and it goes beyond the scope of this work. Here we limit ourselves to discussing the most important displacement noise sources without mentioning the details of the suspension mechanism or the properties of the materials used to build the detectors.
The main noise sources against which we have to deal with are

- **Thermal noise**
  This noise source induces vibrations both on the suspending pendulum and in the mirrors, disturbing the measure process. Regarding the suspension mechanism, we have thermal fluctuations that determine a horizontal displacement of the mirrors due to the induced swinging motion in the suspensions. This noise is the most relevant one between a few Hz and 50 Hz. Besides, because of the Earth curvature, the vertical at the two mirror locations has not the same direction, and the vertical motion induced by thermal fluctuations produces a horizontal-vertical coupling which alters the measure.
  Moreover we have Brownian motion of the atoms of the mirrors due to their kinetic energy [35] and this gives rise to mirror thermal noise, mostly relevant between a

[12]Remember that we are using photons to measures the position of the mirrors.

few tens ad a few hundred Hz. Then we have thermo-elastic fluctuations generated by temperature anomalies that cause the expansion of both the mirror bulk and the mirror coatings.

- **Seismic and Newtonian noise**
  The Earth surface moves continuously with a few microns amplitude. In particular, in the wave band between 1 Hz and 10 Hz this noise is mostly generated by local phenomena[13] and human activity such as train, local traffic and other sources. This constitutes a serious problem for interferometers because they work bouncing the laser beam back and forth in between the mirrors, hence at each reflection further vibrational noise is introduced. This micro-seismic noise can be attenuated -at least in principle- arbitrarily using a cascade set of pendulums able to filter the ground noise. Using a pendulum with resonance frequency $f_\star$ it is possible to attenuate the oscillations by a factor $(f_\star/f)^2$ at frequencies $f \gg f_\star$. Therefore, using a set of N pendulums we can reduce the seismic noise by a factor of $(f_\star/f)^{2N}$. We conclude that the ground noise can be reduced up to the desired level of accuracy just for frequencies above 10 Hz, and that is the main reason why ground-based detectors cannot investigate gravitational wave events with frequency below this limit. The most efficient isolation system has been developed so far for the VIRGO detector [40].
  Besides seismic noise we have to deal with the Newtonian noise, or gravity gradient noise. While the other noise sources can be reduced with apposite filtering system, this noise cannot be attenuated or eliminated, because the gravitational forces cannot be screened out. The Newtonian noise arises from changes in the gravitational field produced by seismic waves, air density fluctuations and man-made sources. All these effects sum up in a non-negligible contribution to the gravity gradient noise and this is the main reason why the detection of gravitational waves in the band below 1 Hz must be done in space.

- **Other noises**
  There are many other subtle effects, besides displacement and read-out noise, that must be kept under control in order to achieve the desired level of accuracy. In particular, fluctuations of the laser input power have to be controlled with great precision and the laser beam must travel in a vacuum tubes in order to avoid fluctuations of the index of refraction that could alter the accuracy of the instrument. Moreover, the residual gases inside the high vacuum pipe must be kept free of or-

[13] Wind and atmospheric cyclonic systems over the oceans [35].

ganic molecules such as hydrocarbons, in order to avoid the cumulative deposit of such molecules in the optical surfaces.

We discussed so far the most important noise sources that could alter the precision of the instrument if they are not kept under control to great accuracy. Next we focus on the plot of the sensitivity curve and, as mention earlier, we need an expression for the one-sided noise PSD, the latter being the quantity that completely characterize the performance of a gravitational wave detector. The noise power spectral density for the advanced LIGO interferometer, according to [34], is well fitted by the expression

$$S_n(x) = S_0\left[x^{-4.14} - 5x^2 + \frac{111(1 - x^2 + 0.5x^4)}{1 + 0.5x^2}\right] \tag{3.79}$$

where we gave the PSD in terms of a dimensionless frequency $x = f/f_0$, with $f_0 = 215$ Hz and $S_0 = 10^{-49}$ Hz^{-1}.
The expression in 3.79 holds true just for frequencies above the cut-off $f_s = 20$ Hz and for data analysis purposes for $f \leq f_s$ the noise PSD is assumed to be essentially divergent. Indeed, due to low frequency seismic vibrations and other noise sources, the sensitivity of ground based interferometers is restricted at frequencies less than a Hertz [34], [15].
Combining again 3.77 with the PSD given in 3.79 we get the aLIGO sensitivity curves in the desired convention

$$\Omega_{aLIGO}(f)h_0^2 = 10^{-15} \times 6\pi^2 f^3\left[x^{-4.14} - 5x^2 + \frac{111(1 - x^2 + 0.5x^4)}{1 + 0.5x^2}\right] \tag{3.80}$$

LISA antenna

Ground-based interferometers such as LIGO and VIRGO can not access the region below about 10 Hz of the gravitational wave spectrum because of the wall due to the Newtonian and seismic noise [35], but there are many expected sources in this wave band such as the coalescence of supermassive black holes at the center of galaxies. These ground-related noises fall down rapidly as we move away from Earth and the only way to observe the low band frequency is to go in space.
The Laser Interferometer Space Antenna (LISA) project, developed in collaboration between ESA and NASA, is a quite impressive mission that would open up for the first time the frequency window between 0.1 mHz and 0.1 Hz [34].
The LISA mission consists of three different spacecraft separated by 2.5 Gm and arranged in a equilateral triangle array orbiting the sun at a distance of about 1 AU, about 20° behind the Earth.
We will not go through a detailed description of the experimental apparatus, but for

the sake of clarity we briefly discuss its most remarkable aspects. The LISA mission incorporates drag-free technique, i.e. inside each spacecraft there are two unattached test masses that fall freely. Using micro-thrusters, the spacecraft adjusts its position with respect to the masses and it is kept stationary relative to them[14]. Hence, the job of the spacecraft is to isolate these masses from the main external influences such as solar radiation pressure, solar wind and micro-meteorite that would affect the measure process.
The spacecraft are way too far to use mirrors reflection[15] similarly to the ground-based interferometers. Instead, LISA uses a system of laser transponders: each spacecraft has an on-board laser that sends signals to the others. Once this laser light is received the signal is sent back using a laser locked exactly at the same phase of the incoming signal [34].

In what follow we present a method to construct and plot the LISA sensitivity curve, and we compare the curve with the signal strength of a gravitational wave event.
According to [36] the LISA sensitivity curve can be well approximated by the expression

$$S_n(f) = \frac{10}{3L^2}\left(P_{oms}(f) + \frac{4P_{acc}(f)}{(2\pi f)^4}\right)\left(1 + \frac{6}{10}\left(\frac{f}{f_*}\right)^2\right) + S_c(f) \tag{3.81}$$

and here we show how this curve is derived. We denote with $f_* = 19.09$ mHz a reference frequency, while $L = 2.5$ Gm is the length of its arms. $P_{oms}(f)$ is the so-called optical metrology noise and P_{acc} is the single test mass acceleration noise and they are quoted as

$$P_{oms} = (1.5 \times 10^{-11}\ \text{m})^2\left(1 + \left(\frac{2\ \text{mHz}}{f}\right)^4\right)\ \text{Hz}^{-1} \tag{3.82a}$$

$$P_{acc} = (3 \times 10^{-15} m\ s^{-2})^2\left(1 + \left(\frac{0.4\ \text{mHz}}{f}\right)^2\right)\left(1 + \left(\frac{f}{8\ \text{mHz}}\right)^4\right)\ \text{Hz}^{-1} \tag{3.82b}$$

$S_c(f)$ stands for the galactic confusion noise due to the unresolved binaries that will interfere with measurements as an effective noise source. An estimate on the confusion noise for LISA interferometer can be found in [37] and it is well fitted by the expression[16]

$$S_c(f) = Af^{-7/3}e^{-f\alpha+\beta f\sin(kf)}[1 + \tanh(\gamma(f_k - f))]\ \text{Hz}^{-1} \tag{3.83}$$

As the mission progresses and more binaries sources are removed from the background, the $S_c(f)$ noise is reduced and in a good analytical model sufficient for most purpose

[14]The LISA pathfinder is a ESA mission launched on December 2015 to demonstrate the drag-free technology at the desired accuracy.

[15]Indeed, reflection is impossible due to power losses when the light travels from one spacecraft to the other.

[16]For the fit parameters consult [36].

it can be neglected. According to [38] the total noise in a LISA-style interferometer is given by

$$P_n(f) = \frac{P_{oms}}{L^2} + 2(1+\cos^2(f/f_*))\frac{P_{acc}}{(2\pi f)^4} \tag{3.84}$$

Combining this expression with the transfer function[17], well-fitted by [15]

$$\mathcal{R}(f) = \frac{3}{10}\frac{1}{(1+0.6(f/f_*)^2)} \tag{3.85}$$

we end up with the final expression for the LISA effective noise power spectral density function

$$S_n(f) = \frac{P_n(f)}{\mathcal{R}(f)} = \frac{10}{3L^2}\left(P_{oms}(f) + 2(1+\cos^2(f/f_*))\frac{4P_{acc}(f)}{(2\pi f)^4}\right)\left(1+\frac{6}{10}\left(\frac{f}{f_*}\right)^2\right) \tag{3.86}$$

Combining this result with relation 3.77 we obtain the LISA sensitivity curve expressed in term of the energy density

$$\Omega_{LISA}(f)h_0^2 = 6\pi^2 f^3 \times 10^{34}\frac{10}{3L^2}\left(P_{oms}(f) + 2(1+\cos^2(f/f_*))\frac{4P_{acc}(f)}{(2\pi f)^4}\right)\left(1+\frac{6}{10}\left(\frac{f}{f_*}\right)^2\right) \tag{3.87}$$

PTA

Pulsars are highly magnetized and rapidly rotating neutron stars that emit electromagnetic radiation. These objects formed with the supernovae explosion of stars with masses between 5 and 10 times the solar mass. The extreme density and the short, regular rotational period of pulsars make these objects excellent clocks: there is a very accurate interval between pulses that goes from milliseconds to seconds for a single pulsar. In particular, these milliseconds pulsars are an impressive source of high precision measurements [12]. This amazing stability allows us to use pulsars as natural gravitational wave detector. Assuming that pulsars emit perfectly regular pulses, we can measure the time irregularities of a single object to set upper limits on the stochastic gravitational wave energy density. On the other hand, if we observe simultaneously more pulsars we end up with a natural gravitational wave detector. Indeed, the perturbation produced by such a wave passing between us and the pulsars induces a fluctuation that causes a delay in the time of arrival of the pulses, proportional to the amplitude of the gravitational wave. It is interesting to note that the sensitivity of a pulsar timing array depends on

[17]This quantity takes into account the averaged signal response function of the instrument due to sky and polarization effects.

the sampling properties of the data set [33]: if we assume a total length of observation time T and each measurement is spaced in time by Δt, then the PTA sensitivity falls in the frequency range between $1/T < f < 1/\Delta t$. Pulsars are typically detected once every few weeks, hence the maximum detectable gravitational wave frequency is limited by the data sampling around $f \sim 10^{-7}$ Hz [41].
Thus, PTA allows us to observe the very low frequency band and we chose to focus on these three different type of detectors[18] in order to cover almost the entire frequency range of the background gravitational wave spectrum.

We summarized the main properties of PTA technique and we now move on with the study of its sensitivity curve. In this work we consider the International Pulsar Timing Network (IPTA) project: it consists of a network of 20 pulsars, and we assume as cadence of the measurements the value $1/\Delta t = 20$ yr^{-1} with an ambitious value of the root mean square error in each timing residual of $\sigma = 100$ ns. We also assumed as total observation time $T = 5$ yr, and this value sets the lower frequency limit on the power spectral density. Finally, we consider identical white timing noise power spectral density [41]

$$P_n(f) = 2\Delta t \sigma^2 \tag{3.88}$$

and using these data sampling it can be shown [42] that the effective noise power spectral density for the IPTA project is given by

$$S_{eff}(f) = S_n(f)\left[\sum_{i=1}^{20}\sum_{j>i}^{20}\zeta_{ij}^2\right]^{1/2} \tag{3.89}$$

where the standard PSD, given by the ratio between the total noise and the transfer function $\mathcal{R}(f)$, takes the form

$$S_n(f) = \frac{P_n(f)}{\mathcal{R}(f)} = 12\pi^2 f^2 P_n(f) \tag{3.90}$$

and the latter is weighted over the Hellings and Downs factors ζ_{ij} [43]. Choosing a set of 20 pulsars we find a value

$$\sum_{i=1}^{20}\sum_{j>i}^{20}\zeta_{ij}^2 = 4.74 \tag{3.91}$$

and it can be thought as the effective number of pulsars of the network array [42].
In this work we present a graphical representation of the sensitivity curve of the IPTA obtained with an analytical fit built with the data discussed above: the lower frequency

[18] LISA, aLIGO and PTA.

range is constrained by the vertical line $f = f_{cutoff} \equiv 1/T$, while for higher frequencies, up to $f_{max} \equiv 1/\Delta t$, there is a growing factor of f^5. In particular, we developed the following analytical fit, in good accordance with the existing literature [41],[42]

$$\Omega_{PTA}(f)h_0^2 = 10^{-10} \times \mathcal{H}(f_{cutoff} - f)\left(\frac{f}{f_{cutoff}}\right)^{-26} + 10^{31} \times \mathcal{H}(f - f_{cutoff})f^5 \quad (3.92)$$

where $\mathcal{H}(x - x_0)$ is the Heaviside step function. It is interesting to note from figure 3.4 that, while the LISA and aLIGO sensitivity curves have a rounded shape, the PTA curve is wedge-shaped: this is due to the fact that the low frequency wall is determined by the total observation time, while for higher frequency the energy density goes like $\Omega_{gw}(f)h_0^2 \propto f^5$: a factor of f^2 is given by the transfer function$\mathcal{R}(f)$, and an additional factor of f^3 comes from the PSD to energy density conversion[19].

3.6 Conclusions

In section 3.4 we discussed the effects of a non-attractor phase of the tensor sector, which allowed us to enhance the primordial power spectrum, and consequently the gravitational wave energy density. In particular we examined how many e-folds of non attractor inflation are necessary in order to ensure that the energy density intersects the sensitivity curves of the three detectors under exam.
In section 3.5 we studied how to characterize the performance of a GW detector, presenting different conventions commonly used in the literature to plot the relative sensitivity curve. Then we discussed the possible noise sources of LISA, aLIGO and PTA detectors, and we presented a good analytical fit for the sensitivity curve of each detector, expressed in terms of the energy density convention.

We can now plot, using a consistent protocol, both the detectors and sources curves in the same graph, showing how the enhanced GW energy density intersects the sensitivity of the detectors.
In figure 3.3 we showed the behaviour of the amplified primordial energy density as a function of the e-folds number, assuming the inflation to end at $N = 60$ e-folds. Here we want to plot the same curves as a function of the frequency f. This can be easily achieved starting from the relation[20]

$$k = \frac{2\pi}{\lambda} = \frac{2\pi f}{c}$$

[19]See the equation 3.77.
[20]We denote with λ and c the wavelength and the speed of light respectively.

Now, using the wave number e-fold relation from eq. 3.60

$$k = k_\star e^{N(\eta_k) - N(\eta_{k_\star})} \tag{3.93}$$

with the reference value

$$k_\star = k_{cmb} = 0.05 \text{ Mpc}^{-1}$$

we obtain the desired frequency e-fold relation

$$f = 10^{-16} \times \frac{1}{40\pi} e^{N(\eta_k)} \tag{3.94}$$

Substituting this result in the expression 3.64 we get the analytical fit of the enhanced primordial energy density as a function of the frequency

$$\Omega_{gw}(f)h_0^2 = 10^{-19} \frac{1 + (40\pi 10^{16} f^6) e^{-6N_i)}}{1 + (40\pi 10^{16} f)^6 e^{-6(N_i + \Delta N)}} \tag{3.95}$$

With all these ingredients we can finally plot the LISA, aLIGO and PTA curves from eqs. 3.87, 3.80, 3.92 respectively, together with the analytical fit of eq. 3.95. The latter was plotted for each detector using the results of table 3.2

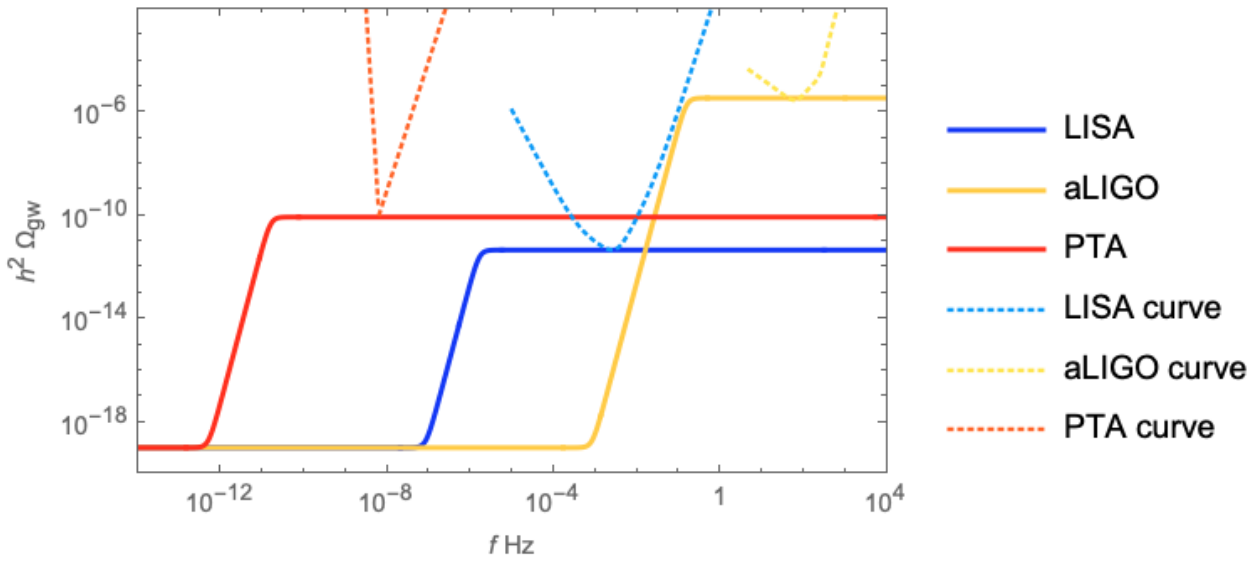

Figure 3.4: The dashed curves stand for the analytical fit of the three detectors sensitivities: starting from the left we have PTA, LISA and aLIGO curves. The solid curves denote the enhanced primordial energy density, relative to each detector.

The plot in figure 3.4 summarize the results discussed in this chapter. Arguably we showed that the assumption of a non-attractor phase for a brief time interval really amplifies the energy density of the gravitational wave background. Indeed, if the growing phase takes place for a sufficiently large number of e-folds, there is a chance for the detectors to measure the gravitational wave event. We highlight that we specifically focused on these three experiments since they cover almost the entire predicted frequency spectrum.

Chapter 4

Model building

In the second chapter we studied a new mechanism to enhance the power spectrum in single field inflation which relies on a transitory non-attractor regime and it can be controlled via a tensor duality between an attractor and non-attractor phase. Then we focused on the phenomenology predicted by this model and we were able to amplify the stochastic background gravitational wave energy density up to the sensitivity curves of different experiments, as we showed in fig 3.4.
In this chapter we study a new model based on the effective field theory approach which allows us to amplify the primordial power spectrum on superhorizon scales avoiding the tensor duality developed by [16], hence with less mathematical effort.
We consider a lagrangian for two tensor field system at superhorizon scales with a non minimal coupling between the two fields, studying whether or not one of the two tensor modes can be enhanced due to the coupling. As we will see later on, this result can be achieved assuming one of the fields to be tachyon like. Indeed, it is the imaginary mass of one of the two fields[1] that introduces instability in the system, allowing the other field to grow exponentially in time when the coupling is on.
We begin studying the analogy with the scalar sector and we briefly investigate a model of hybrid inflation where for the first time it was used a tachyon-like scalar field in order to easily amplify the production of primordial black holes, good candidates for dark matter [30].
After that we introduce the basic ideas behind the effective field theory of inflation, which gives us the most general way to describe fluctuations around a quasi de Sitter background in single field inflation models [19]. This approach allows us to justify the lagrangian chosen for the development of our model and provides an alternative picture to describe the primordial power spectrum enhancement. Then we move towards a

[1]The other being massless.

quantitative study of the model, solving the Euler-Lagrange equations. After that we determine the conditions under which the would-be decaying modes can be amplified at superhorizon scales. Finally, once we determined the growing-modes predicted by the model, we compute the power spectrum for the massless field and, in analogy with the previous chapter, we try to determine how many e-folds of non attractor regime are necessary to ensure that the gravitational wave energy density crosses the sensitivity curves of the detectors.

Primordial black hole formation

In this section we briefly discuss an hybrid inflation model which consist of two different stages of chaotic inflation discussed by [31]. When inflationary theory was first proposed it was believed to begin after the high temperature phase transition in the early phase of the Universe [44]. Then it was proposed to consider all possible initial conditions without assuming necessarily initial thermal equilibrium, and this is what we call chaotic inflation[45]. It took many years to accept this scenario, but later it was understood that thermal initial conditions are neither natural or helpful for inflationary theory.
Recently there has been a renewed interest in the hybrid inflation, which belongs to the more general class of chaotic inflation as well. In particular, hybrid inflation describes the dynamic of two scalar inflaton field, ϕ and ψ. Here we try to explain the distinctive feature of this scenario: at the beginning one of the two fields, say ϕ, moves very slowly while ψ does not move at all and the false vacuum energy density of the latter supports the inflation process. As soon as the slowly rolling field ϕ reaches a critical value $\phi_\star$ it starts a rapid motion of the other field, inducing a transition to a waterfall regime [31]. Eventually the field ψ reaches its real minimum and its energy density degrades rapidly, determining the end of inflation regime.
In particular, in their work [31], Bellido et al. investigated the simplest hybrid inflation model given by the potential

$$V(\phi,\psi) = \left(M^2 - \frac{\sqrt{\lambda}}{2}\psi^2\right)^2 + \frac{1}{2}m^2\phi^2 + \frac{1}{2}\gamma\phi^2\psi^2$$

and assuming a negative square mass $-m_\psi^2 = 2\sqrt{\lambda}M^2$ around the real minumum $\psi = 0$ they were able to amplify density perturbation on the exponentially large scales, allowing the production of primordial black holes.
For many years it was believed that inflation reduced exponentially all the pre-existing inhomogeneities, but they showed that in a simple hybrid inflation model you can pro-

duced in a specific mass range a large amount of black holes, assuming the driving field ψ to be tachyon-like.

We chose to discuss this interesting model because in what follow we try to apply a similar technique at the tensor sector: starting from a super-horizon two tensor fields lagrangian we show how the instability induced by negative square mass field ensures the amplification of the other massless field.

4.1 Effective field theory: an introduction

The effective field theory (EFT) is considered one of the most widely applicable concepts in theoretical physics and in the last decades it has been very fruitful in numerous fields such as particle physics, cosmology and condensed matter physics thanks to its power and universality. EFT techniques give us valuable ideas on the physics behind inflation in the absence of a fundamental theory of gravity.
EFT consists in the description of a system through the isolation of its relevant low-energy degrees of freedom and the systematically inclusion, as non-renormalizable corrections, of the high-energy degrees of freedom effects [6]. Hence, the first step in EFT consists in the identification of the relevant degrees of freedom for the energy scale on interest: this allows us to describe the low-energy physics in term of an effective action for the light fields through the lowest dimension operator compatible with the underlying symmetries of the system [19]. The border between light and heavy degrees of freedom is whether or not the corresponding particles can be produced on shell at a given energy scale of the experiment [32].

4.1.1 EFT techniques

As we said, the starting point in constructing EFT consists in integrate out the heavy degrees of freedom, performing a path integral over them. This allows us to build an effective action for the low-energy fields only

$$e^{iS_{eff}(\psi_L)} \equiv \int \mathcal{D}\psi_H e^{iS(\psi_L,\psi_H)} \tag{4.1}$$

where ψ_L and ψ_H denotes the light and heavy fields respectively. With this method, the effective lagrangian can be written as an expansion into a finite number of terms of dimension four or less, and an infinite sequence of non-renormalizable terms with

dimension higher than four

$$\mathcal{L}_{eff}(\psi_L) = \mathcal{L}_{\Delta<4} + \sum_j \frac{\mathcal{O}_j(\psi_L)}{\Lambda^{\Delta_j - 4}} \tag{4.2}$$

where we denote with $\Delta_j = \dim(\mathcal{O}_j)$ the dimension of the the operator $\mathcal{O}_j$, while Λ is an arbitrary energy scale above which the effective theory breaks down. The expansion in 4.2 is performed in terms of the operators $\mathcal{O}_j$, the latter being made out of light degrees of freedom and they are local in time if we consider processes at energies lower than the heavy fields masses, *i.e.* when $E < M_H \sim \Lambda$.
In principle the sum in 4.2 takes into account an infinite number of terms, but in practice just a few of them are relevant: indeed, we want to reproduce the experiments with a finite level of accuracy [32], hence this requires just a finite number of terms.[2]

Typically EFTs techniques are used in one of the following cases

- If the full theory $S(\psi_L, \psi_H)$ is known, you may use the path integral 4.1 to systematically integrate out the heavy degrees of freedom and focus on the low-energy observables only. In this case, calculations are heavily simplified than in the full theory.

- On the other hand it could happen that the full theory is unknown and once we fixed the energy scale Λ it is possible to decouple the high-energy physics and work with an effective lagrangian such as 4.2. If this happens, then the operators $\mathcal{O}_j(\psi_L)$ that enters $\mathcal{L}_{eff}(\psi_L)$ must respect the underlying symmetries that survive at low energies. Hence, given the most general set of such operators we can write down, taking into account the UV physics in a model independent way, the effective lagrangian of the theory under exam. This is exactly what happens when we try to describe inflation as an effective field theory.

The EFT approach to inflation has been introduced in [19] by analysing the dynamics of Goldstone bosons associated with the breaking of time translation symmetry in a quasi de Sitter, single field inflationary phase. During the past years this approach has been developed considerably, also including extra fields, deriving a general effective action for light modes with spin in inflation. It is well outside the scope of this thesis to develop in detail the subject of EFT of inflation, and we refer the reader to [20] for a comprehensive review. In the next Section, we use some of the results of [21], a recent work which applies EFT techniques to couple the massless tensor mode predicted by general relativity to an

[2]This approach allows us to treat non-renormalizable theories as well.

extra massive spin two field during inflation. In particular, we focus on specific couplings between these two fields that can enhance the amplitude of the primordial spectrum of the massless tensor mode.

4.2 Lagrangian for two-field tensors system

In this section we can finally focus on the phenomenology of a spin-2 tensor fields model. We consider a FRW background with the metric given by

$$\mathrm{d}s^2 = -\mathrm{d}t^2 + a^2(t)\mathrm{d}\Sigma^2 \qquad \mathrm{d}\Sigma^2 = \mathrm{d}r^2 + r^2(\mathrm{d}\theta^2 + \sin^2(\theta)\mathrm{d}\phi^2) \tag{4.3}$$

where we used the physical time t and we assumed a flat background space-time.
First of all we focus on the superhorizon regime characterized by the presence - for a brief time interval - of a coupling term in the lagrangian between the massless graviton and the massive field. In this phase the dynamics of the physical tensor fluctuations strongly depends on the massive term. Indeed we were able to find a specific constrain on the value of the mass parameter in order to enhance the massless tensor fluctuations. Moreover, the standard prediction of a scale invariant spectrum might be always restored if we turn off the coupling term between the two field.
Then we focus on subhorizon scales, where the coupling is absent and the standard Bunch-Davies vacuum can be chosen following the same line of reasoning of section 2.3.1. Thanks to this procedure we can unequivocally fix the integration constants which is of fundamental importance for the primordial power spectrum computation, the latter being the quantity related with the today observed energy density.

4.2.1 Superhorizon dynamics

The starting point is the lagrangian for the two-field system. In the appendix A we show how to obtain the lagrangian in eq. 4.4 starting from a more general one with non canonical kinetic and mass terms.
At super-horizon scales, neglecting the spatial kinetic terms[3], we have

$$\mathcal{L} = a^3(t)\left[\frac{1}{2}\dot{h}_1(t)^2 + \frac{1}{2}\dot{h}_2(t)^2 + \lambda H \dot{h}_1(t) h_2(t) - \frac{1}{2}m^2 h_2(t)^2\right] \tag{4.4}$$

where we consider a massless tensor field $h_1(t)$ describing primordial gravitational waves and a second auxiliary massive field $h_2(t)$ with mass m. We indicate with H the Hubble parameter, while λ is a dimensionless coupling constant. As we will see later on it's the coupling term that allows the tensor mode $h_1(t)$ to grow with time.

[3]This is possible thanks to the very definition of super-horizon scales, $k \ll aH$.

Massive gravity and bigravity

Before exploring deep down the physics predicted by the lagrangian 4.4 we first need to step back for a while and talk about interacting massive spin-2 theories. From particle physics we know that the Standard Model contains massless and massive fields with spin 0, 1/2 and 1, while gravitational interactions are described by a self-interacting massless spin-2 tensors. Even though these theories are well-tested experimentally, the study of new theories behind the standard picture is motivated by several unexplained phenomena and the introduction of new physics becomes unavoidable.
In the framework of general relativity one of the simplest additional degrees of freedom that could be added to the already known theory is a massive spin-2 field, whose presence is expected to modify the gravitational sector [22]. The early attempts of investigating massive gravity were developed by Fierz and Pauli in 1939 and since then there have been important ideas towards the construction of the modern theory. Two review article focused on massive gravity have been written by de Rham [23] and Hinterbichler [24].
It was shown by Boulanger et al. [25] that there is no consistent (ghost-free) coupling that can mix various massless gravitons: most of the interaction observed in natures are described with Yang-Mills' theory by non-linearly interacting massless spin-1 fields. Besides, gravity involves just a single spin-2 massless field and there exists no analog of Yang-Mills' theory with multiplets of interacting massless spin-2 fields.
The main difference between the standard general relativity and bigravity is that the latter uses two different metric, a physical one coupled to matter and a sterile one that does not couple. In such a theory, gravitational interactions are mediated by two gravitons composed of different superposition of the two metric, and so they couple in different ways to the surrounding matter. In particular, one of the graviton is massive while the other one is massless, and this is exactly the case we consider in the next section. Finally, it can be shown that such a theory is a consistent effective field theory valid up to energies parametrically above the particle mass [26].

Equation of motion and growing modes

So far we gave a first introduction of the model under exam, explaining how the lagrangian 4.4 can be derived in term of the effective field theory of inflation and we briefly reviewed the massive graviton approach.
After this remarks we would like to proceed with a quantitative approach and we start studying the Euler-Lagrange equations for the two fields $h_1(t)$ and $h_2(t)$. Explicitly, the

equations of motions are

$$\ddot{h}_1(t) + 3H\dot{h}_1(t) + \lambda H\dot{h}_2(t) + 3\lambda H^2 h_2(t) = 0 \tag{4.5a}$$
$$\ddot{h}_2(t) + 3H\dot{h}_2(t) - \lambda H\dot{h}_1(t) + m^2 h_2(t) = 0 \tag{4.5b}$$

and we recognize them as a coupled ordinary differential equations system, whose solution is in general difficult to understand, but we were able to obtain an analytical solution, as it is shown later on. We remind the reader that we are working in a pure de Sitter space where the expansion is truly exponential and some calculations involving inflation during the early universe can be simplified.
Notice that in the limit $\lambda \to 0$ the equations decoupled and they reduce to the simple form

$$\ddot{h}_1(t) + 3H\dot{h}_1(t) = 0 \tag{4.6a}$$
$$\ddot{h}_2(t) + 3H\dot{h}_2(t) + m^2 h_2(t) = 0 \tag{4.6b}$$

Hence, turning off the coupling we recover the usual equations of motion studied in the previous chapter and they can be easily solved analytically. It is worth to stress out that the $h_1(t)$ tensor mode behaves like in section 3.1.1: indeed the general solution of 4.6a is given by the sum of two terms, a constant and a decaying mode, the latter being negligible at horizon re-entry

$$h_1(t) = \mathcal{C}_1 - \mathcal{C}_2 \frac{e^{-3Ht}}{3H} \tag{4.7}$$

where $\mathcal{C}_1$ and $\mathcal{C}_2$ are two integration constant to be determined once the initial conditions are given. Hence, as we expected the model reduces to the classical form if we turn off the coupling.

Going beyond the decoupling limit analysis of 4.6a and 4.6b we consider again the general equations of motion 4.5a and 4.5b studying their solutions. The complete solutions of the equations of motions are written down in the appendix B and here we would rather focus on the $h_1(t)$ tensor field, writing down the two exponent that can be collected apart. In particular, we try to understand whether or not we have growing or decaying modes. It can be shown that the two possible time behaviours are

$$\log\left(h_1^{decaying}\right) \approx -\frac{3}{2}Ht - \frac{1}{2}t\sqrt{-4m^2 + H^2(9 - 4\lambda^2)} \tag{4.8a}$$
$$\log\left(h_1^{growing}\right) \approx -\frac{3}{2}Ht + \frac{1}{2}t\sqrt{-4m^2 + H^2(9 - 4\lambda^2)} \tag{4.8b}$$

It is easy to determine the time evolution of these two expression: indeed we notice that the r.h.s of eq. 4.8a is always smaller than zero, hence all the terms in the solution of

4.5a that evolve in time according with this behaviour are decaying modes and they can be neglected for the very same reason we explained in section 3.1.1.
On the other hand things can be different for all those terms whose time evolution is governed by 4.8b. Indeed, if the expression under the square root dominates over the first term we might have growing modes. This actually happen if

$$-\frac{3}{2}Ht+\frac{1}{2}t\sqrt{-4m^2+H^2(9-4\lambda^2)}>0 \qquad \Longleftrightarrow \qquad m^2<-H^2\lambda^2 \tag{4.9}$$

where m is the mass of $h_2(t)$ tensor field.
Thus, if we assume $h_2(t)$ to be tachyon-like there is a chance to amplify the gravitational wave amplitude predicted by the lagrangian 4.4 and eventually enhance the primordial power spectrum produced during inflation.
At first, it was believed that tachyon fields permitted faster than light propagation [27] however it was soon realized that excitations of such imaginary mass fields do not propagate faster than light, but they are just some unstable states that need to decay [28],[29]. Indeed, in the context of modern quantum field theory tachyons are viewed as an instability of the system, rather than faster than light particles, treated using tachyon condensation and the causality is preserved.
As we notice in our example, it is the imaginary mass that causes instability and leads the massless field amplitude to increases exponentially. From now on we shall focus on the growing modes only[4]. The complete solution for the growing modes is given by

$$\begin{aligned} h_1^{growing}(t) = \frac{3e^{-\frac{3}{2}Ht+\frac{1}{2}t\sqrt{-4m^2+H^2(9-4\lambda^2)}}}{6H(m^2+H^2\lambda^2)\sqrt{-4m^2+H^2(9-4\lambda^2)}}H^2\lambda\Big[2H\lambda\mathcal{C}_1+ \\ +(9H^2-2m^2)\mathcal{C}_2+\sqrt{-4m^2+H^2(9-4\lambda^2)}\mathcal{C}_3+ \\ +3H\big(\sqrt{-4m^2+H^2(9-4\lambda^2)}\mathcal{C}_2+\mathcal{C}_3\big)\Big] \end{aligned} \tag{4.10}$$

where we introduced the integration constants $\mathcal{C}_1, \mathcal{C}_2, \mathcal{C}_3$ yet to be determined. Once again it is evident that turning off the coupling, *i.e* $\lambda = 0$, the growing modes are suppressed and we restore the classical limit.

From equation 4.10 we see that the time profile is completely determined by the exponent, while all other terms are just constants. Hence we might rewrite the solution in a more convenient way as

$$h_1(t)=h_i(k)\lambda\exp\left(-\frac{3}{2}Ht+\frac{1}{2}t\sqrt{-4m^2+H^2(9-4\lambda^2)}\right) \tag{4.11}$$

[4]Assuming a tachyion like $h_2(t)$ field.

were we incorporated all the constants in a single initial amplitude $h_{(i)}$.
The latter might be determined after matching the solution with the subhorizon evolution, as we show in the next section.
If we introduce the dimensionless parameter

$$\mu^2 = -\frac{4}{9}\left(\lambda^2 + \frac{m^2}{H^2}\right) \tag{4.12}$$

the previous expression takes the form

$$h_1(t) = h_i(k)\lambda \exp\left(\frac{3}{2}Ht\big(\sqrt{1+\mu^2}-1\big)\right) \tag{4.13}$$

where $\mu^2 > 0$. It is now evident that for $\lambda \neq 0$ the time evolution of the tensor amplitude is completely determined by the value of the parameter μ^2. In particular this quantity determines how fast the tensor fluctuations $h_1(t)$ might be enhanced on superhorizon scales.

In what follow we consider $\lambda \neq 0$ just for a brief time interval in between standard slow-roll inflation, in analogy with the non-attractor phase. Therefore it is legit to assume a quasi de Sitter background which allows us to further simplify the expression of the massless tensor modes. Indeed, recalling the time evolution of the scale factor during inflation

$$a(t) \propto e^{Ht} \tag{4.14}$$

with the Hubble parameter H almost constant, and taking the logarithm of 4.13 we have

$$\begin{aligned} \ln\left(\frac{h_1(t)}{h_{(i)}}\right) &= \frac{3}{2}\lambda Ht\big(\sqrt{1+\mu^2}-1\big) \\ &= \frac{3}{2}\lambda\big(\sqrt{1+\mu^2}-1\big)\ln(a(t)) \\ &= \ln(a(t))^{\frac{3}{2}\lambda\left(\sqrt{1+\mu^2}-1\right)} \end{aligned} \tag{4.15}$$

Then if we take the exponential of the above expression and we switch to conformal time η we get the final expression for the growing tensor mode

$$h_1(\eta) = h_{(i)}a(\eta)^{\frac{3}{2}\lambda\left(\sqrt{1+\mu^2}-1\right)} \tag{4.16}$$

In this final form the time evolution of $h_1(\eta)$ is completely determined by the μ^2 parameter which appears as an exponent of the scale factor. In particular it is worthwhile to stress out that if we turn off the coupling $\lambda = 0$ the standard slow-roll model which predicts a constant power spectrum on superhorizon scales is recovered. On the other

hand if we take into account the interaction term *i.e.* $\lambda \neq 0$ then we might enhance the tensor fluctuations on such scales.

Finally we can compute the power spectrum predicted by this model and then translate it into late time energy density of gravitational waves. Before going through the explicit computation we first evaluate the integration constant $h_{(i)}$ by matching the equation 4.16 with the subhorizon modes. This is going to be the topic of the next section.

4.2.2 Subhorizon regime

So far we just focused on superhorizon scales where we considered the lagrangian 4.4 with a coupling term between two tensor field. We studied how such a term completely modify the dynamics of tensor perturbations and we ended up with eq. 4.16 which determines the fluctuations evolution on superhorizon regime if the coupling is on[5].
On the other hand in this paragraph we discuss the subhorizon evolution assuming the coupling term to be negligible during this phase. Eventually this allows us to fix the constant initial amplitude $h_{(i)}$ of equation 4.16 .

We already know from chapter 3 that on subhorizon scales physical wavelengths are smaller than the comoving Hubble radius, *i.e.*

$$k \gg a(\eta)H(\eta) \qquad \Longleftrightarrow \qquad |k\eta| \gg 1 \tag{4.17}$$

This means that the contribution from the spatial derivative of the two tensor field cannot be neglected on this scales.
Actually the subhorizon dynamics is governed by the action

$$S = \int \mathrm{d}^4x a^3(t)\left[\dot{h}_1^2(t) + \dot{h}_2^2(t) - (\partial_i h_1)^2 - (\partial_i h_2)^2 - m^2 h_2^2\right] \tag{4.18}$$

As early disclosed, we did not considered the coupling term between the massive and massless filed, since we suppose the interaction to be relevant for a short time interval only on superhorizon scales.
If we redefine the time variable

$$\mathrm{d}\eta = \frac{\mathrm{d}t}{a(t)} \tag{4.19}$$

with η conformal time, the above action might be written as

$$S = \frac{1}{2}\int \mathrm{d}\eta \mathrm{d}^3x a^2\left[h_1^{2\prime}(\eta) + h_2^{2\prime}(\eta) - (\partial_i h_1)^2 - (\partial_i h_2)^2 - m^2 h_2^2\right] \tag{4.20}$$

[5]Turning off the coupling in 4.16 restores the fluctuations dynamics in standard slow-roll inflation.

In complete analogy with 2.3.2 we proceed with a Fourier expansion of the two tensor field. This is given by

$$h_1(\eta) = \sum_{s=+,\times} \int \frac{\mathrm{d}^3k}{(2\pi)^3} \epsilon^s(k) h^s_{1,k}(\eta) e^{i\boldsymbol{k}\cdot\boldsymbol{x}} \tag{4.21a}$$

$$h_2(\eta) = \sum_{s=+,\times} \int \frac{\mathrm{d}^3k}{(2\pi)^3} \epsilon^s(k) h^s_{2,k}(\eta) e^{i\boldsymbol{k}\cdot\boldsymbol{x}} \tag{4.21b}$$

where $\epsilon^s(k)\epsilon^{s'}(k) = 2\delta_{ss'}$ and $\epsilon_{ii} = k^i\epsilon_{ij} = 0$. With the above decomposition the tensor action in momentum space takes the form

$$S = \sum_s \frac{1}{32\pi G} \int \mathrm{d}\eta \mathrm{d}^3k a^2 \left[(h^{'}_{1,s})^2 + (h^{'}_{2,s})^2 - k^2 (h_{1,s})^2 - \left(k^2 + m^2\right)(h_{2,s})^2 \right] \tag{4.22}$$

where we neglected for simplicity the subscript k of the Fourier modes.
The analogies with equation 2.73 are evident, except for the presence of a second massive tensor field which does not affect the dynamics of the physical tensor fluctuations, since there is no coupling between them.
If we introduce the canonical normalized fields, defined by

$$v_{1,s} = \frac{a}{\sqrt{32\pi G}} h_{1,s} \qquad v_{2,s} = \frac{a}{\sqrt{32\pi G}} h_{2,s} \tag{4.23}$$

the action 4.22 reduces to the standard form

$$S = \sum_s \frac{1}{2} \int \mathrm{d}\eta \mathrm{d}^3k \left[(v'_{1,s})^2 + (v'_{2,s})^2 - \left(k^2 - \frac{a''}{a}\right)(v_{1,s})^2 - \left(k^2 + m^2 - \frac{a''}{a}\right)(v_{2,s})^2 \right] \tag{4.24}$$

This might be easily recognised as the action of two uncoupled harmonic oscillator with time dependent masses in a de Sitter background. Hence the system can be analytically controlled and its dynamics its completely determined by the motion equations. In particular we might derive them for each polarization mode starting from the action:

$$\begin{aligned} \frac{\delta S}{\delta v_{1,s}} = 0 \quad &\Longrightarrow \quad v''_{1,s} + \left(k^2 - \frac{a''}{a}\right) v_{1,s} = 0 \\ \frac{\delta S}{\delta v_{2,s}} = 0 \quad &\Longrightarrow \quad v''_{2,s} + \left(k^2 + m^2 - \frac{a''}{a}\right) v_{2,s} = 0 \end{aligned} \tag{4.25}$$

We ended up with a very similar result as discussed in chapter 2 because we did not consider the coupling between the two fields. The only difference is the presence of the second massive field $v_{2,s}$ which does not alter the evolution of $v_{1,s}$ on these scales.

From now on we focus exclusively on the physically relevant field $v_{1,s}$, trying to solve its equation of motion. Recalling the subhorizon regime approximation, i.e. $|k\eta| \gg 1$ we might neglect the last term of the $v_{1,s}$ motion equation and we are left with

$$v_1'' + k^2 v_1 = 0 \tag{4.26}$$

where we focused on a single polarization, neglecting the subscript s. This is easily recognised as the equation of a harmonic oscillator with time independent frequency. Indeed we already discussed in chapter 2 how such equation admits a unique solution if we require the ground state of the theory to be the minimum energy eigenstate of the hamiltonian functional. This procedure allows us to choose the so called Bunch-Davies vacuum if we impose the initial condition

$$\lim_{\eta \to -\infty} v_1 = \frac{e^{-ik\eta}}{\sqrt{2k}} \tag{4.27}$$

This requirement completely fix the mode functions v_1 on all scales. In particular this solution tells us that inside the horizon all the fluctuations behave like if they were in a flat space. This is not surprising since for physical wavelengths considerably smaller than the Hubble radius we expect the flat space-time to be good approximation for most purposes.
Finally, we might recast the solution in term of the field h_1 and we get

$$h_1 = \frac{\sqrt{32\pi G}}{a(\eta)} \frac{e^{-ik\eta}}{\sqrt{2k}} \tag{4.28}$$

Therefore each polarization might be thought of as a renormalized massless field in a de Sitter background.

4.2.3 Modes matching and power spectrum

In the previous paragraphs we obtain the expression for tensor fluctuations both outside and inside the horizon. In particular the inside horizon solution is uniquely fixed by the Bunch Davies vacuum choice, while the superhorizon has an integration constant yet to be determined. For the sake of clarity we report here both these quantity: on superhorizon regime, determined by $k \ll aH$, we obtained the following time evolution

$$h_1(\eta) = h_{(i)} a(\eta)^{\frac{3}{2}\lambda\left(\sqrt{1+\mu^2}-1\right)} \tag{4.29}$$

which might increase in time if $\lambda \neq 0$, otherwise we recover the standard behaviour. On the other hand on subhorizon scales we got

$$h_1 = \frac{\sqrt{32\pi G}}{a(\eta)} \frac{e^{-ik\eta}}{\sqrt{2k}} \tag{4.30}$$

Hence we have two expression for the perturbation h_1 in the two extremes regimes $k \ll aH$ and $k \gg aH$. If we require the continuity of the function at horizon crossing we might determine the desired integration constant $h_{(i)}$. Indeed, roughly matching the absolute value of the above solutions at $k = aH$ we get

$$h_{(i)} a(\eta_\times)^{\frac{3}{2}\lambda\left(\sqrt{1+\mu^2}-1\right)} = \frac{\sqrt{32\pi G}}{a(\eta_\times)} \frac{1}{\sqrt{2k}} = \frac{\sqrt{32\pi G}}{\sqrt{2k^3}} H_\times \tag{4.31}$$

where with the subscript $\times$ we denote quantities evaluated at horizon crossing. In the last step we used the condition $k = aH$.
Eventually we can determine the value of the constant $h_{(i)}$ as

$$h_{(i)} = \frac{\sqrt{32\pi G} H_\times}{\sqrt{2k^3}} a(\eta_\times)^{-\frac{3}{2}\lambda\left(\sqrt{1+\mu^2}-1\right)} \tag{4.32}$$

This actually allows us to rewrite the final expression for h_1 tensor fluctuations on superhorizon scales: keeping in mind equation 4.16 we simply have

$$h_1(\eta) = \frac{\sqrt{32\pi G} H_\times}{\sqrt{2k^3}} \left(\frac{a(\eta)}{a(\eta_\times)}\right)^{\frac{3}{2}\lambda\left(\sqrt{1+\mu^2}-1\right)} \tag{4.33}$$

The matching procedure allowed us to determine uniquely the fluctuations behaviour on superhorizon scales whether or not we consider a coupling term[6].
Therefore we can proceed with the primordial power spectrum computation, since we already discussed all the required ingredients. This actually help us to estimate the perturbations growing rate in the presence of a coupling term with a tachyon like massive field. Recalling its definition from section 2.3.1, we have

$$\begin{aligned} \langle h_1(k) h_1(k') \rangle &= (2\pi)^3 \delta(\boldsymbol{k} + \boldsymbol{k'}) P_{h_1}(k) \\ &= (2\pi)^3 \delta(\boldsymbol{k} + \boldsymbol{k'}) \frac{16\pi G}{k^3} H_\times^2 \left(\frac{a(\eta)}{a(\eta_\times)}\right)^{3\lambda\left(\sqrt{1+\mu^2}-1\right)} \end{aligned} \tag{4.34}$$

Hence, the dimensionless power spectrum defined by

$$\Delta_h^2 \equiv \frac{k^3}{2\pi^2} P_h(k) \tag{4.35}$$

is simply given by

$$\Delta_{h_1}^2 = \frac{H_\times^2}{\pi^2 M_{pl}^2} \left(\frac{a(\eta)}{a(\eta_\times)}\right)^{3\lambda\left(\sqrt{1+\mu^2}-1\right)} \tag{4.36}$$

[6]Again, if $\lambda = 0$ tensor modes remains constant outside the horizon, as in standard inflation.

where we re-introduced the Planck mass $M_{pl}^2 = 1/8\pi G$. This expression is valid for a single polarization of the tensor fluctuations. Therefore keeping in mind both the polarizations we might actually write down the correct expression for the primordial power spectrum predicted by our massive bigravity model

$$\Delta_T^2 = 2\Delta_{h_1}^2 = \frac{2H_\times^2}{\pi^2 M_{pl}^2}\left(\frac{a(\eta)}{a(\eta_\times)}\right)^{3\lambda\left(\sqrt{1+\mu^2}-1\right)} \tag{4.37}$$

This is going to be the quantity related with the today-observed gravitational wave energy density. In particular we will study the prediction of the model for different values of the parameters λ and μ^2 since they completely determine the dynamics. This eventually allows us to compute how many e-folds of inflation the coupling must be turned on to ensure that the energy density intersects the sensitivity curves of the detectors. Before discussing the phenomenology of the model we note that the above result for the power spectrum is in complete agreement with what we did in section 2.3.2: indeed, if we substitute $\lambda = 0$ in 4.37 we recover the scale invariant primordial power spectrum, constant on superhorizon scales.

4.3 Energy density

So far we computed the primordial spectrum on superhorizon regime predicted by the model introduced in this chapter. Besides proving the power spectrum amplification due to the coupling with the tachyon like massive field we are interested in the phenomenology of the model itself. Therefore the aim of this section is to connect the primordial spectrum with an observable quantity *i.e.* the energy density, which might be measured by different detectors. We know already that the intensity of a gravitational wave background can be characterized by the dimensionless energy density

$$\Omega_{gw}(k) \equiv \frac{1}{\rho_c}\frac{\mathrm{d}\rho_{gw}}{\mathrm{d}\log(k)} \tag{4.38}$$

where we denote with ρ_c the critical energy density

$$\rho_c = \frac{3H_0^2}{8\pi G} \tag{4.39}$$

while ρ_{gw} stands for the stochastic gravitational wave energy density, strictly connected with the primordial power spectrum.
In section 3.2 we already computed the today observed energy density starting from the primordial spectrum, and we took into account the modes that re-entered the horizon

during radiation domination, the latter being the cosmologically relevant ones since they match with the range of frequencies probed by detectors.
In particular we obtained the relation between Ω_{gw} and the primordial spectrum in eq. 3.23:

$$\Omega_{gw} = \frac{1}{12}\Omega_{rad}\left(\frac{g_{\star,0}}{g_\star(\eta_\times)}\right)^{1/3}\Delta_T^2 \tag{4.40}$$

In standard single field inflationary models the predicted energy density is very small, hence the detection of relic gravity waves is unlucky. However we saw in section 3.3 a new mechanism developed by [16] which relies on a non-attractor phase, and it allowed us to enhance the energy density, ensuring it crosses LISA, aLIGO and PTA sensitivity curves - see figure 3.4.
Here we might follow a similar approach for the model discussed in this chapter and we will see whether or not the energy density can be amplified to the desired level tested by the three detectors. As we said earlier we assume the coupling term - responsible for the enhancement - between the two fields to be dominant for a brief time interval, hence for few e-folds, during the inflationary phase. In other words, the modes at horizon exit have a constant power spectrum until the parameter λ is turned on: after that they evolve according to eq. 4.37 and fluctuations are amplified. Then the coupling si switched off and inflation proceeds with standard slow-roll evolution with constant power spectrum. Thus, only the modes that exit the horizon when the coupling is on might be enhanced on superhorizon scales.
Actually, keeping in mind what we just said, the power spectrum profile is given by

$$\Delta_T^2 = \frac{2H_\times^2}{\pi^2 M_{pl}^2} \times \begin{cases} 1 & a < a_i, \qquad \lambda = 0 \\ \left(\frac{a(\eta)}{a(\eta_i)}\right)^{3\lambda\left(\sqrt{1+\mu^2}-1\right)} & a_i < a < a_f, \quad \lambda \neq 0 \\ 1 & a > a_f, \qquad \lambda = 0 \end{cases} \tag{4.41}$$

where we denote with a_i and a_f the value of the scale factor before and after the growing phase respectively.
It is already evident one of the main differences with respect to the non-attractor approach discussed in chapter 3: here we see that the power spectrum falls down as soon as we turn off the coupling term, and the standard slow-roll primordial amplitude is recovered. On the other hand, if we recall the power spectrum evolution 3.57 predicted by the non-attractor model we see that in this case the spectrum remains constant after the growing phase: this means that even the modes that exit the horizon after the non-attractor regime might be amplified.

GW @	k [Mpc^{-1}]	$N_{estim.}$	$(\Omega_{gw}h_0^2)_{min}$
LISA	$10^{11} - 10^{14}$	$28.3 - 35.2$	4.5×10^{-12}
aLIGO	$10^{16} - 10^{17}$	$39.8 - 42.13$	3.2×10^{-6}
PTA	$10^{6} - 10^{8}$	$16.8 - 21.4$	0.9×10^{-10}

[h!]

Table 4.1: First column: list of different interferometers under exam. Second columns: observational windows in terms of the order of magnitude of the wave number of the primordial modes. Third column: estimate number of e-folds at which those modes exit the horizon. Fourth column: minimum value of gravitational wave amplitude detectable by each experiment.

In essence this was possible thanks to the non canonical kinetic terms of the model: the time dependent function $\mathcal{G}_T(t), \mathcal{F}_T(t)$ have a different time profile before and after the non-attractor regime, hence we had the chance to keep constant, but still amplified, the power spectrum at the end of the growing phase.

After these considerations we might actually focus on the gravitational wave energy density: keeping in mind 4.40 and the expression of the power spectrum 4.41 we have

$$\Omega_{gw} = \frac{1}{6}\Omega_{rad}\left(\frac{g_{\star,0}}{g_\star(\eta_\times)}\right)^{1/3}\frac{H_\times^2}{\pi^2 M_{pl}^2} \times \begin{cases} 1 & a < a_i, \qquad \lambda = 0 \\ \left(\frac{a(\eta)}{a(\eta_i)}\right)^{3\lambda\left(\sqrt{1+\mu^2}-1\right)} & a_i < a < a_f, \quad \lambda \neq 0 \\ 1 & a > a_f, \qquad \lambda = 0 \end{cases} \tag{4.42}$$

We note that the effective growing rate of the fluctuations depends on the values of the parameters λ and μ^2. Thus we expect that this mechanism ensures that the energy density really intersect the detectors sensitivity curves with just few e-folds of growing phase. The latter depends explicitly on the values of the two parameters, as we see in a while.

Before going through the direct computation of the number of necessary e-folds for each detectors, we recall the observational windows of the experiments under exam, together with the minimum value of gravitational wave energy density detectable by each of them. These results, already encountered in 3.4, are summarised in table 4.1, reported here for the sake of clarity.

Finally we might estimate the duration of the growing regime in order to get the desired amplification. This can be easily computed keeping in mind the e-folds number definition

$$\mathrm{d}N = \mathrm{d}\ln(a) = H\mathrm{d}t \qquad \Rightarrow \qquad N = \log\left(\frac{a_f}{a_i}\right) \tag{4.43}$$

and taking into account the energy density value $\Omega_{gw}h_0^2 \sim 10^{-19}$ predicted by usual slow-roll inflation before the coupling is turned on. Then the number of necessary e-folds ΔN is given by

$$\left(\frac{a_f}{a_i}\right)^{3\lambda\left(\sqrt{1+\mu^2}-1\right)} = e^{3\lambda\left(\sqrt{1+\mu^2}-1\right)\Delta N} = \frac{(\Omega_{gw}h_0^2)_{min}}{\Omega_{gw}h_0^2} = \frac{(\Omega_{gw}h_0^2)_{min}}{10^{-19}} \tag{4.44}$$

Hence, we get

$$\Delta N = \frac{1}{3\lambda\left(\sqrt{1+\mu^2}-1\right)}\ln\left(\frac{(\Omega_{gw}h_0^2)_{min}}{10^{-19}}\right) \tag{4.45}$$

where with $(\Omega_{gw}h_0^2)_{min}$ we denote again the minimum value of energy density detectable by each experiments.
Therefore, if we take into account the fourth column of table 4.1, the above formula gives us the value ΔN for the three different detectors. Moreover we might actually fix the value $N_i = N_{estim} - \Delta N$ at which the coupling term should be turned on to ensure te amplification of the energy density at the desired frequencies. However, while for the non-attractor regime of section 3.4 the growing rate was fixed as

$$\left(\frac{a_f}{a_i}\right)^6 = e^{6\Delta N} \tag{4.46}$$

in this case it depends on the values of the free parameters λ and μ^2. Indeed if choose

$$\lambda = 1 \qquad \mu^2 = 8 \tag{4.47}$$

we have the same growing rate of the non-attractor model, *i.e.*

$$\Omega_{gw} = \frac{1}{6}\Omega_{rad}\left(\frac{g_{\star,0}}{g_\star(\eta_\times)}\right)^{1/3}\frac{H_\times^2}{\pi^2 M_{pl}^2} \times \begin{cases} 1 & a < a_i, \qquad \lambda = 0 \\ \left(\frac{a(\eta)}{a(\eta_i)}\right)^6 & a_i < a < a_f, \quad \lambda \neq 0 \\ 1 & a > a_f, \qquad \lambda = 0 \end{cases} \tag{4.48}$$

and the number of e-folds ΔN, according to 4.45, is given by

$$\Delta N = \frac{1}{6}\ln\left(\frac{(\Omega_{gw}h^2)_{min}}{10^{-19}}\right) \tag{4.49}$$

GW @	ΔN	N_i
LISA	2.9	$25.4 - 32.3$
aLIGO	5.2	$34.6 - 36.9$
PTA	3.4	$13.4 - 18$

Table 4.2: First column: estimated duration of the growing phase. Second column: number of e-folds at which the coupling term should have turned on. Here we assumed $\lambda = 1$ and $\mu^2 = 8$.

In particular this gives us the values of ΔN and N_i reported in table 4.2, in complete analogy with table 3.2.
We conclude that the values 4.47 give us the same results of the previous model.
On the other hand, if we choose different values, such as

$$\lambda = 1 \qquad \mu^2 = 15 \tag{4.50}$$

we get a faster growing rate on superhorizon scales: with these values the gravitational wave energy density profile is given by

$$\Omega_{gw} = \frac{1}{6}\Omega_{rad}\left(\frac{g_{\star,0}}{g_\star(\eta_\times)}\right)^{1/3}\frac{H_\times^2}{\pi^2 M_{pl}^2} \times \begin{cases} 1 & a < a_i, \quad \lambda = 0 \\ \left(\frac{a(\eta)}{a(\eta_i)}\right)^9 & a_i < a < a_f, \quad \lambda \neq 0 \\ 1 & a > a_f, \quad \lambda = 0 \end{cases} \tag{4.51}$$

while eq. 4.45 gives us the estimated number of e-folds necessary to get the desired amplification

$$\Delta N = \frac{1}{9}\ln\left(\frac{(\Omega_{gw}h^2)_{min}}{10^{-19}}\right) \tag{4.52}$$

Again, taking into account the fourth column of table 4.1 we find the values of ΔN and N_i reported in table 4.3, corresponding to the parameters choice of eq. 4.50:
Here we see that this second choice of the parameters λ and μ^2 gave us a faster growing rate, therefore the number of necessary e-folds ΔN to ensure that the energy density intersects the sensitivity curves is slightly decreased. Physical constraints on the values of the two free parameters might be obtained from specific model of massive gravity and bigravity, and this actually goes behind the aim of this work.

GW @	ΔN	N_i
LISA	1.96	$26.3 - 33.2$
aLIGO	3.4	$36.4 - 38.7$
PTA	2.3	$14.5 - 19.1$

Table 4.3: First column: estimated duration of the growing phase. Second column: number of e-folds at which the coupling term should have turned on. Here we assumed $\lambda = 1$ and $\mu^2 = 15$.

4.4 Outcomes

In the previous sections we discussed the effects of an interaction term between the massless graviton and a spin-2 massive fields. In particular we showed that if the coupling is turned on - even for a brief time interval in between standard slow-roll inflation - it is possible to enhance the primordial power spectrum, and consequently the today observed energy density up to the magnitude probed by the detectors. In particular, we showed that this is possible only if we assume

$$m^2 < H^2\lambda^2 \tag{4.53}$$

where m denotes as usually the h_2 field mass. Then, we examined for how many e-folds of inflation the parameter λ must be different from zero in order to have the desired amplification and the results are summarized in table 4.3, where we assumed $\lambda = 1$ and $\mu^2 = 15$.
In this section we try to plot the profile of the energy density 4.42 for the above values of the free parameters.
The performance of gravitational wave detectors have already been discussed in section 3.5, where we studied the possible noise sources and we provided good analytical fit for the sensitivity curve of LISA, aLIGO and PTA detectors.
As a final step we can actually plot both the detectors and sources curves in the same graph using the developed standard protocol[7] We will use the analytical fit for the detectors sensitivity curves introduced in chapter 3, while the gravitational energy density profile of eq. 4.51 might be expressed as a function of the frequency with the following fit

$$\Omega_{gw}(f)h_0^2 = 10^{-19}\left(1 + \frac{(40\pi 10^{16} f)^9 e^{-9N_i}}{1 + e^{f/f_c}}\right) \tag{4.54}$$

[7]We expressed all the quantities in term of the energy denity as a function of the frequency.

Here we denote with N_i the number of e-folds at which the coupling term should be turned on[8]. This value is given in the second column ot table 4.3 for each detector. While with f_c we denote a cut-off frequency which corresponds to the frequency associated with the minimum value of gravitational wave amplitude detectable by each experiment.
Arguably the energy density analytical fit is merely phenomenological and it does not descend from specific models of massive gravity and bigravity. However it gives us a good example of amplified power spectrum with a profile that evolves in time according to eq 4.51.
We report in the next paragraphs the plot of the sensitivity curve together with the analytical fit 4.54 for each detector.

LISA

Actually the LISA sensitivity curve, expressed in term of the energy density is

$$\Omega_{LISA}(f)h_0^2 = 6\pi^2 f^3 \times 10^{34}\frac{10}{3L^2}\left(P_{oms}(f) + 2(1+\cos^2(f/f_*))\frac{4P_{acc}(f)}{(2\pi f)^4}\right)\left(1+\frac{6}{10}\left(\frac{f}{f_*}\right)^2\right) \tag{4.55}$$

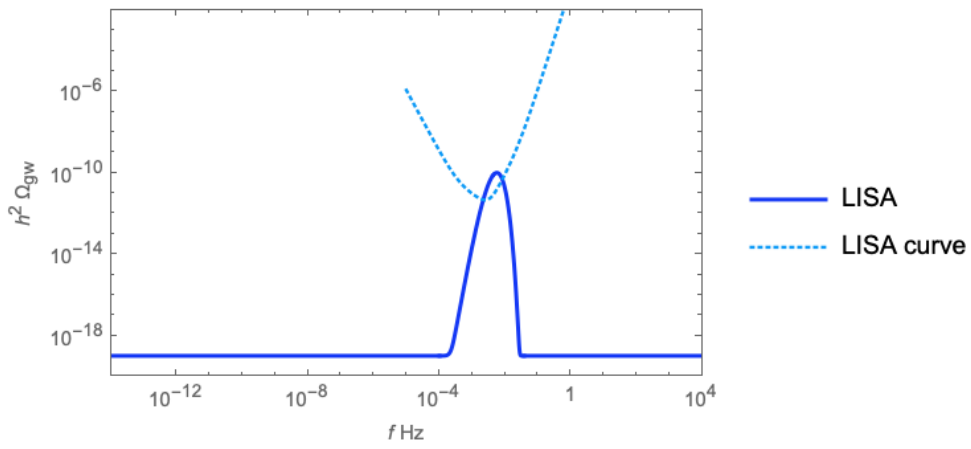

Figure 4.1: Sensitivity curve and amplified power spectrum of LISA interferometer. The dashed curves stand for the analytical fit of the sensitivity while the solid curves denote the enhanced primordial energy density.

[8]We are assuming inflation to end at $N = 60$ e-folds.

aLIGO

For aLIGO interferometer the sensitivity curve is well fitted by

$$\Omega_{aLIGO}(f)h_0^2 = 10^{-15} \times 6\pi^2 f^3 \left[x^{-4.14} - 5x^2 + \frac{111(1 - x^2 + 0.5x^4)}{1 + 0.5x^2} \right] \tag{4.56}$$

where the variable $x = f/f_0$ is a dimensionless frequency, while $f_0 = 215$ Hz. We remind the reader that this fit holds true for frequencies above the cutoff $f_s = 20$ Hz. Indeed, for data analysis purposes the noise is assumed to be essentially divergent for frequencies $f \leq f_s$.

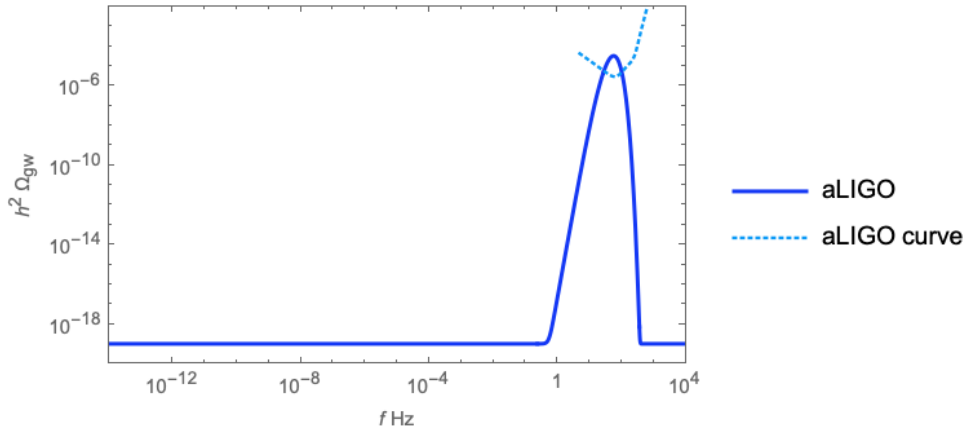

Figure 4.2: Sensitivity curve and amplified power spectrum for aLIGO interferometer. The dashed curves stand for the analytical fit of the sensitivity, while the solid curves denote the enhanced primordial energy density.

PTA

A good analytical fit for the PTA curve is given by

$$\Omega_{PTA}(f)h_0^2 = 10^{-10} \times \mathcal{H}(f_{cutoff} - f)\left(\frac{f}{f_{cutoff}}\right)^{-26} + 10^{31} \times \mathcal{H}(f - f_{cutoff})f^5 \tag{4.57}$$

Here, we considered a network of 20 pulsars, assuming a cadence of the measurements of $1/\Delta t = 20$ yr^{-1} and a root mean square error in each timing residual of $\sigma = 100$ ns.

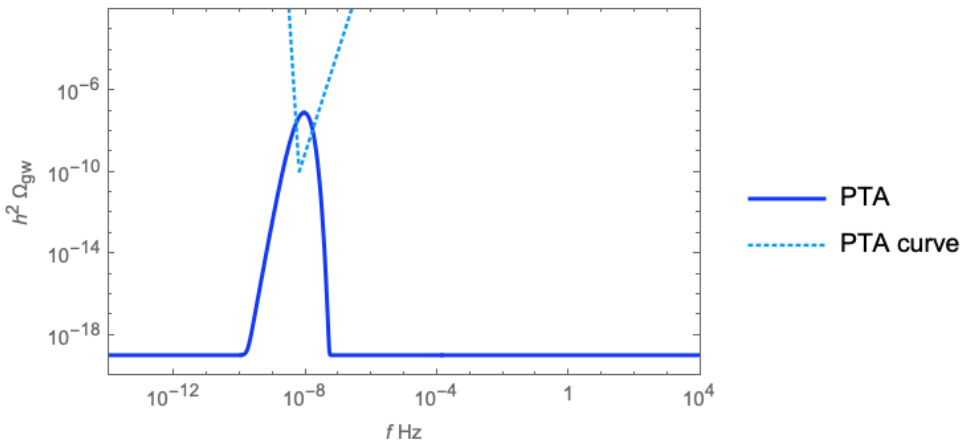

Figure 4.3: Sensitivity curve and amplified power spectrum of PTA detectors. The dashed curves stand for the analytical fit of the sensitivity while the solid curves denote the enhanced primordial energy density.

Figures 4.1, 4.2 and 4.3 explicitly shows us that the energy density, determined by the primordial power spectrum, can be enhanced up to the orders of magnitude probed by the three detectors.
We chose arbitrary values for the free parameters, *i.e.*

$$\lambda = 1 \qquad \mu^2 = 15 \tag{4.58}$$

which give us a faster energy density amplification than the non-attractor model.
However in this case the energy density rapidly falls down as soon as we turn off the coupling term: therefore we might enhance only those modes that exit the horizon when the interaction term is dominant. Finally, we highlight that even in this scenario the detectability of relic gravitational waves might be achieved if coupling constant λ is non-vanishing for a sufficiently large number of e-folds during inflation.

Conclusions

The goal of this thesis was the study of primordial fluctuations of the tensor sector produced during inflation and their relation with late-time observables.
We investigated two new mechanisms which allow us to enhance the primordial spectrum on superhorizon scales. Here we report the main results we obtained and suggest potential future prospects.

This dissertation studies the phenomenological aspects of inflation and its ability to solve the standard big bang drawbacks. We gave special attention to the predicted stochastic gravitational wave background and its possible detectability. Indeed, a potential detection would give us a completely new method to investigate the dynamics of the early universe, with an exclusive access at ultra-high energy scales, otherwise inaccessible with standard experiments. This constitutes the main reason why the scientific community is involved with large effort in the construction of advanced gravitational wave detectors. However we showed that the predicted energy density by standard slow-roll inflation is very small, and direct detectability of stochastic background is so far unlikely.

The first purpose of this thesis was to investigate new models that allow us to amplify the tensor perturbations on superhorizon scales. We focused on two different mechanism: firstly we discussed a non-attractor regime based on non-canonical kinetic term for the inflaton field. Then we proposed a new model which relies on the existence of a second massive spin-2 field coupled with the standard massless tensor fluctuations.
For both these cases we assumed the breakdown of standard slow-roll inflation for a brief time interval, during which the non-attractor phase and the presence of a coupling term respectively sets in.
We analysed in detail the phenomenology predicted by these two mechanisms and we showed that the primordial power spectrum of the tensor sector may be amplified on superhorizon scales up to the desired level for both the models.

In chapter 3 we focused on the non-attractor mechanism and we investigated how many e-folds of transitory non-attractor inflation are necessary in order to amplify the would-

be decaying mode up to the energy density scales accessible with LISA, aLIGO and PTA detectors.
Then in chapter 4 we discussed the interacting model and we showed that the primordial power spectrum might be enhanced if we assume the massive field to be tachyon-like. In particular we obtained specific constrains on the value of the mass parameter. We then turned into the phenomenological analysis of the model: in analogy with what we did for non-attractor model, we computed the number of e-folds of interaction between the two field required to ensure that the primordial spectrum crosses the sensitivity curves. While in the non-attractor regime the spectrum enhancement was proportional to the sixth power of the scale factor, in the interacting model the growing rate depends on the strength of the interaction constant and on the value of the mass parameter. The latter might be constrained from specific model of massive gravity and bigravity, which may be taken into account in future projects. In this work we considered fictitious values for the two parameter: first we showed that is always possible to obtain a growing rate analogous to the non-attractor model, hence like the sixth power of the scale factor. Then we considered different values of the parameters in order to obtain a faster growing profile. In this case the number of necessary e-folds to get the desired amplification was slightly smaller than in the previous situation.

In conclusion, we were able to correctly amplify the tensor primordial spectrum for both the models. However, while the non-attractor regime has a fixed growing rate, the interacting model admits different time evolution, depending on the values of the free parameters of the theory. Among this, another main difference between the two model is given by the power spectrum behaviour once the growing phase ends and standard slow-roll is restored: while for the non-attractor regime the power spectrum remains amplified, but constant, even after the end of the non-attractor phase, in the interacting model the primordial spectrum falls down as soon as we turn off the coupling term, and standard slow-roll spectrum amplitude is restored. This means that only the modes that exit the horizon when the coupling term is on might be amplified. On the other hand, in the non-attractor model even the modes that exit the horizon after the non-attractor phase could in principle be amplified.

In the future it will be interesting to further develop these two models and complete this study by building concrete and realistic scenarios of inflation where the two amplification mechanism might be inserted in.
The comprehension of the early universe physics is an ongoing adventure and we hope to face this challenge together with all the curious and interested people.

Appendix A

Diagonalization Procedure

The starting point of the model we developed in chapter 4 is the lagrangian 4.4 for the two tensor field system. The latter can be obtained starting from a more general lagrangian with non-canonical kinetic and mass terms

$$\begin{aligned}\mathcal{L} = a^3(t)\Big[&\frac{1}{2}\dot{h}_1(t)^2 + \frac{1}{2}\dot{h}_2(t)^2 + \mu\dot{h}_1(t)\dot{h}_2(t) + \lambda H\dot{h}_1(t)h_2(t) + \\ &+ \lambda_1 h_1(t)\dot{h}_2(t) - \frac{1}{2}m^2 h_2(t)^2 + \sigma h_1(t)h_2(t)\Big]\end{aligned} \tag{A.1}$$

where we introduce the new parameters μ for the non-canonical kinetic term, σ for the mass term and λ_1, λ as coupling constant.
We ask ourselves if this general lagrangian can be further simplified without affecting the dynamics of the system, hence with a diagonalization process.
We start studying the simplest term of A.1, which is the interaction lagrangian

$$\mathcal{L}_{int} = \lambda H\dot{h}_1(t)h_2(t) + \lambda_1 h_1(t)\dot{h}_2(t) \tag{A.2}$$

The second term on the r.h.s can be reabsorbed with a integration by part if we re-define the coupling constant and we obtain, up to a total derivative, the standard interaction lagrangian used in eq. 4.4

$$\mathcal{L}_{int} = \tilde{\lambda} H\dot{h}_1(t)h_2(t), \qquad \tilde{\lambda} = \lambda - \frac{\lambda_1}{H} \tag{A.3}$$

A more interesting term is the non-canonical kinetic lagrangian

$$\mathcal{L}_{kin} = \frac{1}{2}\dot{h}_1(t)^2 + \frac{1}{2}\dot{h}_2(t)^2 + \mu\dot{h}_1(t)\dot{h}_2(t) \tag{A.4}$$

The latter can be diagonalized with an orthogonal transformation, as we show in the next steps. The non diagonal kinetic matrix has the form

$$K = \frac{1}{2}\begin{bmatrix} 1 & \mu \\ \mu & 1 \end{bmatrix} \tag{A.5}$$

with the following eigenvalues and eigenvector

$$\xi_1 = \frac{1-\mu}{2}, \quad \xi_2 = \frac{1+\mu}{2} \qquad\qquad \boldsymbol{v_1} = \frac{1}{\sqrt{2}}\begin{bmatrix} -1 \\ 1 \end{bmatrix}, \quad \boldsymbol{v_2} = \frac{1}{\sqrt{2}}\begin{bmatrix} 1 \\ 1 \end{bmatrix} \tag{A.6}$$

Therefore, we can diagonalize the kinetic matrix with the orthogonal transformation given by the matrix of the eigenvectors

$$K_{diag} = U^T K U = \frac{1}{2}\begin{bmatrix} 1-\mu & 0 \\ 0 & 1+\mu \end{bmatrix}, \qquad\qquad U = \frac{1}{\sqrt{2}}\begin{bmatrix} -1 & 1 \\ 1 & 1 \end{bmatrix} \tag{A.7}$$

We have found the diagonal form of the kinetic matrix and we can finally re-define the fields $h_1(t)$ and $h_2(t)$ using the matrices U and U^T in order to get the standard kinetic term. Hence, we define two new field $w_1(t)$ and $w_2(t)$ such that

$$\begin{aligned} h_1(t) &\to \frac{-w_1(t) + w_2(t)}{\sqrt{2(1-\mu)}} \\ h_2(t) &\to \frac{+w_1(t) + w_2(t)}{\sqrt{2(1+\mu)}} \end{aligned} \tag{A.8}$$

where we rescaled the two fields with the coefficient $\sqrt{1-\mu}$ and $\sqrt{1+\mu}$ respectively in order to get the correct $1/2$ coefficient in front of the kinetics terms.
Substituting these expression into the general lagrangian A.1 we get

$$\begin{aligned} \mathcal{L} = \frac{1}{4(-1+\mu^2)} a^3(t) \Big[& 2(-1+\mu^2)\big(\dot{w}_1(t)^2 + \dot{w}_2(t)^2\big) + (1+\mu)(m^2+2\sigma)w_1(t)^2 - \\ & - (-1+\mu)(m^2-2\sigma)w_2(t)^2 + 2H\lambda w_2(t)\big(\sqrt{1-\mu^2}\dot{w}_1(t) + (1-\mu)\dot{w}_2(t)\big) + \\ & + 2w_1(t)\big(H\lambda(1+\mu)\dot{w}_1(t) + \sqrt{1-\mu^2}(m^2 w_2(t) - H\lambda\dot{w}_2(t)\big) \Big] \end{aligned} \tag{A.9}$$

We finally obtained the desired canonical kinetic term and we can now focus on the mass matrix and diagonalized it. According to A.9 the latter matrix is given by

$$M = \frac{1}{4(-1+\mu^2)}\begin{bmatrix} (1+\mu)(m^2+2\sigma) & m^2\sqrt{1-\mu^2} \\ m^2\sqrt{1-\mu^2} & (1-\mu)(m^2-2\sigma) \end{bmatrix} \tag{A.10}$$

Given the matrix M, we ask ourselves what rotation needs to be performed such that M is diagonalized

$$M_{diag} = R^T M R, \qquad R = \begin{bmatrix} \cos(\theta) & -\sin(\theta) \\ \sin(\theta) & \cos(\theta) \end{bmatrix} \tag{A.11}$$

It is easy, but a bit tedious, to obtain the expression for M_{diag} and we will write down the final result only. Imposing the anti-diagonal term of M_{diag} to vanish, we obtain the following condition on the value of the angle θ

$$\theta = \frac{1}{2}\arctan\left(\frac{m^2\sqrt{1-\mu^2}}{m^2\mu - 3H^2\lambda + 2\sigma}\right) \tag{A.12}$$

Therefore, substituting the latter into the explicit expression for M_{diag} we finally obtain

$$M_{diag} = \frac{3H^2\lambda - 2\sigma}{4}\begin{bmatrix} \alpha_1 & 0 \\ 0 & \alpha_2 \end{bmatrix} \tag{A.13}$$

where we defined

$$\begin{aligned} \alpha_1 &:= \frac{1}{\left(\mu + \sqrt{1 - \frac{m^4(-1+\mu^2)}{(m^2\mu+2\sigma-3H^2\lambda)^2}}\right) - 4m^2\left(1 + \mu\sqrt{1 - \frac{m^4(-1+\mu^2)}{(m^2\mu+2\sigma-3H^2\lambda)^2}}\right)} \\ \alpha_2 &:= \frac{1}{\left(\mu - \sqrt{1 - \frac{m^4(-1+\mu^2)}{(m^2\mu+2\sigma-3H^2\lambda)^2}}\right) + 4m^2\left(1 - \mu\sqrt{1 - \frac{m^4(-1+\mu^2)}{(m^2\mu+2\sigma-3H^2\lambda)^2}}\right)} \end{aligned} \tag{A.14}$$

It is now straightforward to obtain the final form of the lagrangian: indeed, we have to introduce two new field $\gamma_1(t)$ and $\gamma_2(t)$ using the matrices R , R^T and the value of θ previously found. Then, substituting these new fields in A.9 we finally get the lagrangian

in its diagonal form

$$\begin{aligned}\mathcal{L} = \frac{a(t)^3}{4\left(1-\mu^2\right)^{3/2}}\Bigg\{ &- \sqrt{1-\mu^2}\Bigg[m^2\left(\mu\sqrt{1-\frac{\left(\mu^2-1\right)m^4}{\left(-3H^2\lambda+\mu m^2+2\sigma\right)^2}}+1\right)- \\ &- \left(3H^2\lambda-2\sigma\right)\left(\sqrt{1-\frac{\left(\mu^2-1\right)m^4}{\left(-3H^2\lambda+\mu m^2+2\sigma\right)^2}}+\mu\right)\Bigg]\gamma_1(t)^2+ \\ &+ \sqrt{1-\mu^2}\Bigg[m^2\left(\mu\sqrt{1-\frac{\left(\mu^2-1\right)m^4}{\left(-3H^2\lambda+\mu m^2+2\sigma\right)^2}}-1\right)- \\ &- \left(3H^2\lambda-2\sigma\right)\left(\sqrt{1-\frac{\left(\mu^2-1\right)m^4}{\left(-3H^2\lambda+\mu m^2+2\sigma\right)^2}}-\mu\right)\Bigg]\gamma_2(t)^2+ \\ &+ 4H\lambda\left(\mu^2-1\right)\gamma_2(t)\dot{\gamma}_1(t)+2\left(1-\mu^2\right)^{3/2}\left(\dot{\gamma}_1(t)^2+\dot{\gamma}_2(t)^2\right)\Bigg\}\end{aligned} \tag{A.15}$$

It is always possible to rewrite this expression as in the standard form used in chapter 4

$$\mathcal{L} = a^3(t)\left[\frac{1}{2}\dot{\gamma}_1(t)^2+\frac{1}{2}\dot{\gamma}_2(t)^2-\frac{1}{2}m_1^2\gamma_1(t)^2-\frac{1}{2}m_2^2\gamma_2(t)^2+\lambda H\dot{\gamma}_1(t)\gamma_2(t)\right] \tag{A.16}$$

where we rescaled the parameter in order to simplify the expression.It is worthwhile to stress out that the kinetic term are invariant under the transformation of the fields into the mass eigenstates: this was possible because we first reduced to the canonical form the kinetic term, and after that we diagonalized the mass matrix. Eventually, after the diagonalization procedure, we end up with two massive fields, but it is always possible to set $m_1 \ll m_2$ and neglect the mass of one of the two field.

Appendix B

General Solutions of the Equation of Motion

Here we present the general solutions of the equation of motion 4.5a and 4.5b derived from the two field system lagrangian 4.4. For the massless field $h_1(t)$ we have

$$h_1(t) = -\frac{9e^{-3Ht-\frac{1}{2}\left(\sqrt{H^2(9-4\lambda^2)-4m^2}-3H\right)t}\lambda c_3 H^3}{2\left(m^2+H^2\lambda^2\right)\sqrt{H^2\left(9-4\lambda^2\right)-4m^2}}$$

$$+\frac{9e^{\frac{1}{2}t\left(3H+\sqrt{H^2(9-4\lambda^2)-4m^2}\right)-3Ht}\lambda c_3 H^3}{2\left(m^2+H^2\lambda^2\right)\sqrt{H^2\left(9-4\lambda^2\right)-4m^2}}$$

$$+\frac{\lambda^2 c_1 H^2}{m^2+H^2\lambda^2}-\frac{e^{-3Ht-\frac{1}{2}\left(\sqrt{H^2(9-4\lambda^2)-4m^2}-3H\right)t}\lambda^2 c_2 H^2}{\left(m^2+H^2\lambda^2\right)\sqrt{H^2\left(9-4\lambda^2\right)-4m^2}}$$

$$+\frac{e^{\frac{1}{2}t\left(3H+\sqrt{H^2(9-4\lambda^2)-4m^2}\right)-3Ht}\lambda^2 c_2 H^2}{\left(m^2+H^2\lambda^2\right)\sqrt{H^2\left(9-4\lambda^2\right)-4m^2}}$$

$$+\frac{3e^{-3Ht-\frac{1}{2}\left(\sqrt{H^2(9-4\lambda^2)-4m^2}-3H\right)t}\lambda c_3 H^2}{2\left(m^2+H^2\lambda^2\right)}$$

$$+\frac{3e^{\frac{1}{2}t\left(3H+\sqrt{H^2(9-4\lambda^2)-4m^2}\right)-3Ht}\lambda c_3 H^2}{2\left(m^2+H^2\lambda^2\right)}-\frac{3\lambda c_3 H^2}{m^2+H^2\lambda^2}$$

$$
\begin{aligned}
&- \frac{3e^{-3Ht-\frac{1}{2}\left(\sqrt{H^2(9-4\lambda^2)-4m^2}-3H\right)t}\lambda c_4 H^2}{2\left(m^2+H^2\lambda^2\right)\sqrt{H^2\left(9-4\lambda^2\right)-4m^2}} \\
&+ \frac{3e^{\frac{1}{2}t\left(3H+\sqrt{H^2(9-4\lambda^2)-4m^2}\right)-3Ht}\lambda c_4 H^2}{2\left(m^2+H^2\lambda^2\right)\sqrt{H^2\left(9-4\lambda^2\right)-4m^2}} \\
&+ \frac{e^{-3Ht-\frac{1}{2}\left(\sqrt{H^2(9-4\lambda^2)-4m^2}-3H\right)t}m^2\lambda c_3 H}{\left(m^2+H^2\lambda^2\right)\sqrt{H^2\left(9-4\lambda^2\right)-4m^2}} \\
&- \frac{e^{\frac{1}{2}t\left(3H+\sqrt{H^2(9-4\lambda^2)-4m^2}\right)-3Ht}m^2\lambda c_3 H}{\left(m^2+H^2\lambda^2\right)\sqrt{H^2\left(9-4\lambda^2\right)-4m^2}} \\
&+ \frac{e^{-3Ht-\frac{1}{2}\left(\sqrt{H^2(9-4\lambda^2)-4m^2}-3H\right)t}\lambda c_4 H}{2\left(m^2+H^2\lambda^2\right)} \\
&+ \frac{e^{\frac{1}{2}t\left(3H+\sqrt{H^2(9-4\lambda^2)-4m^2}\right)-3Ht}\lambda c_4 H}{2\left(m^2+H^2\lambda^2\right)} \\
&- \frac{\lambda c_4 H}{m^2+H^2\lambda^2} + \frac{m^2 c_1}{m^2+H^2\lambda^2} - \frac{e^{-3Ht}m^2\lambda c_3}{3\left(m^2+H^2\lambda^2\right)} \\
&+ \frac{m^2\lambda c_3}{3\left(m^2+H^2\lambda^2\right)} - \frac{e^{-3Ht}m^2 c_2}{3\left(m^2+H^2\lambda^2\right)H} + \frac{m^2 c_2}{3\left(m^2+H^2\lambda^2\right)H}
\end{aligned}
\tag{B.1}
$$

On the other hand, for the massive field $h_2(t)$ we obtain

$$h_2(t) = -\frac{3e^{\frac{3Ht}{2}-\frac{1}{2}t\left(6H+\sqrt{H^2(9-4\lambda^2)-4m^2}\right)}\lambda^2 c_3 H^3}{\left(m^2+H^2\lambda^2\right)\sqrt{H^2\left(9-4\lambda^2\right)-4m^2}}$$

$$-\frac{3e^{\frac{3Ht}{2}-\frac{1}{2}t\left(6H+\sqrt{H^2(9-4\lambda^2)-4m^2}\right)}\lambda c_2 H^2}{2\left(m^2+H^2\lambda^2\right)\sqrt{H^2\left(9-4\lambda^2\right)-4m^2}}$$

$$+\frac{3e^{\frac{3Ht}{2}-\frac{1}{2}\left(6H+\sqrt{H^2(9-4\lambda^2)-4m^2}\right)t+\sqrt{H^2(9-4\lambda^2)-4m^2}t}\lambda^2 c_3 H^3}{\left(m^2+H^2\lambda^2\right)\sqrt{H^2\left(9-4\lambda^2\right)-4m^2}}$$

$$-\frac{e^{\frac{3Ht}{2}-\frac{1}{2}t\left(6H+\sqrt{H^2(9-4\lambda^2)-4m^2}\right)}\lambda^2 c_4 H^2}{\left(m^2+H^2\lambda^2\right)\sqrt{H^2\left(9-4\lambda^2\right)-4m^2}}$$

$$+\frac{3e^{\frac{3Ht}{2}-\frac{1}{2}\left(6H+\sqrt{H^2(9-4\lambda^2)-4m^2}\right)t+\sqrt{H^2(9-4\lambda^2)-4m^2}t}\lambda c_2 H^2}{2\left(m^2+H^2\lambda^2\right)\sqrt{H^2\left(9-4\lambda^2\right)-4m^2}}$$

$$-\frac{e^{\frac{3Ht}{2}-\frac{1}{2}t\left(6H+\sqrt{H^2(9-4\lambda^2)-4m^2}\right)}\lambda c_2 H}{2\left(m^2+H^2\lambda^2\right)}$$

$$+\frac{e^{\frac{1}{2}t\sqrt{H^2(9-4\lambda^2)-4m^2}-\frac{1}{2}t\left(6H+\sqrt{H^2(9-4\lambda^2)-4m^2}\right)}\lambda^2 c_3 H^2}{m^2+H^2\lambda^2}$$

$$-\frac{3e^{\frac{3Ht}{2}-\frac{1}{2}t\left(6H+\sqrt{H^2(9-4\lambda^2)-4m^2}\right)}m^2 c_3 H}{2\left(m^2+H^2\lambda^2\right)\sqrt{H^2\left(9-4\lambda^2\right)-4m^2}}$$

$$+\frac{e^{\frac{3Ht}{2}-\frac{1}{2}\left(6H+\sqrt{H^2(9-4\lambda^2)-4m^2}\right)t+\sqrt{H^2(9-4\lambda^2)-4m^2}t}\lambda^2 c_4 H^2}{\left(m^2+H^2\lambda^2\right)\sqrt{H^2\left(9-4\lambda^2\right)-4m^2}}$$

$$+\frac{e^{\frac{3Ht}{2}-\frac{1}{2}t\left(6H+\sqrt{H^2(9-4\lambda^2)-4m^2}\right)}m^2 c_3}{2\left(m^2+H^2\lambda^2\right)}$$

$$
\begin{aligned}
&+\frac{e^{\frac{1}{2}t\sqrt{H^2(9-4\lambda^2)-4m^2}-\frac{1}{2}t\left(6H+\sqrt{H^2(9-4\lambda^2)-4m^2}\right)}\lambda c_2 H}{m^2+H^2\lambda^2}\\
&-\frac{e^{\frac{3Ht}{2}-\frac{1}{2}t\left(6H+\sqrt{H^2(9-4\lambda^2)-4m^2}\right)}m^2 c_4}{\left(m^2+H^2\lambda^2\right)\sqrt{H^2\left(9-4\lambda^2\right)-4m^2}}\\
&-\frac{e^{\frac{3Ht}{2}-\frac{1}{2}\left(6H+\sqrt{H^2(9-4\lambda^2)-4m^2}\right)t+\sqrt{H^2(9-4\lambda^2)-4m^2}t}\lambda c_2 H}{2\left(m^2+H^2\lambda^2\right)}\\
&+\frac{3e^{\frac{3Ht}{2}-\frac{1}{2}\left(6H+\sqrt{H^2(9-4\lambda^2)-4m^2}\right)t+\sqrt{H^2(9-4\lambda^2)-4m^2}t}m^2 c_3 H}{2\left(m^2+H^2\lambda^2\right)\sqrt{H^2\left(9-4\lambda^2\right)-4m^2}}\\
&+\frac{e^{\frac{3Ht}{2}-\frac{1}{2}\left(6H+\sqrt{H^2(9-4\lambda^2)-4m^2}\right)t+\sqrt{H^2(9-4\lambda^2)-4m^2}t}m^2 c_3}{2\left(m^2+H^2\lambda^2\right)}\\
&+\frac{e^{\frac{3Ht}{2}-\frac{1}{2}\left(6H+\sqrt{H^2(9-4\lambda^2)-4m^2}\right)t+\sqrt{H^2(9-4\lambda^2)-4m^2}t}m^2 c_4}{\left(m^2+H^2\lambda^2\right)\sqrt{H^2\left(9-4\lambda^2\right)-4m^2}}
\end{aligned}
\tag{B.2}
$$

Acknowledgements

There are many important people with whom I shared this amazing journey which I would like to thanks. First of all I want to thanks Prof. Michele Cicoli for his support and encouragement on this project. Then, it is a pleasure to thanks Prof. Gianmassimo Tasinato, who introduced me to world of early universe cosmology.
He helped me with patient, giving constant advice. I really appreciate his time and I am grateful for his scientific interest in this work.
I would like to express my deepest gratitude to my Mom and Dad who guided me in this five years path, putting their faith in me. They gave me the opportunity to study and always helped me with enthusiasm since I was a child.
I can't help to thanks my friends, with whom I spent beautiful years. I learned a lot from them and they delighted me with jokes even when it was time to get back to work. It is a pleasure to thanks the *Band of Physicist* who made my work environment a very kind one. A special thanks to the *BDSP family* for their constant presence and for all the dinner parties organised together among these year and all the ones to come.
Finally, thanks to *K.* for being awesome.

Bibliography

[1] A. Riotto, *Inflation and the Theory of Cosmological Perturbation*, (2002)

[2] D. Baumann, *TASI Lectures on Inflation*, arXiv:0907.5424v2, (2002)

[3] Dimitry S. Gorbunov, Valery A. Rubakov, *Introduction to the Theory of the Early Universe*, (2011)

[4] V. Mukhanov *Physical Foundation of Cosmology*, Cambridge University Press, (2005)

[5] S. Dodelson, *Modern Cosmology*, Academic Press, (2003)

[6] D. Baumann, *The Physics of Inflation*

[7] D. Baumann, *Inflation and String Theory*, Cambridge University Press, (2005)

[8] S. Dodelson, W. H. Kinney, E. W. Kolb,*Cosmic microwave background measurements can discriminate among inflation models*, Phys. Rev. D 56 3207 (1997).

[9] J. M. Bardeen, P. J. Steinhardt, M. S. Turner, *Spontaneous creation of almost scale-free density perturbations in an inflationary universe*, Phys. Rev. D28, 679 (1983).

[10] J. M. Maldacena, *Non-Gaussian features of primordial fluctuations in single field inflationary models*, JHEP 05, 013, astro-ph/0210603, (2003)

[11] K. Dimopoulos, *Ultra slow-roll inflation demystified*, arXiv:1707.05644v3, (2017)

[12] M. Maggiore, *Gravitational Wave Experiments and Early Universe Cosmology*, arXiv:gr-qc/9909001, (2000)

[13] Tristan L. Smith, Marc Kamionkowski, Asantha Cooray, *Direct detection of the inflationary gravitational wave background*, arXiv:astro-ph/0506422, (2006)

[14] Juan Garcìa-Bellido, Marco Peloso, Caner Unal, *Gravitational wave at interferometer scales and primordial black holes in axion inflation*, arXiv:1610.03763, (2016)

[15] Shane L. Larson, Wiliam A. Hiscock, Ronald W. Hellings, *Sensitivity curves for spaceborne gravitational wave interferometers*, arXiv:gr-qc/9909080 (2000)

[16] M. Mylova, O. Özsoy, S. Parameswaran, G. Tasinato, I. Zavala *A new mechanism to enhance primordial tensor fluctuations in single field inflation*, arXiv:1808.10475, (2018)

[17] T. Kobayashi, M. Yamaguchi, J. Yokoyama, *Generalized G-inlation: Inlation with the most general second-order field equations*, Prog. Theor. Phys. 126 511529, arXiv:1105.5723, (2011)

[18] D. Wands, *Duality Invariance of Cosmological Perturbation Spectra*, arXiv:gr-qc/9809062, (1999)

[19] C.Cheung, P. Creminelli, A. Liam Fitzpatrick, J. Kaplan, L. Senatore, *The Effective Field Theory of Inflation*, arXiv:0709.0293, (2008)

[20] F.Piazza, F.Vernizzi, *Effective Field Theory of Cosmological Perturbations*, [arXiv:1307.4350 [hep-th]], (2013)

[21] L.Bordin, P.Creminelli, A.Khmelnitsky, L.Senatore, *Light Particles with Spin in Inflation*, [arXiv:1806.10587 [hep-th]], (2018)

[22] A. Schmidt-May, M. von Strauss, *Recent developments in bimetric theory*, arXiv:1512.00021, (2016)

[23] C. de Rham, *Massive Gravity*, arXiv:1401.4173, (2014)

[24] K. Hinterbichler, *Theoretical Aspects of Massive Gravity*, arXiv:1105.3735, (2012)

[25] N.Boulanger, T. Damour, L.Gualtieri, M. Henneaux, *Inconsistency of interacting, multi-graviton theories*, arXiv:hep-th/0007220, (2000)

[26] N Arkani-Hamed, H. Georgi, M.D. Schwartz, *Effective field theory for massive gravitons and gravity in theory spaces*, arXiv:hep-th/0210184, (2002)

[27] G.Feinberg, *Possibility of Faster-Than-Light Particles*, (1967) https://doi.org/10.1103/PhysRev.159.1089

[28] Y. Aharonov, A. Komar and L. Susskind, *Superluminal Behaviour, Causality and Instability*, Phys. Rev. 182 , 1400 (1969).

[29] C. Schwarz, *Toward a Quantum Theory of Tachyon Fields*, arXiv:1603.01294, (2016)

[30] P. Ivanov, P. Naselsky, and I. Novikov, *Inflation and primordial black hole as dark matter*, Phys. Rev. D 50, 7173 (1994)

[31] J.G.Bellido, A.Linde, D.Wands, *Density perturbation and balck hole formation in hybrid inflation*, arXiv:astro-ph/9605094, (1996)

[32] W. Skiba, *TASI Lectures on Effective Field Theory and Precision Electroweak Measurements*, arXiv:1006.2142, (2010)

[33] C.J. Moore, R.H. Cole, C.P.L. Berry, *Gravitational-wave sensitivity curves*, arXiv:1408.0740 , (2014)

[34] B.S. Sathyaprakash, B.F Schutz, *Physics, Astrophysics and Cosmology with Gravitational Waves*, arXiv:0903.0338, (2009)

[35] M. Maggiore, *Gravitational Waves volume 1: theory and experiments*, (2007)

[36] T. Robson, N.J. Cornish, C. Liu, *The construction and use of LISA sensitivity curves*, arXiv:1803.01944, (2018)

[37] N. Cornish, T. Robson, C. Liu *The construction and use of LISA sensitivity curves*, arXiv:1803.01944v2, (2018)

[38] N.Cornish,*Detecting a stochastic gravitational wave background with the Laser Interferometer Space Antenna*, arXiv:gr-qc/0106058, (2002)

[39] H. Vahlbruch, M. Mehmet, S. Chelkowski, B. Hage, A. Franzen, N. Lastzka, S. Gossler, K. Danzmann, R. Schnabel, *Observation of Squeezed Light with 10-dB QuantumNoise Reduction*, Phys. Rev. Lett., 100, 033602, (2008).

[40] A. Giazotto et al., *The VIRGO Experiment: Status of the Art*, (World Scienti?c, Singapore; River Edge, NJ, 1995).

[41] G. Hobbs et al., *The International Pulsar Timing Array Project: using pulsars as a gravitational wave detector*, Class. Quantum Grav. 27 084013, (2010)

[42] E.Thrane, J.D. Romano, *Sensitivity curves for searches for gravitational-wave backgrounds*, arXiv:1310.5300v2, (2013)

[43] R.W. Hellings, G.S. Downs, *Upper limits on the isotropic gravitational radiation background from pulsar timing analysis*, Astrophyis. J. Lett. 265 39?42, (1983)

[44] A.H. Guth, *Inflationary universe: A possible solution to the horizon and flatness problems*, Phys. Rev. D 23, 347,(1981)

[45] A.D. Linde, *Chaotic Inflation*, Phys. Lett. 129B, 177, (1983)